Advanced ultrafast fiber laser sources enabled by fiber nonlinearities

Wei Liu

Fachbereich Physik
Universität Hamburg

This dissertation is submitted to the University of Hamburg for the degree of
Doctor rerum naturalium

Fakultät für Mathematik,
Informatik und
Naturwissenschaften

September 2016

Date of Oral defense: 20 December, 2016

The following evaluators recommend the admission of the dissertation:

Prof. Dr. Franz X. Kärtner

Dr. Guoqing Chang

Prof. Dr. Michael A. Rübhausen

Prof. Dr. Florian Grüner

Prof. Dr. Ludwig Mathey

I would like to dedicate this thesis to my loving parents ...

Declaration

I hereby declare that except where specific reference is made to the work of others, the contents of this dissertation are original and have not been submitted in whole or in part for consideration for any other degree or qualification in this, or any other university. This dissertation is my own work and contains nothing which is the outcome of work done in collaboration with others, except as specified in the text and Acknowledgements.

Wei Liu
September 2016

Acknowledgements

First of all, I would like to thank Prof. Franz X. Kärtner for giving me the opportunity to work in the excellent working environment with excellent and motivated colleagues.

I am extremely grateful to Noah, my supervisor and spiritual mentor, for his guidance and encouragement in all aspects. He has supported me in virtually all aspects of my work (including proofreading this thesis), giving me that large degree of independence in my research work and always anticipating a successful outcome of my experiments. I will never forget the exciting discussions during the lunches and coffee breaks with Noah. His patience, clear explanation, and continuous support are always available to me for solving problems. All this helped me gain a lot of experience and professional confidence. Besides, his personality and his attitude towards work and life really set him as a role model for me. From him I can really draw inspiration and determination for my future work and life.

I would like to thank Dr. Damian Barre for his dedicated work in helping me develop the CPA system. Obviously the large-pitch fiber amplifier could not be installed without his countless effort. I always benefited from numerous stimulating discussions with Damian.

Further more, I appreciate the cooperation work with Jan Schulte, who gave me valuable suggestions and help on adapting our CPA laser system for enhancement cavity project. Special thanks go to Chen Li, who built a stable mode-locked oscillator for my experiments in developing SPM-enabled ultrafast fiber sources. I would like to thank Hsiang-Yu and Shih-Hsuan for applying my laser system to their multiphoton microscopy project. They offered me valuable comments on improving the laser performance.

I also would like to thank the secretary Christine Berber for her dedicated work to take care of numerous organizational challenges.

I wish to thank all members in our group for the nice and friendly environment.

Finally, I would like to thank my parents and my brother for their endless love and constant support.

Abstract

Development of high power/energy ultrafast fiber lasers for scientific research and industrial applications is one of the most exciting fields in ultrafast optics. This thesis demonstrated new means to improve two essential properties—which are indispensable for novel applications such as high-harmonic generation (HHG) and multiphoton microscopy (MPM)—of an ultrafast fiber laser system: energy scaling capability and wavelength tunability.

High photon-flux extreme ultraviolet sources enabled by HHG desire high power (>100 W), high repetition-rate (>1 MHz) ultrafast driving laser sources. We have constructed from scratch a high-power Yb-fiber laser system using the well-known chirped-pulse amplification (CPA) technique. Such a CPA system capable of producing $\sim$200-W average power consists of a monolithic Yb-fiber oscillator, an all-fiber stretcher, a pre-amplifier chain, a main amplifier constructed from rode-type large pitch fiber, and a diffraction-grating based compressor. To increase the HHG efficiency, ultrafast pulses with duration <60 fs are highly desired. We proposed and demonstrated a novel amplification technique, named as pre-chirp managed amplification (PCMA). We successfully constructed an Yb-fiber based PCMA system that outputs 75-MHz spectrally broadened pulses with >130-W average power. The amplified pulses are compressed to 60-fs pulses with 100-W average power, constituting a suitable HHG driving source.

MPM is a powerful biomedical imaging tool, featuring larger penetration depth while providing the capability of optical sectioning. Although femtosecond solid-state lasers have been widely accepted as the standard option as MPM driving sources, fiber-based sources have received growing research efforts due to their superior performance. In the second part of this thesis, we both theoretically and experimentally demonstrated a new method of producing wavelength widely tunable femtosecond pulses for driving MPM. We employed self-phase modulation to broaden a narrowband spectrum followed by bandpass filters to select the rightmost/leftmost spectral lobes. Widely tunable in 820-1225 nm, the resulting sources generated nearly transform-limited, $\sim$100 fs pulses. Using short fibers with large mode-field-diameter for spectral broadening, we obtained ultrashort pulses with the pulse energies up to 20 nJ. We applied such an enabling source to drive MPM imaging of both cancer cells and skin samples.

Zusammenfassung

Die Entwicklung von Ultrakurzpuls-Faserlasern mit hoher Leistung und Energie für Anwendungen in der wissenschaftlichen Forschung und Industrie ist eines der spannendsten Gebiete ultraschneller Optik und das Hauptthema dieser Dissertation. Diese Dissertation zeigt neue Mittel zur Verbesserung von zwei wesentlichen Eigenschaften eines Ultrakurzpuls-Faserlasersystems: die Energieskalierungsfähigkeit und Durchstimmbarkeit der Wellenlänge, die unentbehrlich für neue Anwendungen wie die Erzeugung höherer Harmonischer in Edelgasen (Englisch: High Harmonics Generation, HHG) und Multiphotonen-Mikroskopie (MPM) sind.

Ultrakurzpuls-Faserlaser Anwendungen, wie die von HHG erzeugte extreme Ultraviolett-Strahlungsquelle, erfordern Laserquellen die von hoher Leistung (>100 W) und hoher Pulswiederholrate (>1 MHz) gekennzeichnet sind. Um diese Parameter zu demonstrieren wurde ein Lasersystem basierend auf der Verstärkung mit gechirpten Pulsen (Englisch: Chirped Pulse Amplification, CPA) und Verwendung von Ytterbium-dotierten Fasern ein Hochleistungs-Oszillator-Verstärkersystem (Englisch: Master-Oscillator-Power-Amplifier, MOPA) aufgebaut. Dieses CPA-System, das ca. 200W Durchschnittsleistung produzieren kann, besteht aus einem monolithischen Ytterbium-Faser-Oszillator, einem Faserstrecker, einer Vorverstärkerkette, und einem single-modigen Großkernfaser-Hauptverstärker, sowie einem auf dielektrischen Beugungsgitter basiertem Kompressor.

Für viele wissenschaftliche Anwendungen, wie z.B. HHG, erfordern ultrakurze Pulse mit Dauern <60 fs. Wir haben eine neue Verstärkungstechnik vorgeschlagen und demonstriert, die wir als Vorchirp gesteuerte Verstärkung (pre-chirp managed amplification, PCMA) bezeichnen. Mit einem auf Ytterbium-Faser basierten PCMA-System konnten wir 60fs-Pulse bei 100 W durchschnittlicher Leistung und 75 MHz Pulswiederholungsrate erzeugen. Was die Laserquelle für die Erzeugung von HHG interessant macht.

Im zweiten Teil dieser Dissertation zeigen wir theoretisch und experimentell eine neue Methode, die Femtosekundenpulse mit breit durchstimmbarer Wellenlänge als Quelle für die Multiphotonen-Mikroskopie nutzbar macht. Die Multiphotonen-Mikroskopie ist ein vielfach verwendetes biomedizinisches Bildgebungsverfahren zur Untersuchung molecularer und morphologischer Information. Ein entscheidender Vorteil von MPM ist die Bildgebung mit großer Eindringtiefe. Die Entwicklung von angepassten durchstimmbaren faserbasierten Ultrakurzpulslasern führt zu einer entscheidenden Verbesserung in der MPM. Wir benutzen Selbstphasenmodulation, um das schmalbandige Spektrum zu verbreiten. Dann wählen wir die im verbreiterten Spektrum ins Blaue und Rote verschobenen Ränder mittels eines Bandpassfilters. Die entsprechenden Quellen sind von 800-1225nm durchstimmbar und generieren fast Fourier-limitierte Pulse mit Dauern von ca. 100fs. Mittels kurzen Fasern mit

großem Modefelddurchmesser erhalten wir ultrakurze Pulse mit Energien von bis zu 20nJ. Mit dieser neuen Laserquelle wurden mittels MPM Krebszellen und Hautproben abgebildet.

List of Publications

Journal publications

1. **Wei Liu**, Shi-Hsuan Chia, Hsiang-Yu Chung, Franz X. Kaertner and Guoqing Chang, "Energy scalable ultrafast fiber laser sources tunable in 1030-1210 nm for multi-photon microscopy," (2016) (submitted to Optical Express)

2. Yizhou Liu, **Wei Liu**, Damian N Schimpf, Tino Eidam, Jens Limpert, Andreas Tünnermann, Franz X Kärtner, Guoqing Chang, "100-W few-cycle Yb-fiber laser source based on pre-chirp managed amplification employing circular polarization," (2016) (submitted to optics letters)

3. **Wei Liu**, Chen Li, Zhigang Zhang, Franz X Kärtner, Guoqing Chang, "Self-phase modulation enabled, wavelength-tunable ultrafast fiber laser sources: an energy scalable approach," Optics Express, 24(14), 15328-15340. (2016)

4. **Wei Liu**, Damian N Schimpf, Tino Eidam, Jens Limpert, Andreas Tünnermann, Franz X Kärtner, Guoqing Chang, "Pre-chirp managed nonlinear amplification in fibers delivering 100 W, 60 fs pulses," Optics letters, 40(2), 151-154. (2015)

Conference Proceedings

1. **Wei Liu**, Yizhou Liu, Damian N Schimpf, Tino Eidam, Jens Limpert, Andreas Tünnermann, Franz X Kärtner, Guoqing Chang. Pre-chirp managed nonlinear amplification in fibers delivering 100 W, 60 fs pulses.paper PA16-PA115-22, SPIE/COS Photonics Asia, Beijing (2016) (invited paper)

Conference talks

1. **Wei Liu**, Yizhou Liu, Damian N Schimpf, Tino Eidam, Jens Limpert, Andreas Tünnermann, Franz X Kärtner, Guoqing Chang. Pre-chirp managed nonlinear amplification in fibers delivering 100 W, 60 fs pulses.paper PA16-PA115-22, SPIE/COS Photonics Asia, Beijing (2016) (invited talk)

2. **Wei Liu**, Shi-Hsuan Chia, Hsiang-Yu Chung, Franz X. Kaertner and Guoqing Chang, "Energy scalable ultrafast fiber laser sources tunable in 1030-1200 nm for multiphoton microscopy," Advanced Solid-State Lasers, Massachusetts (2016)

3. **Wei Liu**, Chen Li, Hsiang-Yu Chung, Shih-Hsuan Chia, Zhigang Zhang, Franz X. Kärtner, Guoqing Chang, "Ultrafast fiber laser source tunable in 825-1210 nm for multi-photon microscopy," EPS-QEOD Europhoton Conference, Vienna (2016)

4. **Wei Liu**, Chen Li, Shi-Hsuan Chia, Hsiang-Yu Chung, Zhigang Zhang, Franz X Kärtner, Guoqing Chang, "Widely tunable ultrafast sources for multi-photon microscopy," paper SM2I-7, CLEO/QELS, San Jose (2016)

5. **Wei Liu**, Chen Li, Zhigang Zhang, Franz X. Kärtner and Guoqing Chang, "Yb-fiber laser based ultrafast source emitting 50-fs pulses at 920 nm," paper UFO0123, Ultrafast optics, Beijing (2015)

6. **Wei Liu**, Damian N Schimpf, Tino Eidam, Jens Limpert, Andreas Tünnermann, Franz X Kärtner, Guoqing Chang, "Pre-chirp managed amplification (PCMA) in fibers to 100 W with 60-fs output pulse duration," paper AW4A.2, Advanced Solid-State Lasers, Shanghai (2014)

7. **Wei Liu**, Gengji Zhou, J. K. Lim, H. –W. Chen, Franz X. Kaertner, and Guoqing Chang, "Relative intensity noise of Raman solitons: which one is more noisy," paper SM4N.7, CLEO/QELS, San Jose (2014)

Table of contents

List of figures

List of tables

Nomenclature

Acronyms / Abbreviations

CFBG chirped fiber bragg grating

FSR free-spectral range

GDD group delay dispersion

GNLSE generalized nonlinear Schrödinger equation

GVD group velocity dispersion

HC hollow-core

HDM highly dispersive mirror

LMA large mode area

LPF large pitch fiber

MFA mode field area

MFD mode field diameter

MOPA master oscillator power amplifier

OPO optical parametric oscillator

PBGF photonic band-gap fiber

PCMA pre-chirp managed amplification

PZT piezo actuator

SAM saturable absorber mirror

SHG second harmonic generation

SMF single mode fiber

SPM self-phase modulation

SRS stimulated Raman scattering

SSFS soliton self-frequency shift

SS self-steepening

THG third harmonic generation

TOD third-order dispersion

WDM wavelength division multiplexer

YDFA ytterbium doped fiber amplifier

Chapter 1

Introduction

Ultrafast lasers have found many important applications such as frequency metrology, high-harmonic generation (HHG), precision machining, and multiphoton imaging. Among many ultrafast laser systems, ultrafast Yb-fiber lasers have attracted intensive research efforts because of their superior power scalability, small footprint, excellent beam quality, and potential maintenance-free operation. In this thesis, we employ fiber-optic nonlinearities to expand the capabilities of current Yb-fiber laser technology. In this chapter, I will first briefly discuss the basics about optical fibers, fiber lasers, and nonlinear fiber optics. Then I will address the motivation of my thesis work. Finally I will give the structure of this thesis.

1.1 Fiber, fiber lasers, and nonlinear fiber optics

1.1.1 Passive fiber

Optical fibers are the core components of fiber optics. As a type of cylindrical waveguides, they are usually made of some kind of glass. Optical fibers made of fused silica—the most commonly used glass material—can be hundreds of kilometers in length.

Most optical fibers used in laser technology have a core with a refractive index higher than that of the surrounding medium (known as cladding). For step-index optical fibers, the refractive indices are constant for both the core and the cladding. Light launched into the fiber is guided by the core; that is, the light propagates mainly in the core region though the intensity distribution may extend beyond the core. Due to the guidance and the low propagation losses, the optical power can be maintained in the fiber for long propagation distance.

The design of a step-index fiber can be characterized with only three parameters: the core radius and the refractive indices of the core and the cladding. SMFs for guiding light at about

1.03 μm (the Yb-fiber laser wavelength) have a nominal core diameter of a few microns. The core-cladding refractive index contrast determines the fiber's numerical aperture (NA), which is defined as

$$NA = \frac{1}{n_0}\sqrt{n_{core}^2 - n_{cladding}^2} \tag{1.1}$$

NA corresponds to the sine of the maximum acceptable angle of an incident beam with respect to the fiber axis (considering the launch from air into the core in a ray-optic picture). (n_0 is the refractive index of the surrounding medium – close to 1 in case of air.) NA also quantifies the strength of fiber guidance. NA values vary in a relatively large range for SMFs. Typical NA values are $\sim$0.1 for conventional SMFs while large mode-area SMFs can have low NA below 0.05.

Photonic crystal fiber (PCF), also known microstructure fiber or holey fiber, is a special type of optical fiber. A typical PCF consists of only one material (usually fused silica), containing small air holes with diameters well below 1 µm. PCFs are fabricated by drawing fiber preforms that are prepared by stacking capillary tubes.

By varying the arrangement of air holes, PCFs can be fabricated with customized properties [1–4]:

- Extremely large or small mode area, leading to extremely weak or strong nonlinearity.
- Single-mode guidance in very large wavelength regions (e.g., endlessly SMFs).
- Guidance with the light field dominantly propagating in an air hole (air-guiding photonic bandgap fibers).
- Unusual chromatic dispersion properties, e.g. anomalous dispersion in the visible wavelength region.

PCFs have found many important applications, such as fabrication of extremely nonlinear fiber devices, high-energy and high-power laser beam delivery, and construction of high-energy fiber amplifiers, to name a few.

1.1.2 Fiber lasers

If the core of an optical fiber is doped with rare-earth ions, such as ytterbium, erbium, thulium and so on, the fiber now becomes an active fiber and can work as a gain medium to construct ultrafast fiber lasers. Single-pass of an Yb-doped fiber can provide small signal gain up

to >30 dB, which offers large optical alignment tolerance and reduces the complexity of opto-mechanic system construction. Ultrafast fiber lasers are widely used in many areas of optical science and technology, including modern ophthalmology, optical microscopy, laser micromachining, optical communication, and precision metrology [5].

Mode-locked Yb-fiber lasers emit in a typical wavelength range of 1020–1060 nm. In this wavelength range, most SMFs exhibit positive group-velocity dispersion (GVD). However, generation of femtosecond pulses often requires managing the total cavity dispersion, which in turn demands devices that can provide negative GVD. These devices may be a fiber Bragg grating or a bulk grating pair. Depending on the sign and the amount of net cavity dispersion, an Yb-fiber mode-locked laser outputs pulses with the duration ranging from sub-ps to $\sim$ 10 ps, corresponding to different mode-locking regimes (i.e. dissipative soliton, similariton, stretched-pulse, and soliton) [6]. An Yb-fiber laser can be configured with different cavity structures, such as linear cavity [7], ring cavity [8], figure of eight [9, 10], and figure of nine [11].

1.1.3 Nonlinear fiber optics

As ultrafast pulses propagate inside the core (with a nominal diameter of several microns) of an optical fiber, the intense peak power modifies the refractive index of the fiber material and leads to nonlinear fiber-optic effects. This material response can be represented by an expansion of the material polarization [12]:

$$P = \chi^{(1)}E + \chi^{(2)}EE + \chi^{(3)}EEE \tag{1.2}$$

where $\chi^{(n)}$ is the $n^{th} - order$ susceptibility at optical frequencies. Glasses are optically isotropic material and the second-order susceptibility vanishes. The various types of nonlinearities considered here can be expressed in terms of the real and imaginary parts of the third-order nonlinear susceptibility appearing in Eq. 1.2. The real part of the susceptibility is associated with the refractive index; the imaginary part corresponds to a time or phase delay in the material response, giving rise to either loss or gain. For instance, the nuclear contribution to stimulated Raman scattering (SRS) or the electrostrictive stimulated Brillouin effect (both resulting in loss or gain) can be expressed in terms of the imaginary part of a $\chi^{(3)}$ susceptibility, while four-wave mixing (a purely electronic and almost instantaneous effect resulting in frequency conversion) is associated with the real part of the $\chi^{(3)}$ susceptibility [13–15].

It might be counter-intuitive that nonlinear effects are so prominent in optical fibers given a small nonlinear index of silica ($n_2 = 2.6 \times 10^{-26} cm^2/W$). However, two other fiber

parameters—mode field area (MFA) A_{eff} and effective length L_{eff}— strongly enhance the light-fiber nonlinear interaction. These two parameters are given by[16]:

$$A_{eff} = \frac{\left\{\int_{-\infty}^{+\infty} |A(x,y)|^2 dx dy\right\}^2}{\int_{-\infty}^{+\infty} |A(x,y)|^4 dx dy} \tag{1.3}$$

$$L_{eff} = \frac{1}{\alpha}(1 - e^{-\alpha L}), \tag{1.4}$$

where $A(x,y)$ is the field distribution and α is the loss coefficient. MFA of conventional SMFs (such as HI1060) is about $80\,\mu m^2$. L_{eff} is the effective propagation length taking into account loss.

We can compare the nonlinearities in bulk media and silica fibers using the following ratio [16]:

$$\frac{I_f L_{eff}(fiber)}{I_b L_{eff}(bulk)} = \frac{\lambda}{\pi r_0^2 \alpha}, \tag{1.5}$$

where I_f and I_b are the intensity (power per unit area) in the fiber and bulk, respectively. λ is the wavelength, and r_0 the mode field radius of the fiber. As seen from Eq. 1.5, a small mode field radius and low loss can greatly enhance the ratio and thus the optical nonlinearities. For example, if we choose the wavelength to be 1 μm and a fiber with a typical loss of 0.2 dB/km, the nonlinear enhancement simply due to the small core can be of the order of 10^8.

GVD is another critical parameter in nonlinear fiber optics. In particular for nonlinear wavelength conversion, GVD has manifold effects, which can be grouped into three categories:

1. It determines the phase matching of parametric nonlinear processes.

2. It causes group velocity mismatch (temporal walk-off, limited phase-matching bandwidth) and thus limits the effective interaction length for ultrashort pulses.

3. It stretches the propagating pulses, reduces the pulse peak power, and therefore weakens the nonlinear interaction.

Fiber-optic nonlinear effects can be a serious disadvantage for high-energy pulse amplification and delivery in fibers because high peak intensities cause many fiber-optic nonlinear effects that distort both the optical pulse and the optical spectrum. As a result, suppressing these nonlinearities is crucial in designing ultrafast fiber laser systems. For example, high-energy (>1 μJ) ultrafast Yb-fiber amplifiers usually employ chirped-pulse amplification

(CPA) to mitigate the detrimental nonlinear effects. In a typical Yb-fiber CPA system, weak pulses are temporally stretched to 100-1000 ps before seeding into an Yb-fiber amplifier followed by a compressor to compress the stretched, amplified pulses to the transform-limited duration.

However, fiber-optic nonlinearities are extremely useful for many applications, such as wavelength conversion, spectral broadening and pulse compression, supercontinuum generation, etc. In fact, development of the next-generation ultrafast sources for clinical applications strongly relies on fiber-optic nonlinearities in order to implement all-fiber integrated sources. Realization of these robust and compact fiber-based sources therefore requires careful investigation of both the advantages and disadvantages of nonlinear effects.

In this thesis, fiber-optical nonlinearities are used to (1) control nonlinear amplification of ultrafast pulses and (2) generate wavelength-tunable femtosecond pulses.

1.2 Why high power fiber lasers?

Ultrafast laser sources featuring high pulse energy (>1 μJ), ultrashort pulse duration (<100 fs), and high average power (>100 W) are desired by numerous ultrafast applications, particularly for those nonlinear optical processes that exhibit low conversion efficiency. For example, generation of ultrashort pulses at the terahertz range via optical rectification pumped by a near-IR femtosecond source has a typical efficiency of $10^{-5} - 10^{-3}$; coherent vacuum extreme ultraviolet sources enabled by HHG in noble gases require laser intensities of > $10^{13} W/cm^2$ and feature conversion efficiencies of $\sim 10^{-7}$ or less. The conversion efficiency can be improved using a passive high-finesse optical cavity pumped by a femtosecond laser source. If the laser repetition rate matches the FSR of the optical cavity, the laser power can be efficiently coupled into the passive optical cavity and the resulting power circulating inside the cavity is much larger than the laser output power; the enhanced factor depends on the cavity finesse [17, 18]. Driving such an enhancement cavity necessitates the development a suitable ultrafast laser source with high pulse energy, well-compressed pulse duration, and preferably a stable carrier-envelope phase for cavity locking.

Among the most promising candidates, high-power Yb-fiber lasers have exhibited superior power scalability because optical fibers possess large surface-to-volume ratio resulting in excellent heat dissipation. Other advantages of Yb-fiber lasers over solid-state lasers include high electrical-to-optical conversion efficiency (>10%), large single-pass gain (30 dB), excellent beam quality (close to diffraction-limited) due to waveguide confinement, and small footprint, to name a few [19]. High-power ultrafast Yb-fiber laser system can be imple-

mented using different technologies, such as CPA, self-similar pulse amplification followed by pulse compression, or CPA plus subsequent pulse compression using hollow-core PCFs.

1.2.1 High-power Yb-fiber CPA system

Due to the rapid advance in developing double-clad Yb-doped fibers and high brightness pump diodes, ultrafast Yb-fiber lasers with proper thermal management are able to output sub-kW average power. The achievable pulse energy from an ultrafast Yb-fiber laser system is mainly limited by fiber-optic nonlinearities inside Yb-fiber amplifiers. To obtain >1-μJ pulse energy, CPA has become the standard technique to mitigate the accumulated nonlinear phase. Thanks to the recent progress in fabrication of large-mode-area (LMA) Yb-doped fiber—such as LMA PCF, rod-type large-pitch fiber, chirally-coupled core fiber, ultrafast Yb-fiber laser systems with > 100-μJ (or even mJ) pulse energy and >100-W average power have been demonstrated.

A typical Yb-fiber CPA system consists of an ultrafast oscillator, a pulse stretcher, fiber amplifiers, and a pulse compressor. To avoid detrimental nonlinearities, the pulse to be amplified is strongly stretched to durations in the range of 0.2-2 ns. Limited by gain narrowing and residual dispersion mismatch, the compressed pulse duration is typically $\geq$ 150-fs for Yb-doped amplifiers [5]. Further reduction of the pulse duration to <100 fs necessitates a subsequent external nonlinear pulse-compression stage, which increases the system complexity and reduces the throughput efficiency.

1.2.2 Post-stage pulse compression

Post-stage nonlinear pulse compression can overcome the limitation of gain bandwidth and produce few-cycle pulses [20–23]. Figure 1.1 shows the typical schematic setup. Several parameters are critical in the nonlinear compression process, including nonlinear strength, dispersion, pump wavelength, pump intensity and so on. The front-end is typically a high power CPA laser system with pulse duration of >200 fs, usually limited by the gain bandwidth.

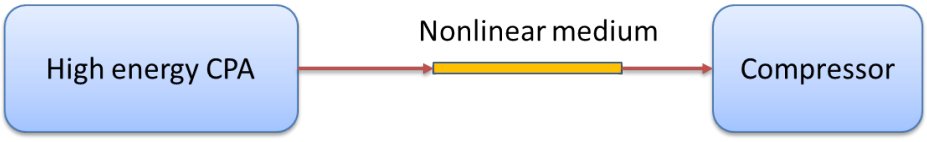

Fig. 1.1 Schematic of the nonlinear pulse compression

Nonlinear medium is the most critical element in the architecture. One of the most important concerns is how to avoid the facet damage of the nonlinear medium and prevent

self-focusing inside it. Different options exist depending on the pulse energy from the CPA system. Figure 1.2 illustrates the nonlinear compression techniques suitable for different pulse energy levels. For mJ-level pulse energy, noble gas-filled glass capillaries with sub-mm mode field diameter are usually adopted as the nonlinear medium [21–25]. This approach has been used to generate the compressed pulses with the highest peak power and average power, and the compressed pulse has a duration of <10 fs, which is less than three optical cycles. For pulse energy about tens of μJ level, hollow-core Kagome PCFs are commonly used for nonlinear compression [26–33]. For pulse energy below μJ level, solid-core LMA fibers are well suited [27, 34]. The physical mechanisms behind spectral broadening in these nonlinear pulse compression approaches can be divided into two categories: (1) self-phase modulation (SPM) dominated spectral broadening in a nonlinear medium with positive GVD and (2) higher-order soliton compression occurring in a nonlinear medium with negative GVD.

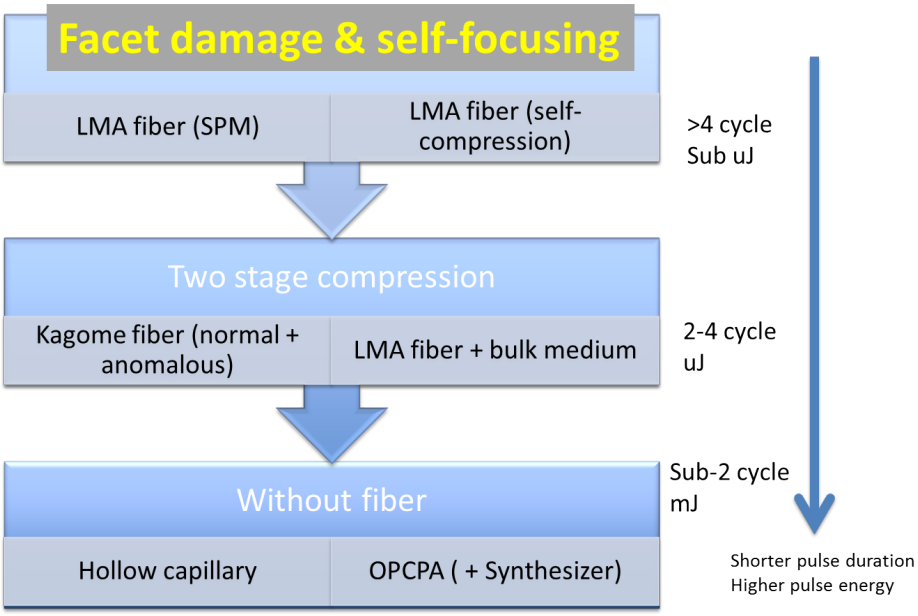

Fig. 1.2 Post-stage pulse compression techniques

1.2.3 Self-similar pulse amplification

Self-similar pulse amplification does not require a stretcher and employs fiber-optic nonlinear effects [35]. In contrast to fiber-based CPA systems avoiding nonlinearities by strongly stretching the pulses, self-similar pulse amplification directly amplifies the pulses [36, 37]. Due to the interplay of SPM, positive GVD, and gain, self-similar pulse amplification inside

an Yb-fiber amplifier gradually reshapes the amplified pulse such that the pulse develops a parabolic temporal intensity profile and a linear chirp after a characteristic self-similar fiber length [38]. This amplification scheme has produced sub-50 fs pulses with $\sim 20\,W$ average powers and $\sim 300\,nJ$ pulse energy [39–41].

Further increase of pulse-energy is limited by the onset of SRS for a long gain fiber and limited by finite gain bandwidth for a short gain fiber [42–44]. Typically, the characteristic self-similar length of Yb-doped fiber is several meters. When reducing the gain-fiber length to $\sim$ 1m the pulse dynamics deviates from self-similar amplification since the parabolic self-similar solution cannot develop in such a short propagation distance. However, fiber amplifiers in this operation regime are still attractive because (1) a shorter gain fiber accumulates less nonlinearity and therefore allows higher amplified pulse energy, and (2) amplified pulse is sub-ps in duration, which can be compressed by loss-free high dispersion mirrors.

In high-gain, short-length fiber amplifiers, the spectrum of an amplified pulse is rapidly broadened beyond the gain bandwidth ($\sim$ 40 nm for Yb-doped fiber), which may impose nonlinear chirp to the amplified pulses and degrade subsequent pulse compression. Nonetheless, by using 0.85 m rod-type fiber amplifier, pulses from an Yb:KYW ultrafast oscillator have been directly amplified to around 10 W average power. After pulse compression with 1250 lines/mm gratings, this results in 49 fs pulses with 870 nJ energy. Using a 1740 line/mm compressor results in 70 fs pulses [45]. However, such direct amplification scheme lacks flexibility because high-quality compressed pulses can be only produced at an optimum operating output-power [45]. In this thesis we proposed and demonstrated pre-chirp managed amplification (PCMA), in which the seeding pulse was nonlinearly amplified such that the amplified spectrum was substantially broadened. By properly pre-chirping the seeding pulse, the amplified pulse can be compressed with a duration much shorter than the transform-limited duration allowed by the seeding spectrum. Using an Yb-doped rod-type large-pitch fiber as the power amplifier, PCMA has enabled us to generate 75 MHz, $\sim$ 60 fs, linearly-polarized pulses with >100-W average power.

1.3 Ultrafast sources with wide wavelength coverage

Multiphoton microscopy (MPM) has been widely used in biomedical imaging due to the unique features such as capability of optical sectioning, various imaging contrast mechanisms, and larger penetration depth in tissue imaging [46]. The success of MPM is largely driven by the rapid advance of femtosecond laser sources in the near infrared wavelength range. For example, femtosecond pulses in the typical wavelength range 800-1300 nm can excite most of the important fluorophores employed in two-photon excited fluorescence microscopy.

Besides causing less potential photo-damage due to less photon energies, the 1200-1300 nm wavelength range enables deep tissue imaging with 1 mm penetration depth thanks to an optimal combination of reduced light scattering and low water absorption [47]. To date, no single laser can provide >1 nJ femtosecond (50-150 fs) pulses tunable in the entire 800-1300 nm wavelength range. Conventional solution relies on multiple laser systems each covering a portion of 800-1300 nm and the stitched spectrum spans the whole wavelength range. A typical combination is a Ti:sapphire laser tunable from 700 to 1040 nm plus a solid-state optical parametric oscillator (OPO) that covers the wavelength tuning range of 1040-1300 nm. However, high complexity (e.g., water cooling required), high cost, and large size of such a solid-state laser solution have spurred intensive development of reliable, cost-effective, and compact ultrafast sources in fiber format [48, 49].

Two types of femtosecond fiber lasers operate in the wavelength range of 800-1300 nm: Yb-fiber laser in 1020-1060 nm and Nd-fiber laser in 910-935 nm [50]. Such a narrowband wavelength coverage can be further expanded using various fiber-optic nonlinear mechanisms, such as dispersive wave generation [51, 52], Raman self-frequency shift [53, 54], supercontinuum generation (SCG) [55], and four-wave mixing [56], to name a few.

Most of the spectral broadening processes favor certain fiber GVD, which can be engineered for PCFs featuring much smaller mode area and thus stronger nonlinearity compared with conventional SMFs. Requiring negative GVD at the laser emission wavelength, dispersive wave generation normally generates femtosecond pulses at shorter wavelength whereas Raman self-frequency shift leads to a wavelength-tunable pulse towards longer wavelength. Limited by strong nonlinearity in PCFs, the resulting wavelength-converted pulses are limited to <1 nJ in pulse energy. SCG broadens the input optical spectrum into both shorter and longer wavelength range, spanning the entire range of 800-1300 nm; a subsequent bandpass (bandwidth of 10-30 nm) filter could select a spectral slice, which after proper phase compensation leads to femtosecond pulses. However, this method has two drawbacks: (1) SCG distributes input pulse energy in the broadened spectrum, and the selected spectral slice with 10-30 nm bandwidth includes little (<1 nJ) pulse energy. (2) SCG exerts strong nonlinear phase on the resulting spectrum, and therefore phase compensation of the filtered spectrum necessitates complex and lossy active devices (e.g., spatial light modulator). At the expense of complexity, four-wave-mixing-based fiber OPO can generate wavelength tunable pulses with much higher pulse energy. For example, Ref. [56] reports such a fiber OPO tunable in 867-918 nm for the signal and in 1200-1300 nm for the idler. Pumped by a μJ-level fiber laser system at 1040 nm, the fiber OPO produces 560-fs pulses after post compression with 30-nJ pulse energy, corresponding to 4.7% energy conversion efficiency from the pump to the idler [56].

In the second part of this thesis, we propose and demonstrate a new type of fiber laser based femtosecond source, which employs fiber-optic nonlinearities (dominated by SPM) in an optical fiber. Both the simulation and experiments demonstrate that this source is energy scalable and has a potential to cover the entire wavelength-tunable range of 800-1300 nm in an all-in-one unit. The resulting filtered spectra correspond to slightly chirped, femtosecond (70-120 fs) pulses, which might be easily compressed to the transform-limited duration by chirped mirrors.

1.4 Structure of the thesis

The thesis is divided into two parts. **Part I** (chapter 2 and 3) discusses the development of high-power/energy femtosecond fiber laser systems for exploring extremely nonlinear optics and **part II** (chapter 4 and 5) describes the development of energy scalable, wavelength widely tunable ultrafast fiber sources for multiphoton imaging application.

Chapter 2 presents the detailed designs of a high power, high repetition-rate ultrafast Yb-fiber CPA system. Especially, I discuss how to construct a low noise Yb-fiber oscillator that can be locked to an enhancement cavity, how to design the monolithic fiber stretcher, and how to manage the nonlinear effects using large-pitch rod-type gain fiber.

Chapter 3 demonstrates a new type of Yb-fiber amplifier based on pre-chirp managed amplification. I will show that the amount of pre-chirping group delay dispersion (GDD) affects the compressed-pulse quality; the optimum pre-chirping GDD that leads to nearly pedestal-free compressed pulses varies at different amplifier power. We successfully implemented an Yb-fiber laser system using this pre-chirp managed amplification technique and obtained >100-W, 75-MHz, 60-fs pulses at 1.03 μm.

In Chapter 4 we propose a new method of producing wavelength widely tunable femtosecond pulses for multi-photon microscopy. The method employs fiber-optic nonlinearities (dominated by SPM) to broaden an input optical spectrum, followed by optical bandpass filters to select the leftmost or rightmost spectral lobes. The filtered spectral lobes correspond to nearly transform-limited pulses with $\sim$ 100 fs pulse duration. In this chapter, I present a detailed numerical modeling of the method and discuss the effects of stimulated-Raman Scattering, self-steepening, dispersion, and nonlinearities.

The simulation results presented in Chapter 4 are confirmed by the experimental results in Chapter 5. More specific, use of 20-mm fiber NL-1050-ZERO-2 enables us to implement an Yb-fiber laser based source, delivering femtosecond (70-120 fs) pulses wavelength tunable from 825 nm to 1210 nm with >1 nJ pulse energy. Then we present another energy scaling method—using LMA fibers for spectral broadening, which allows us to scale the pulse

energies up to 20 nJ in the wavelength range of 1070-1220 nm, enabling nonlinear light excitation even for third-harmonic generation in human skin. Preliminary results of MPM imaging driven by our novel SPM-enabled source are presented in the end of this chapter.

Finally I use Chapter 6 to conclude my thesis.

Chapter 2

High-power Yb-fiber CPA system for cavity enhanced ultrafast optics

Using CPA to stretch the pulse prior to amplification and using LMA Yb-fiber to increase the beam size—both necessary to prevent detrimental nonlinear effects, 640-fs pulses with 830-W average power were produced from a master-oscillator-power-amplifier (MOPA) system operating at 76 MHz [57]. Unfortunately, because of long pulse duration (sub-picosecond) and low pulse energy ($\sim 12\ \mu J$), such a powerful ultrafast source does not have enough pulse peak power to directly drive HHG in noble gases. While the pulse duration can be further reduced via post nonlinear compression, current power scalability of a single Yb-fiber MOPA system always provides relatively low pulse energy ($1-10\ \mu J$) as the pulse repetition rate approaches ~ 100 MHz. Cavity-enhanced nonlinear optics solves this issue via coupling laser pulses into a resonant cavity with its free-spectral range (FSR) equal to the pulse repetition rate [18, 17, 58, 59]. Without any active amplification, the circulating pulse inside the cavity can be constructively enhanced by 2 orders of magnitude. This enhancement technique has enabled HHG driven by high repetition-rate (136 MHz) lasers, generating microwatt-level EUV pulses [60]. It is worth to note that a high repetition rate laser source will not only make the laser system itself compact but also shrink the size of an enhancement cavity. As a result, a table-top experimental platform could be realized.

This chapter is structured as follows. Section 2.1 discusses the basic requirements for the Yb-fiber laser system that is suitable for driving an enhancement cavity. Section 2.2 presents the design and construction of a low-noise Yb-fiber femtosecond oscillator that can be locked to the enhancement cavity. The noise suppression technology and locking interface design will be discussed. In section 2.3, we describe the design and construction of a high-power Yb-fiber CPA system with a detailed discussion of several critical elements. Finally, the output parameters from the pre-amplifiers and the main amplifier are given in section 2.4.

2.1 Laser requirement for driving an enhancement cavity

2.1.1 Design goal

To reach the HHG threshold for the noble gas inside an enhancement cavity, a fundamental requirement is to scale up the peak intensity I_{cir} of the intra-cavity circulating pulse. I_{cir} is given by the following formula:

$$I_{cir} \propto \frac{E_{pulse}}{\tau_{pulse} \cdot A_{\text{focus}}} \cdot Q \tag{2.1}$$

E_{pulse} and τ_{pulse} are the pulse energy and the pulse duration of the external driving Yb-fiber laser, respectively. Q is the cavity enhancement factor and A_{focus} the optical beam area at focus. Apparently, scaling up I_{cir} can be achieved by increasing the pulse energy and the enhancement factor while decreasing the pulse duration and focus size. Since HHG demands pulse energy of hundreds-of-μJ and an enhancement cavity can provide an enhancement factor of ~ 100, the desired Yb-fiber driving laser system should provide μJ-level pulse energy at 10s of MHz repetition-rate.

Table 2.1 Literature survey of μJ-level, fs Yb-fiber laser systems [57, 61–64]

Group	Ave. Power	Rep. Rate	Seed laser	Stretcher	Stret. duration	Compressor	Compre. pulse duration	Fiber of last stage
CELIA (Ref. 61)	28 W (100uJ@max)	100k-1 M	Yb:KGW, 1.7 W, 10 MHz 2.5 nm@1030nm	Offner stretcher Grating @1740/mm	600 ps	Trans. 1740/mm 52% eff.	270 fs	Rod-type PCF with 70 um core
Jena (Ref. 57)	830 W (11uJ@max)	78 MHz	Yb:KYW 150 mW 200 fs@1042 nm	Offner stretcher Grating @1740/mm	800 ps	Trans. 1740/mm 88% eff.	650 fs	8m, 27/500
DESY (Ref. 62)	32 W (530uJ@max)	60 kHz	Ti:sapphire 1030 nm	Offner stretcher Grating @1740/mm	1.5 ns	Trans. 1740/mm	1120 fs	Rod-type PCF with 80 um core
IMRA (Ref. 63)	80 W	154 MHz	Yb-fiber, Linear cavity 45nm@1050 nm	380 m of 3 fibers @double pass 12.4 ps^2 @1070nm	870 ps	Polymer Trans. 1590/mm 74% eff.	120 fs	9m, NKT DC-200/40 @915 nm
Vienna (Ref. 64)	.5 W (5uJ@max)	100 kHz	Yb-fiber, Linear cavity 30nm@1045 nm	100 m OFS fiber @single pass 12.4 ps^2 @1040nm	350 ps	Reflection 1480/mm 55% eff.	160 fs	2m, Nufern 30/250 @976 nm

Besides requirements on pulse energy and average power, the driving laser should exhibit low noise to facilitate the locking to the enhancement cavity. The layout of our enhancement cavity experimental platform is shown in Fig. 2.1. Occupying an optical table of 150 $cm \times 360$ cm, the entire system includes a high power Yb-fiber laser system, an

enhancement cavity, an optical unit to enable mode-matching between the laser output beam and the resonant mode allowed by the enhancement cavity, cavity diagnostic setup, locking setup etc. The overall requirements on the Yb-fiber driving laser are following:

- $\mu J - level$ pulse energy
- short (< 200 fs) pulse duration
- low noise
- variable repetition-rate that can be locked to the enhancement cavity
- small footprint and high stability

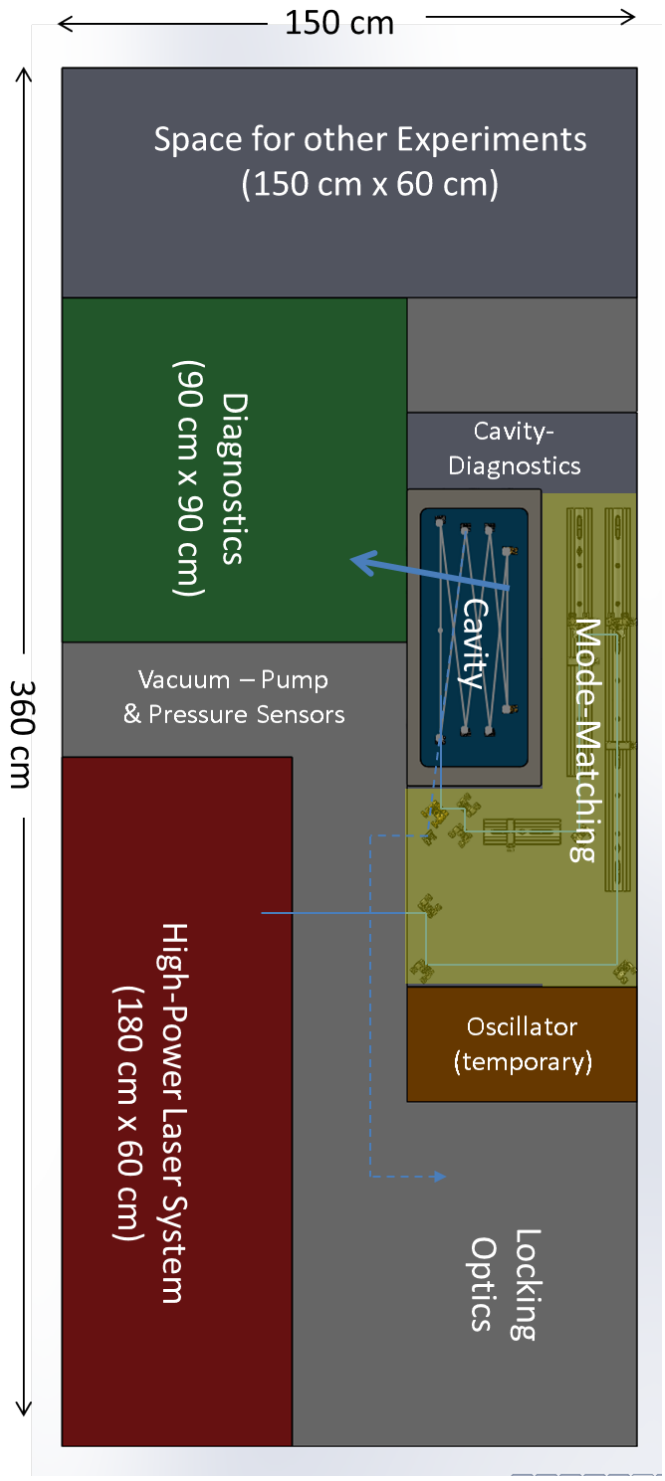

Fig. 2.1 The layout of table top enhancement cavity experimental platform. The platform is planned to build on a 150 cm x 360 cm optical table, which includes the laser system, mode-matching unit, enhancement cavity, diagnostic setup and locking setup.

2.1.2 Design concerns on the high-power Yb-fiber laser system

Current high-power Yb-fiber laser systems rely on LMA fibers to reduce accumulated nonlinear effects and bulky devices (e.g., diffraction-grating pairs) for pulse stretching/compressing [65–68]. To retain diffraction-limited beam quality—one of the most important merits for a fiber laser, special care must be taken to ensure that the LMA Yb-fiber operates at fundamental mode though it also accommodates higher-order modes. Despite remarkable success in implementing high power/energy laser systems, photonic-crystal LMA fibers suffer from long interaction length compared with bulk gain medium; thus special attention should be paid on the nonlinear phase accumulated in the laser system, as well as the self-focusing limitation.

Another pivotal device in high power Yb-fiber lasers (oscillator or MOPA) is the highly dispersive element that can provide substantial GDD to significantly chirp (or de-chirp) incident pulses. For example, in a high-power Yb-fiber CPA system, the input pulses normally are stretched hundreds-to-thousand times longer in order to substantially reduce the pulse peak power before entering power amplifiers. Dielectric diffraction-gratings configured at double-pass are widely used for pulse stretching and compressing.

For a HHG source, avoiding over ionization of the gas sample to fulfill the phase-matching condition and thus achieve better conversion efficiency demands much shorter laser pulses. However, due to relatively narrow gain bandwidth ($\sim$ 40 nm) and the gain narrowing effect during the power amplification, high-power (> 100 W) Yb-fiber CPA systems usually provide pulse durations > 200 fs. Avoiding the gain narrowing effect and achieving as short as possible pulse duration from CPA system is challenging.

2.2 Design and construction of a low-noise Yb-fiber oscillator

Recent experimental study has shown that an Yb-fiber oscillator mode-locked in the stretched-pulse regime with the net-cavity dispersion close to zero exhibits both low relative intensity noise and low timing jitter noise [69]. This provides us with general design guidelines on our Yb-fiber oscillator that will be further amplified to higher average power in a chain of Yb-fiber amplifiers. To further improve the oscillator's noise performance such that it can be conveniently locked to the enhancement cavity, we designed a monolithic Yb-fiber oscillator with minimal free-space elements. The Yb-fiber oscillator is mode-locked by a saturable absorber mirror (SAM); the positive GDD of cavity fibers is compensated by a chirped-fiber Bragg grating (CFBG) to guarantee that the net-cavity dispersion is close to zero.

2.2.1 Determination of GDD for CFBG

To design a CFBG that provides the right amount of GDD to compensate the positive GDD accumulated from the cavity elements (e.g., Yb-doped fiber, passive fibers, SAM etc.), accurate measurement of the net-cavity dispersion is necessary. We first built an Yb-fiber oscillator with a grating pair (instead of a CFBG) placed inside the oscillator cavity for dispersion compensation. The schematic setup of the test-oscillator is shown in Fig. 2.2. The repetition-rate of the final oscillator is designed at 75 MHz to match the cavity length of the enhancement cavity. However, the beam-path of the present diffraction-grating pair increases the round-trip time resulting a 68-MHz oscillator. The grating-pair separation can be freely adjusted to continuously tune the net-cavity dispersion.

The specific parameters of the main components are described in the following list:

- Grating pair: 600 lines/mm (with incident angle at 45 degree)
- L1 and L2: collimators from Thorlabs, f=4.5 mm
- SMF1: passive fiber from WDM, 850 mm (fiber type: HI1060)
- YDF: Ytterbium doped fiber, Yb501 from Coractive, 400 mm
- L3: Lens f=8 mm

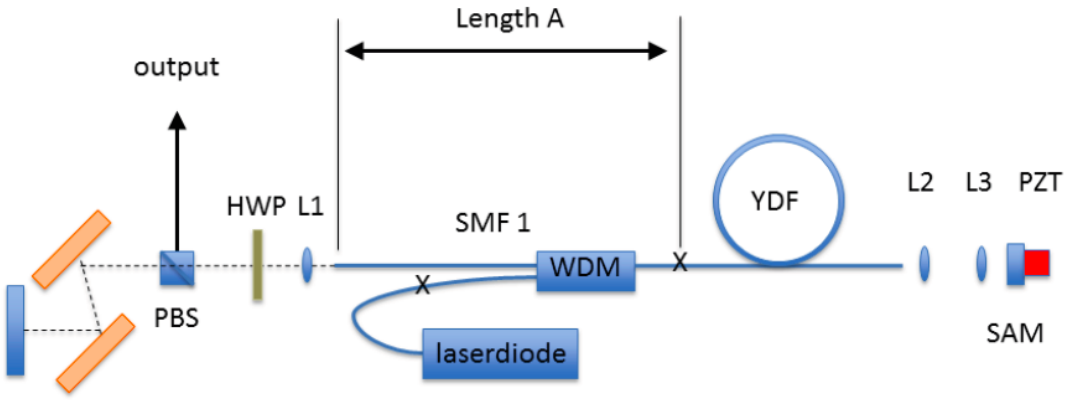

Fig. 2.2 Experimental setup the mode-locked ytterbium-doped fiber oscillator. PZT: piezo actuator, SAM: saturable absorber mirror, L1-3: lenses, YDF: ytterbium-doped fiber, WDM: wavelength-division multiplexer, SMF1: passive single-mode fiber, HWP: half-wave plate, PBS: polarization beam splitter.

To measure the net-cavity dispersion, we adopted the technique developed by Knox [70]. We inserted a slit before the end mirror right after the grating pair such that the spectral

center of the mode-locked oscillator was determined by the slit position. We then spatially translated the slit; at each slit position, the spectral center-wavelength was measured by an optical spectrum analyzer and the oscillator's repetition rate was measured by a RF spectrum analyzer. Figure 2.3 plots the repetition rate versus the center wavelength with the grating pair separated by 36 mm.

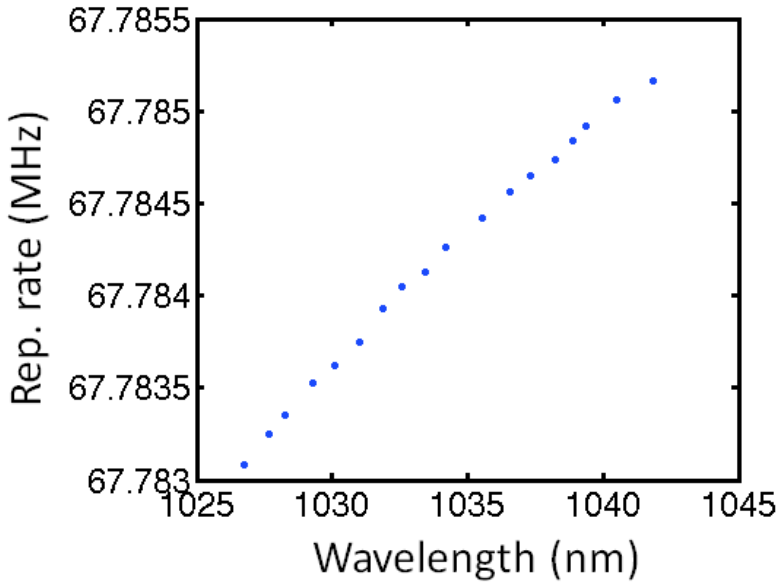

Fig. 2.3 Repetition rate vs. spectral center wavelength with the grating pair separated by 36 mm.

We repeated the same measurements with the grating pair separation at 38 mm and 40 mm. Figure 2.4(a) summarizes the repetition rate versus spectral center-wavelength for the grating pair separated by 36 mm, 38 mm, and 40 mm.

Note that the reciprocal of repetition rate gives the cavity round-trip time, corresponding to the total group delay when the intra-cavity pulse travels exactly one round-trip. Therefore we can calculate from Fig. 2.4(b) the total group delay per round-trip as a function of wavelength, which allows us to further calculate the net-cavity GDD. The calculated GDD is shown in Fig. 2.5. Clearly as we varied the grating separation from 36 mm to 40 mm, the positive net-cavity dispersion decreased and approached almost zero. Further increasing the grating separation beyond 40 mm made the oscillator hard to be mode-locked. Therefore we decided to use the 40-mm grating separation as the reference to calculate the required dispersion for the CFBG. The dispersion of a grating pair is given by [71]:

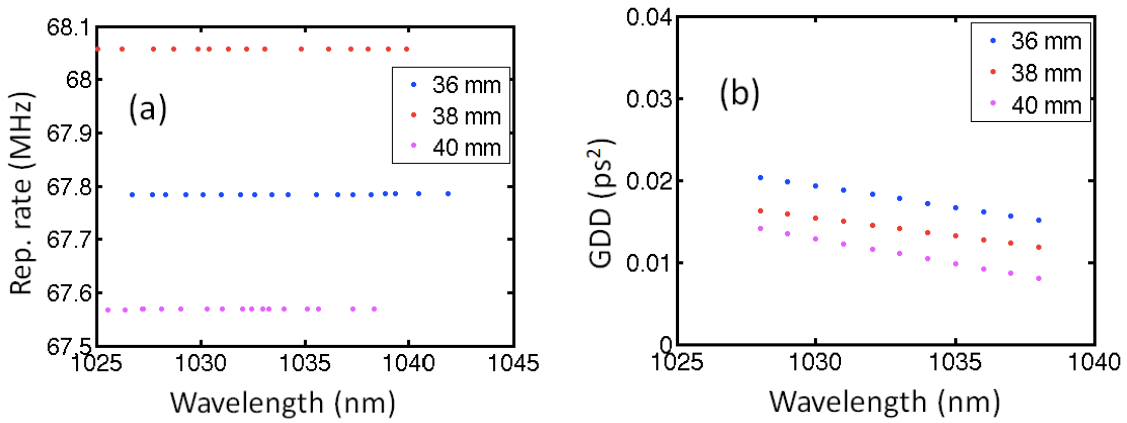

Fig. 2.4 (a) Repetition rate vs. spectral center-wavelength at different grating separation of 36 mm, 38 mm, and 40 mm. (b) The calculated net-cavity GDD at different grating separation of 36 mm, 38 mm, and 40 mm.

$$GDD_{GP}(\lambda) = \frac{-\lambda^3 b}{2\pi c^2 d^2 cos^3(arcsin(\lambda/d - sin\alpha))} \tag{2.2}$$

λ is the wavelength, b the grating separation, c the light speed, d the grating period, and α the incidence angle. For 40-mm grating separation, the calculated GDD is $-57 \times 10^{-3} ps^2$, which means that we can use a CFBG with its GDD at this value to replace the diffraction grating pair and the resulting net cavity dispersion should be close to zero. The CFBG was fabricated by Teraxion with the customized GDD of $-57 \times 10^{-3} ps^2$. The peak reflectivity of the CFBG is 7% at 1040 nm with 25-nm bandwidth; see Fig. 2.5.

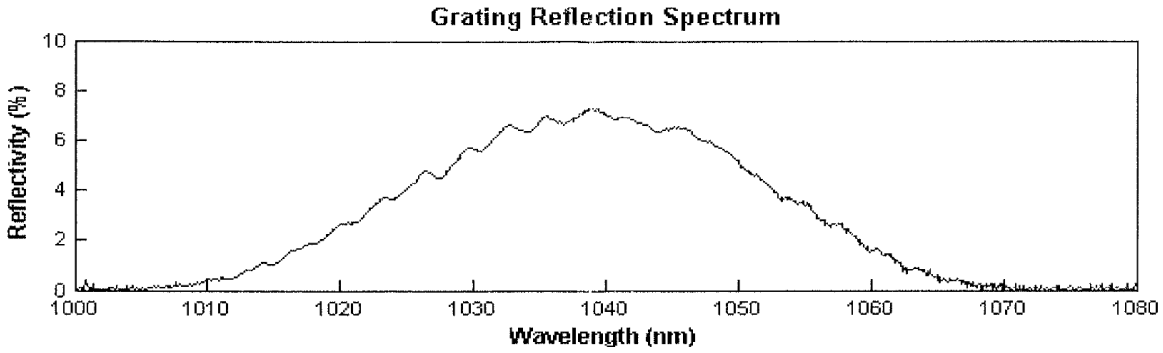

Fig. 2.5 Reflective curve of CFBG (Fabricated by TeraXion).

2.2.2 SAM and locking interface

The Yb-fiber oscillator is mode-locked by a SAM (obtained from Batop), which is also used for actively locking the oscillator to the enhancement cavity. To achieve stable mode-locking, we tested several SAMs with different modulation depths and found that the SAM with 30% modulation depth and 500-fs recovery time showed the best performance, leading to the highest output pulse energy and largest mode-locking range. Because a lighter active locking load will give higher locking frequency, the SAM was chosen to be of small size ($1 \times 1\ mm^2$).

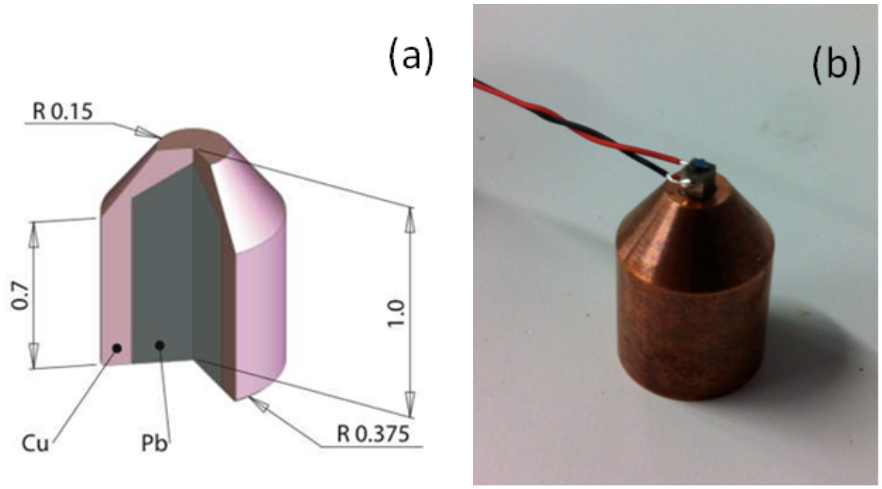

Fig. 2.6 (a) The design of lead-filled copper recoil-body [72]. (b) The picture of SAM mounted on a recoil-body.

To implement broadband locking stabilization, we need to take account two types of noises: high-frequency noise (e.g., quantum noise) and low-frequency noise (e.g., technical

noise due to mirror vibration or temperature fluctuation). High-frequency noise needs to be compensated by a fast PZT with relatively short travel range (2.2 μm). Low-frequency noise can be removed using a slow PZT actuator with much longer travel range.

For fast active locking, the small SAM was glued onto a bulky recoil body. Figure 2.6 shows the design of the recoil body. It is fabricated with brass filled with lead to allow effective cooling of the SAM and avoid mechanical resonances of the oscillator at acoustic frequencies. The fast PZT was sandwiched between the SAM and recoil body by rigid crystal bound (see Fig. 2.6).

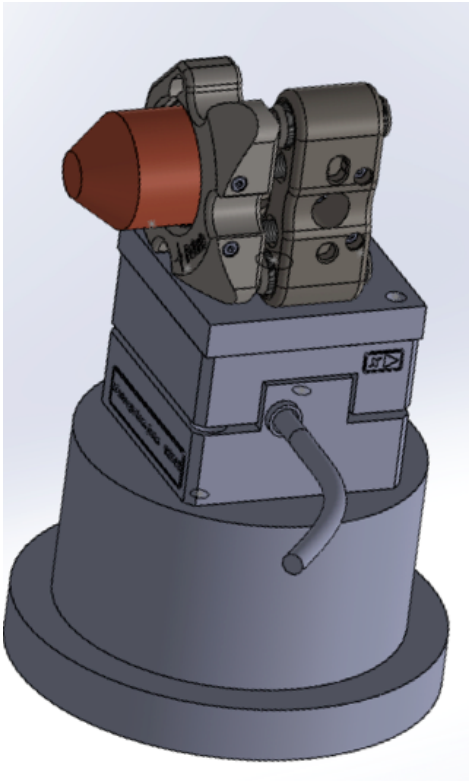

Fig. 2.7 The assemble setup of two locking interfaces. Image courtesy of Jan Schulte.

Figure 2.7 shows the assemble setup of the two locking interfaces. The recoil body was placed on a linear translation PZT stage. With this properly designed locking device, the mirror-on-PZT system could achieve a linear bandwidth in excess of 180 KHz.

2.2.3 Monolithic Yb-fiber ultrafast oscillator

Figure 2.8 shows the final version of our monolithic Yb-fiber oscillator, in which the diffraction grating pair in the original version was replaced by the customized CFBG. With a

repetition rate of 75 MHz, the oscillator also incorporated two active locking loops at the free-space segment.

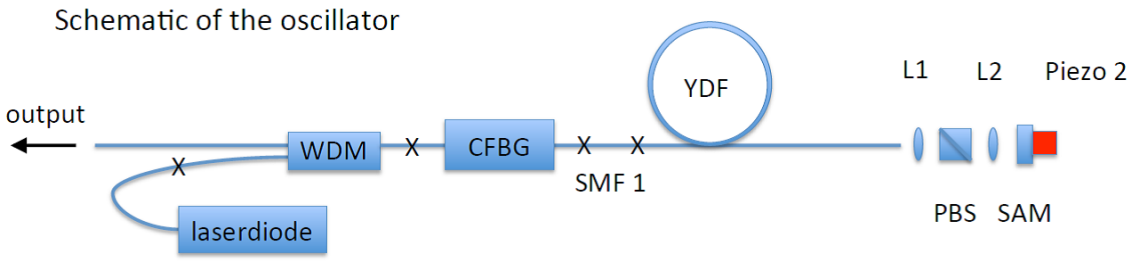

Fig. 2.8 The schematic of fiber oscillator with CFBG.

Although the CFBG has the reflection peak at 1040 nm, the oscillator tends to mode lock at 1030 nm overlapping with the Yb-doped fiber's gain peak. To enforce the oscillator mode locked at longer wavelength to avoid gain narrowing during subsequent amplification, a bandpass filter-polarizer is used to replace the polarization beam splitter inside the cavity such that the oscillator output spectrum centers at 1034.4 nm as shown in Fig. 2.9.

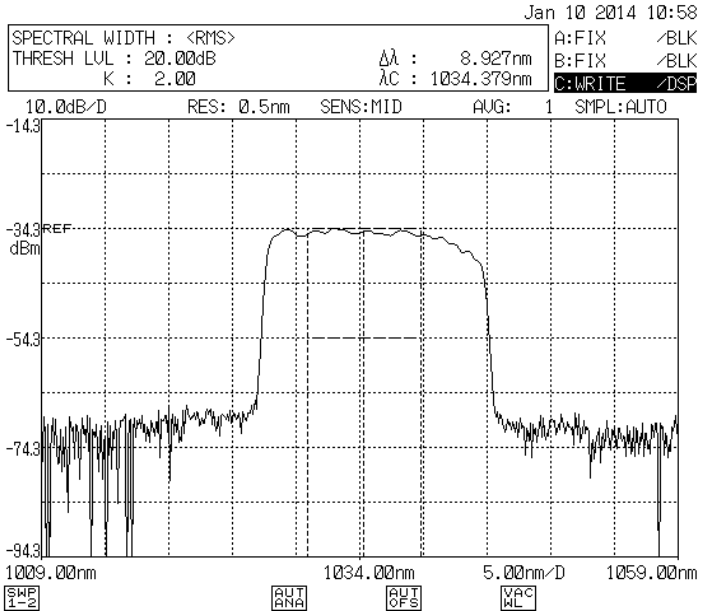

Fig. 2.9 Output spectum from the fiber oscillator.

Figure 2.10 shows the picture of our Yb-fiber oscillator. Compact and self-stating, this oscillator can be easily locked to the enhancement cavity. The only free-space segment is the SAM-PZT unit. It is worth to point out that if locking interface is unnecessary for other applications, we can even use a fiber-pigtailed SAM to eliminate the free space segment.

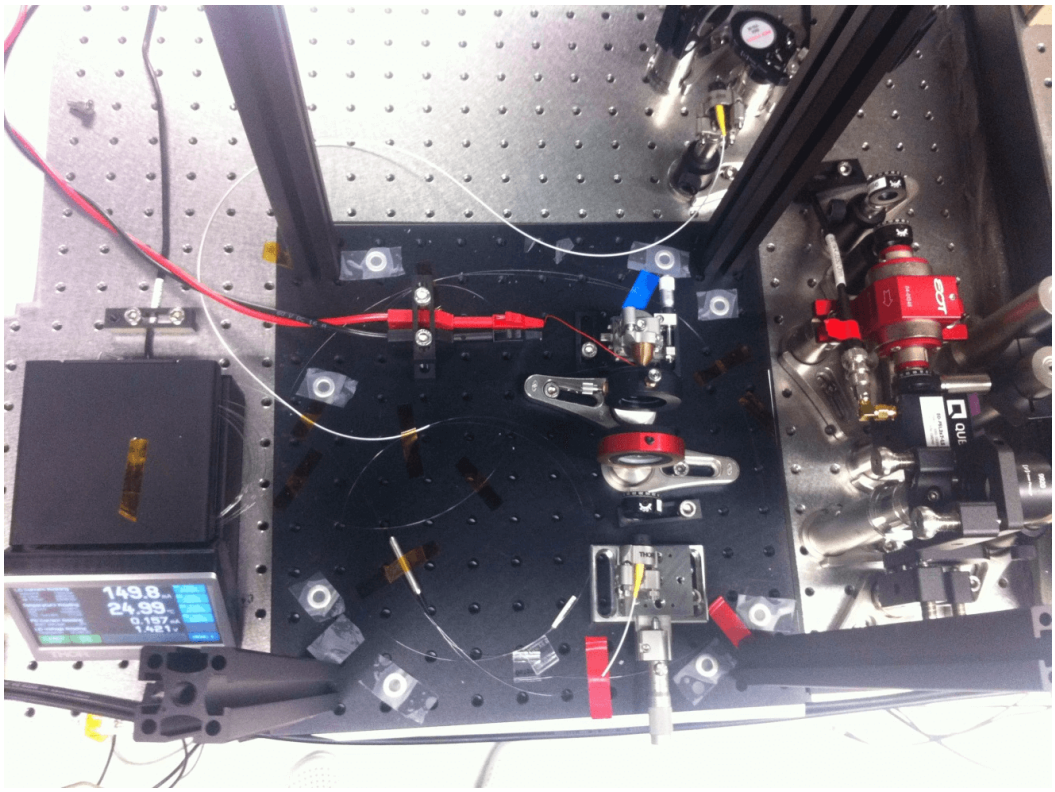

Fig. 2.10 Picture of fiber mode-locked oscillator.

2.3 Yb-fiber CPA system

Figure 2.11 illustrates the schematic of the Yb-fiber CPA system seeded by our monolithic Yb-fiber oscillator described in Sec. 2.2. The pulses generated by the oscillator were stretched to 370 ps in an all-fiber stretcher module with a double-pass configuration. Subsequently, the chirped pulses were first amplified in a single-clad Yb-fiber (6-μm core diameter) amplifier followed by a double-clad Yb-fiber (12-μm core diameter) amplifier, resulting in amplified pulses with 7.8-W average power. Then these amplified pulses were coupled into the main power amplifier constructed from 1.2-m Yb-doped large-pitch PCF (80- μm core diameter). The amplified pulses were compressed by a pair of diffraction gratings (1480 lines/mm groove density), generating $\sim$ 200-fs compressed pulses with > 100-W average power.

Figure 2.12 shows the assemble setup of the whole Yb-fiber MOPA system. Next I will discuss in detail about the key components in constructing the CPA system.

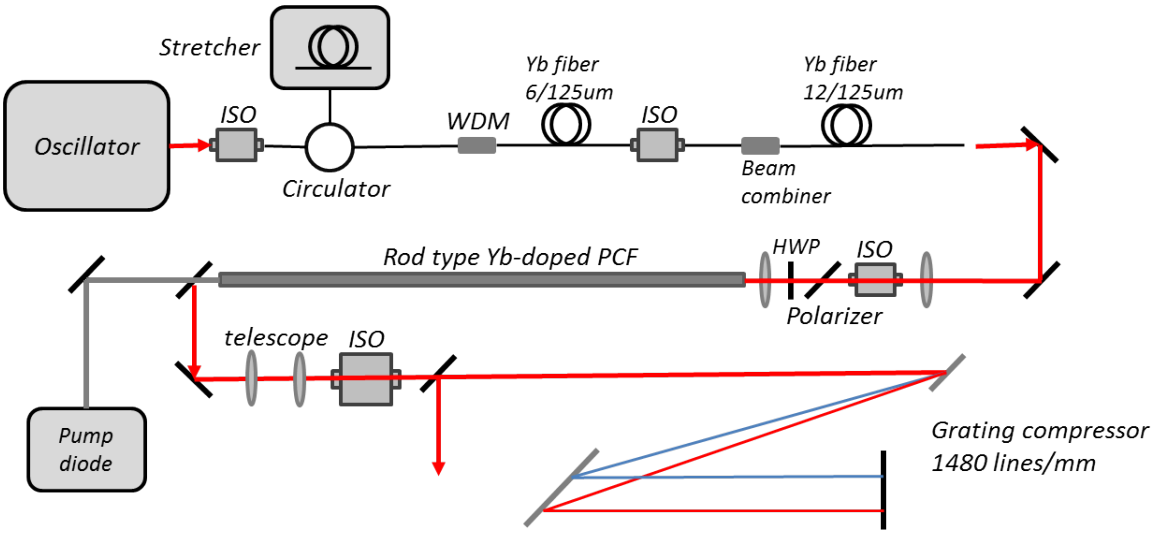

Fig. 2.11 Schematic of the experimental setup. ISO: optical isolator; WDM: wavelength division multiplexer; Yb fiber: yb-doped fiber; HWP: half-wave plate; PCF: photonics crystal fiber.

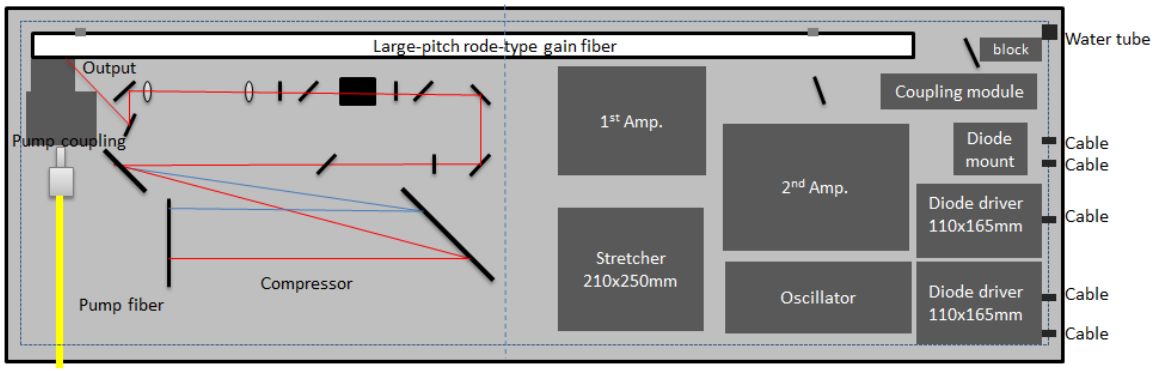

Fig. 2.12 System layout of the high power CPA system. All the optical setup and the electric drivers for seed and amplifiers are installed on a 60 cm x 120 cm optical table.

2.3.1 Stretcher and compressor

For final pulse compression, the diffraction-grating based compressor is configured at double-pass. To reduce the throughput loss, diffraction gratings of high diffraction efficiency are required. We chose the dielectric diffraction gratings from Fraunhofer IOF, which exhibit extremely high diffraction efficiency of > 99% over 20 nm bandwidth at 1040 nm as shown in Fig. 2.13. These gratings are reflective gratings, with 1480 lines/mm groove density. The angle of incidence is designed at 45^0. The substrate material is fused silica, which can handle > 1 kW average power.

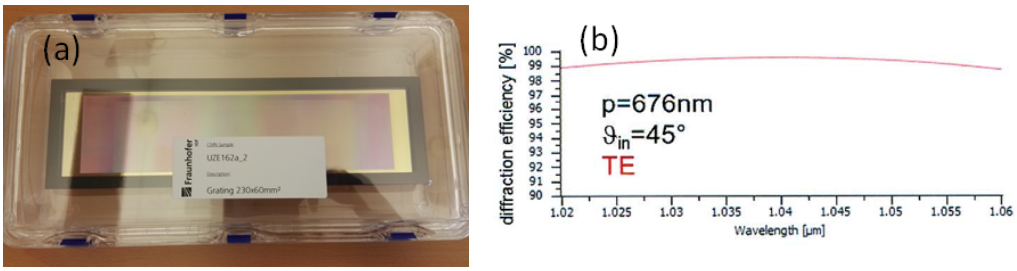

Fig. 2.13 (a) The picture of diffraction grating with dimension of $60\,mm \times 230\,mm$. (b) The diffraction efficiency of the customized-grating.

To make a compact and stable CPA system, the stretcher is of all-fiber format. Conventional SMFs provide positive GVD, which can be compensated by a pair of diffraction gratings that provide negative GVD. Unfortunately both conventional SMFs and diffraction gratings exhibit positive third-order dispersion (TOD). For a CPA system seeded by highly stretched pulses, the uncompensated TOD is huge and dramatically degrades the pulse compression quality. Luckily, a stretcher fiber with positive GVD and negative TOD ($\beta_3/\beta_2 = -7.7$ fs at 1030 nm) has been designed and manufactured. The detailed properties of the stretcher fiber are listed in Table 2.2. The fiber shows a good dispersion match to a compressor grating pair for the GVD, TOD, and even the fourth-order dispersion. Furthermore, this stretcher fiber can be low-loss spliced to conventional SMFs. Different length combination of the stretcher fiber and a conventional SMF allows us to design a fiber stretcher module to match a grating-pair based compressor. Such an all-fiber stretcher also reduces loss, improves stability, and downsizes the CPA system.

Table 2.2 The properties of stretcher fiber at 1030 nm [73]

Parameter	Unit	Value
β_2	ps^2/km	111
β_3/β_2	fs	-7.7
Attenuation	dB/km	2.5
PMD	$\mathrm{ps} \cdot km^{-0.5}$	0.04
Mode-field area	μm^2	6.4
Cut off wavelength	nm	945
Slice loss to SM fiber	dB	0.2

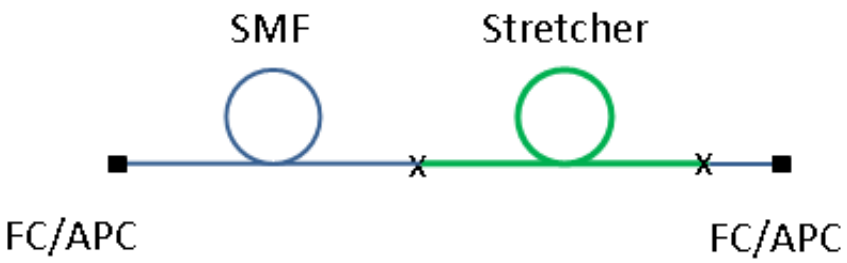

Fig. 2.14 Schematic of all-fiber stretcher.

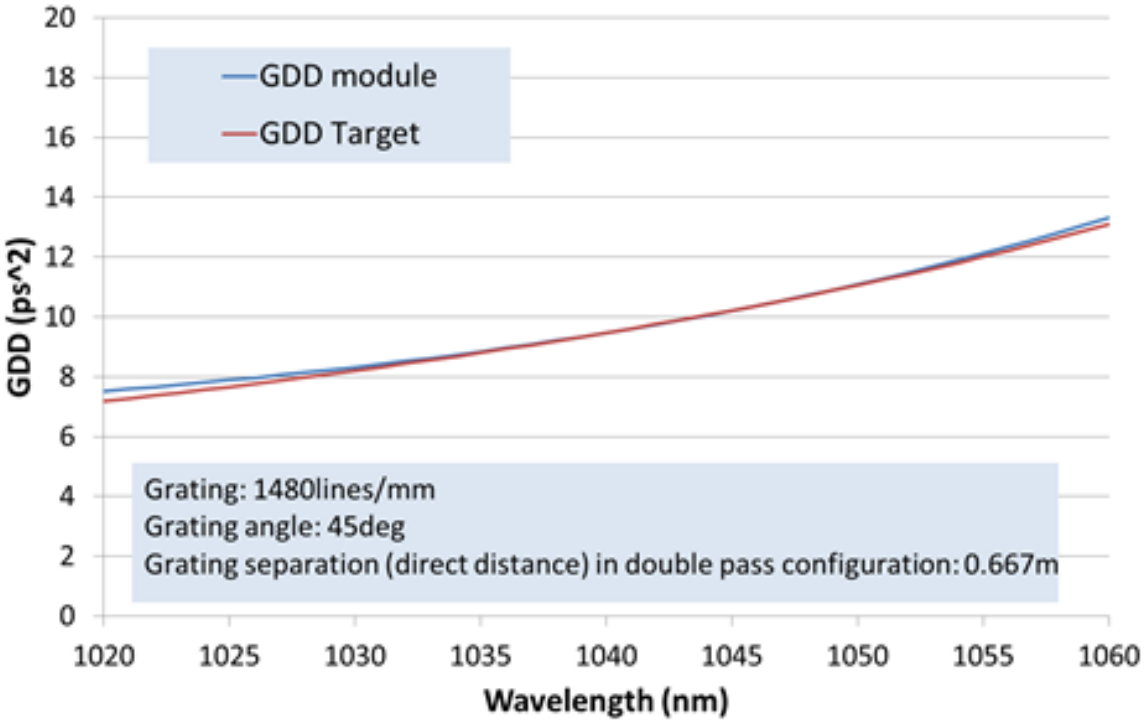

Fig. 2.15 The GDD matching between the stretcher fiber module and a grating-pair compressor made of two1480 lines/mm gratings separated by 66.7 cm.

Figure 2.15 demonstrates how the stretcher fiber can be used to compensate a grating-pair compressor made of two1480 lines/mm gratings separated by 66.7 cm. The optical beam is incident at 45 degree. A double-pass configuration of the stretcher module is applied to suppress the detrimental effect of intrinsic birefringence of the stretcher module. 65 m of stretcher fiber spliced together with 37 m conventional SMF (i.e., fiber HI-1060) can stretch the output pulse from our Yb-fiber oscillator to $\sim$ 370 ps. Figure 2.15 shows the GDD of our fiber stretcher module (blue curve) and the targeted ideal GDD (red curve) that can be exactly compensated by our grating-pair compressor including two diffraction gratings (1480 lines/mm groove density) separated by 66.7 cm. The two curves nearly overlap in the

wavelength range of 1030-1055 nm. Table 2.3 illustrates the detailed design parameters of the stretcher module in our CPA system.

Table 2.3 the detailed design parameters of the stretcher module in our CPA system.

Stretcher fiber length	65 m	±10%
SMF length	37 m	±10%
Group delay dispersion @1040nm	9.468 ps^2	±1%
Third order dispersion @ 1040nm	-0.08097 ps^3	±5%
Mode field diameter of stretcher @ 1040nm	2.9 μm	
Cutoff wavelength of stretcher	945 nm	±40
Insertion loss	<2.5dB	
Proof test level of fiber	100/1.0 kpsi/%	
Connector	FC/APC	
Polarization property	Non-polarization maintaining	

2.3.2 Large-pitch rod-type gain fiber

Large-pitch fibers (LPFs) are the first fiber designs exploiting the mode delocalization concept [74]. They employ a photonic structure consisting of few hexagonally arranged air holes with large hole-to-hole distances (Fig. 2.16) to achieve the delocalization of higher-order modes. Because the design method is not based on resonant effects, the mode field area can be scaled up by increasing the hole-to-hole distance. Using this method, effectively single-mode LPFs with 130 μm core diameter are possible, which significantly improve the highest output average power and highest pulse energy from Yb-fiber amplifiers.

2.3.3 Technical concerns in the system design

Back reflection of laser pulses may break the mode-locking state of the oscillator, disturb the pulse amplification, and even cause serious damage to the laser system. To prevent back reflection, an optical isolator with high isolation is placed after the output of the main

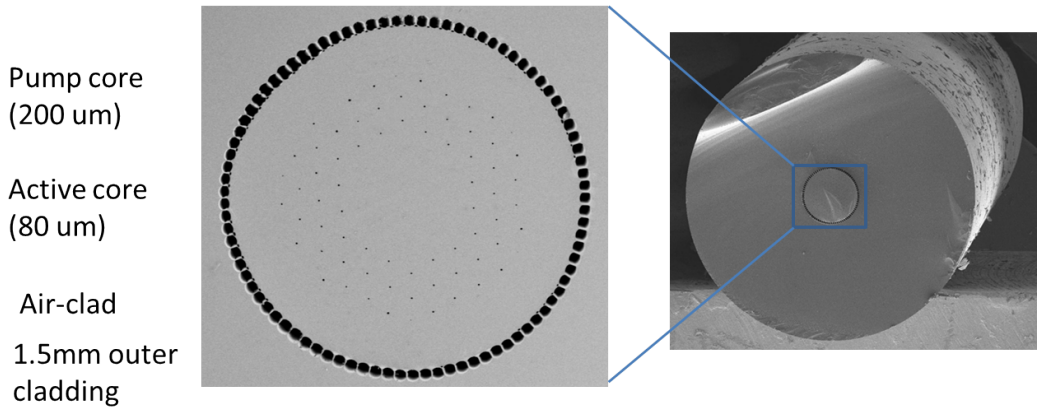

Fig. 2.16 The geometry of the large-pitch rode-type gain fiber [75].

amplifier. For the enhancement cavity application, protecting the laser system from the back reflection caused by the enhancement cavity is extremely important.

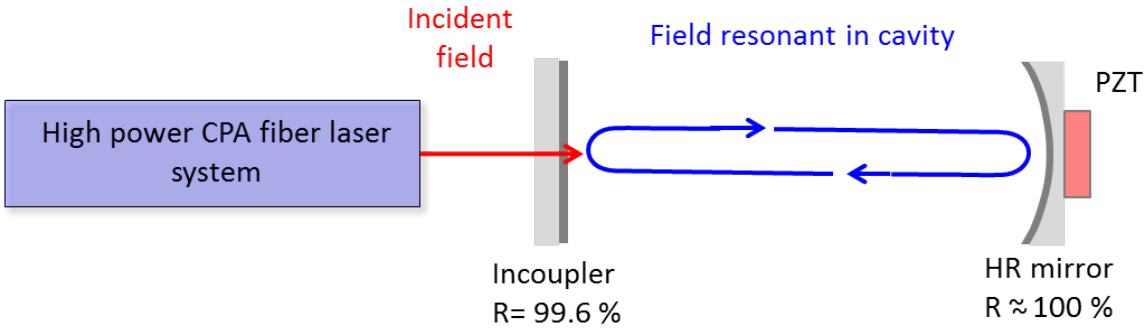

Fig. 2.17 Schematic setup of enhancement cavity.

Figure 2.17 shows the schematic of the enhancement cavity. The cavity consists of several high reflective mirrors with more than 99% reflectivity. That means if the cavity and the high power laser system are not locked, huge back reflection will happen. Thus an optical isolator with extremely high isolation is a must. But the isolation of nearly all the commercially available optical isolator is about 20-30 dB, corresponding to $\sim$ 1-W laser power back-reflected to our laser system when > 100-W power is reflected by the enhancement-cavity mirror.

Figure 2.18 is the schematic of a home-made optical isolator including two polarizing filters with extremely high extinction ratio and a Farady rotator. The polarizing filters (From Semrock) combine a highly efficient polarizer and a bandpass filter in a single optical component. These excellent linear polarizers have a contrast ratio exceeding 1,000,000 to 1. We expect that our home-made optical isolator can provide an isolation of > 60 dB.

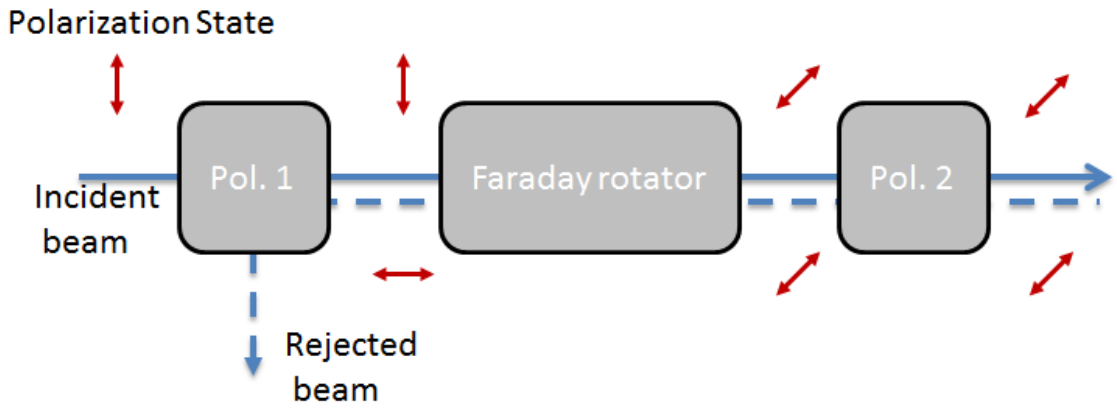

Fig. 2.18 The working principle of customized optical isolator with extremly high isolation [5].

2.4 Experimental results

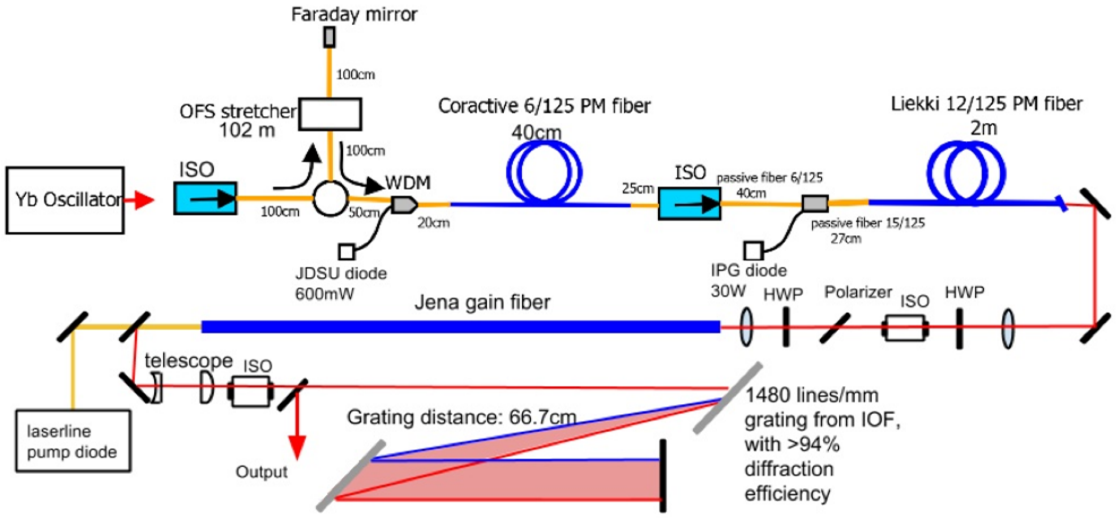

Fig. 2.19 Final version of our high-power Yb-fiber CPA system with detailed information about the optical components.

Figure 2.19 shows the final version of our high-power Yb-fiber CPA system with detailed information about the optical components. The system consists of a mode-locked Yb-fiber oscillator (described in Sec. 2.2), a fiber stretcher module (Sec. 2.3.1), two pre-amplifiers, one main amplifier based on large pitch Yb-doped PCF (Sec. 2.3.2), and a grating-based compressor (Sec. 2.3.1). The oscillator delivers slightly chirped 2-ps pulses at 75-MHz repetition rate with 50-mW average power at 1033-nm center wavelength. After propagating

through the double-pass configuration fiber stretcher, the pulses were stretched to $\sim$ 370 ps. Due to the transmission loss of the stretcher module, the average power is reduced to 3 mW.

The stretched pulses were amplified in two preamplifiers, which were constructed from a single-clad PM Yb-fiber and a double-clad PM Yb-fiber, respectively. The single-clad Yb-fiber is 40-cm long and commercially available from Coractive. The double-clad Yb-fiber is 1.2-m long with a core diameter of 12 μm pumped by a fiber-coupled multimode diode laser emitting at 976 nm. After these pre-amplifiers, the stretched pulses were amplified to 7 W average power with >30-dB suppression of amplified spontaneous emission.

The main amplifier, constructed from a 1.2-m air-cladding rod-type LPF, was pumped by a fiber-coupled, 500-W diode module emitting at 976 nm. By properly matching the input beam to the LPF fundamental mode, stable excitation of the fundamental mode was achieved. It is noteworthy that the mode matching was quite sensitive to the launching position of the seed. A slight position shift will excite more modes, indicating that the rod-type LPF supports a few transverse modes. Figure 2.20 shows the beam quality measurement and the near-field beam profile at the LPF output. The M^2 value of the output beam is $\sim$ 1.31.

In practice, we operated the preamplifiers to output 2-W for seeding the LPF-based main amplifier because reducing the seed power can mitigate excessive accumulation of nonlinear phase. With $\sim$ 85% coupling efficiency, we coupled about 1.7-W average power

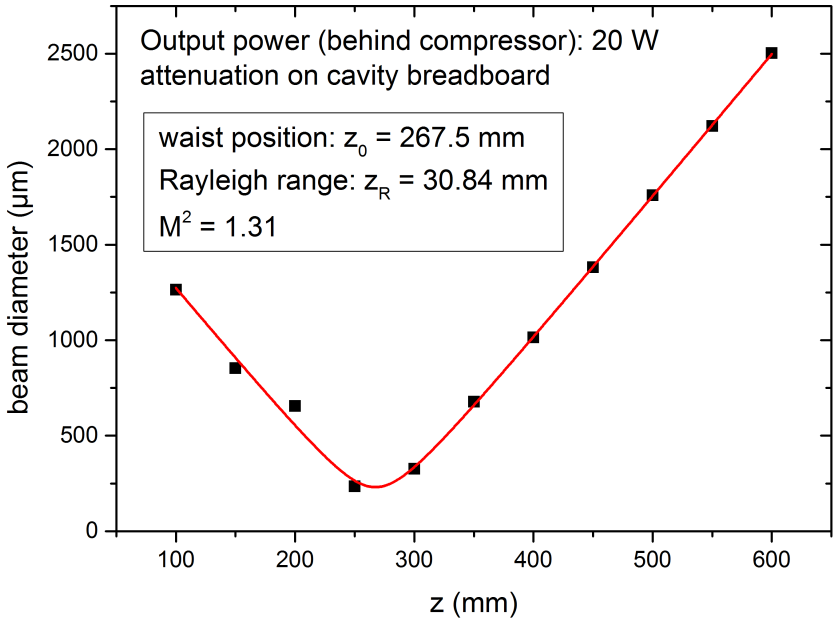

Fig. 2.20 Measured beam quality at 20 W compressed output power.

into the LPF amplifier and we obtain >100-W amplified power at the LPF output. For the initial optimization of the enhancement cavity, we tuned down the pump power into the LPF amplifier such that the system produced 20-W average power after the compressor. Figure 2.21 shows the output spectrum and the corresponding measured autocorrelation trace.

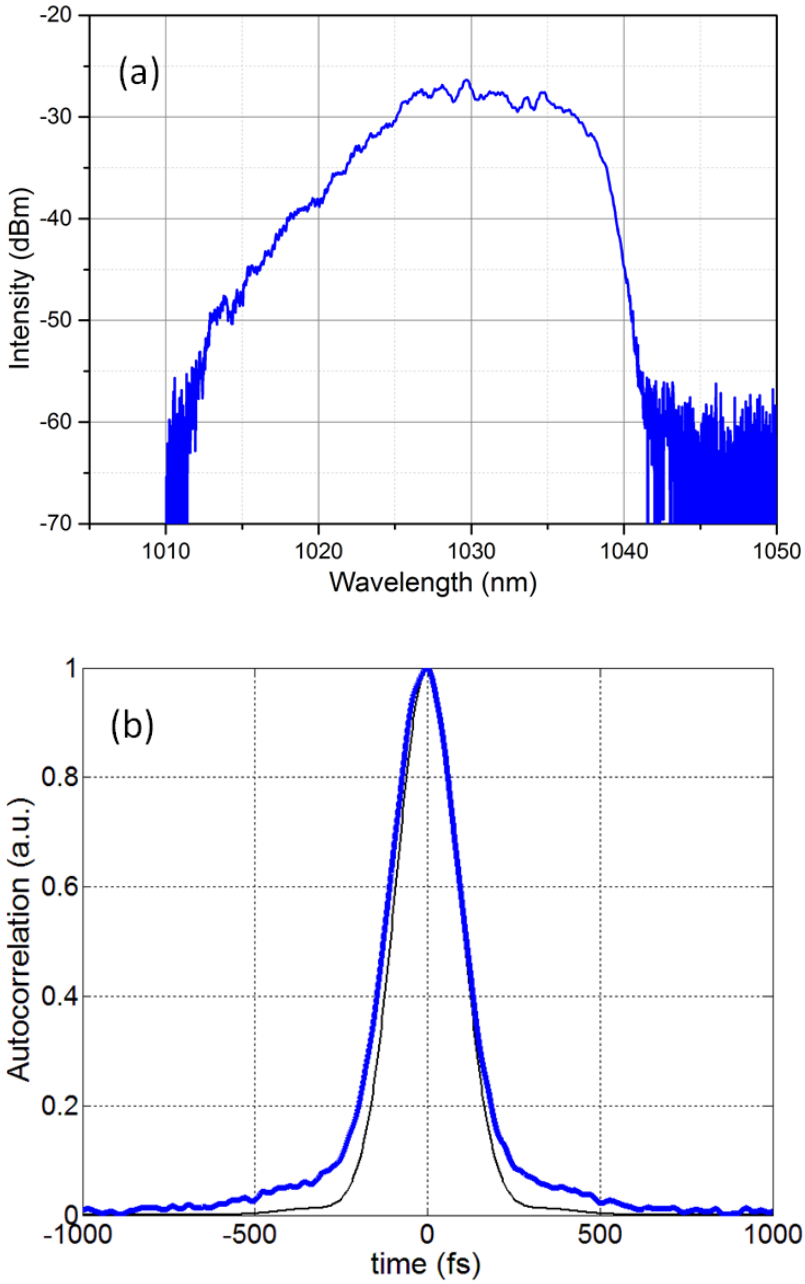

Fig. 2.21 (a) Output spectrum from the main amplifier. (b) Optimized compression autocorrelation trace.

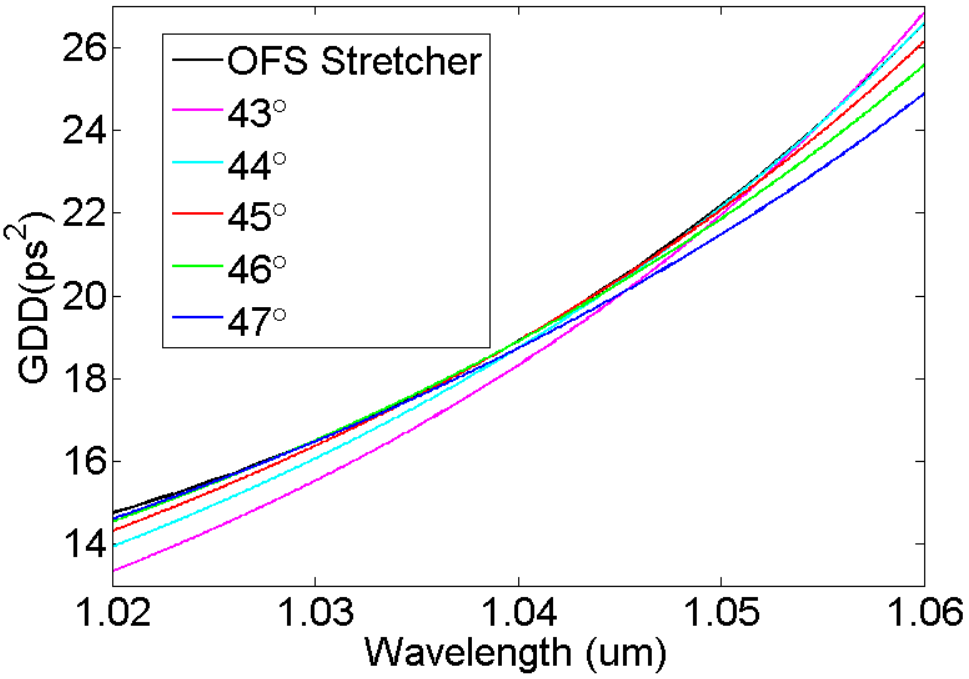

Fig. 2.22 Optimization of compression quality by adjusting the incident angle of grating compressor.

The output spectrum is centered at 1033 nm, the same as the oscillator. As discussed in Sec. 2.2, our stretcher and compressor were designed for GDD matching in the wavelength range of 1030-1055 nm. However the experimental spectrum has a large portion below 1030 nm, where the mismatch for higher-order dispersion exists between the stretcher and the compressor. As a result, the compressed pulse quality was compromised. To solve this issue, we fine tuned the stretcher GDD by changing stretcher fiber length. We also slightly tuned the beam incident angle onto the compressor grating to adjust the β_3/β_2 ratio. It can be shown that increasing the incidence angle will decrease the β_3/β_2 ratio. Figure 2.22 plots the GDD of the grating pair with different incident angles as well as the stretcher GDD. Clearly, increasing the incident angle by 1-2 degree shifts the matching central wavelength to shorter wavelength. With the incident angle set at 47 degree, gradually changing the grating separation allowed optimizing pulse compression. Figure 2.21 shows the optimized autocorrelation trace corresponding to 210 fs pulse duration, which is quite close to transform-limited duration. No significant pedestal appears indicating that the dispersion was managed and most of the pulse energy was concentrated in the main peak.

2.5 Conclusion of Chapter 2

To conclude, we have constructed from starch a high-power Yb-fiber MOPA system, consisting of a monolithic Yb-fiber oscillator, an all-fiber stretcher, a pre-amplifier chain, a LPF-based main amplifier, and a diffraction-grating based compressor. The whole system was installed on one optical breadboard with the dimension of $60 \times 120\,mm$, as depicted in Fig. 2.23. To further improve the system stability, the entire laser system is enclosed by aluminum walls.

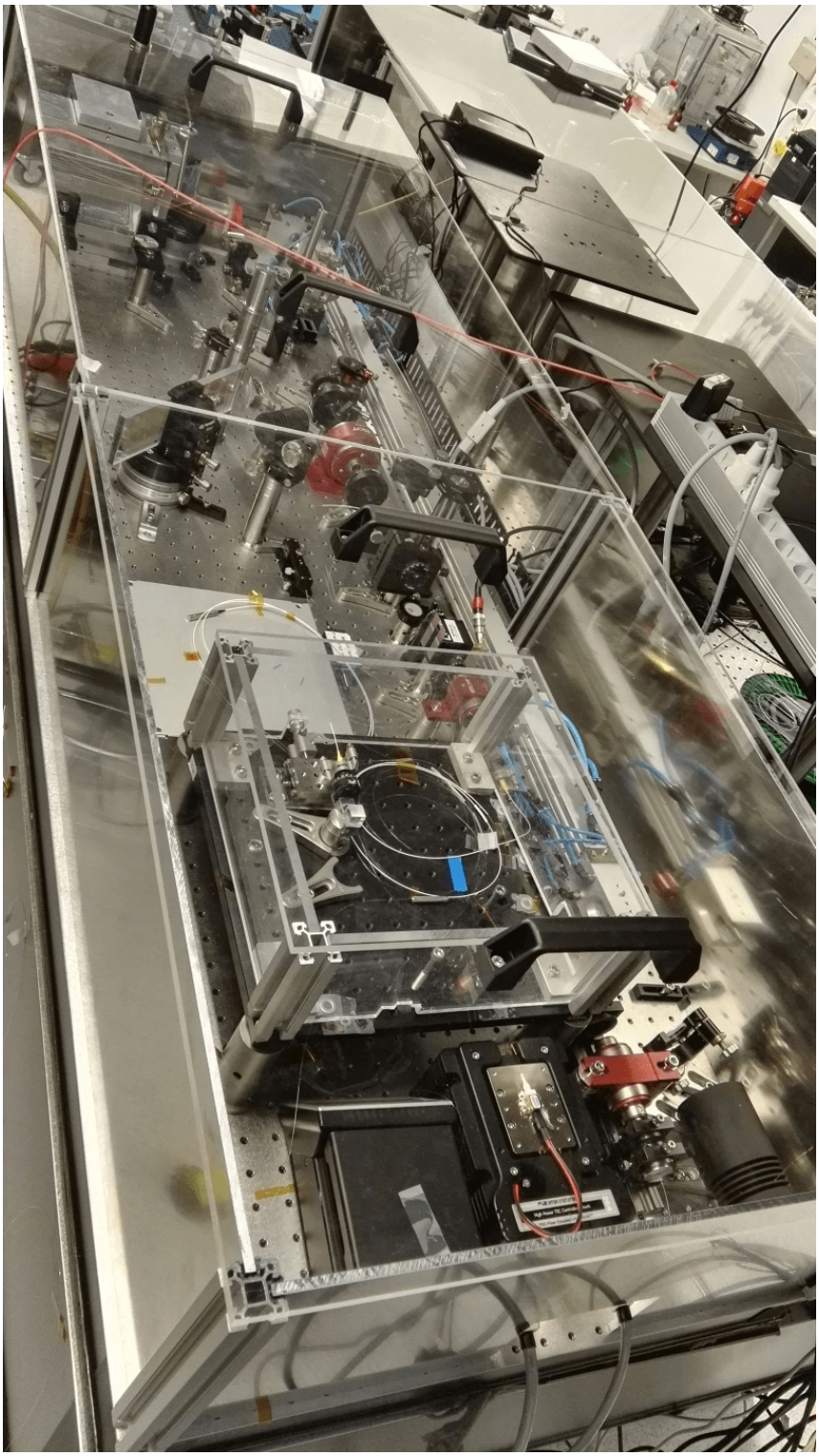

Fig. 2.23 Picture of CPA system,well enclosed by aluminum walls.

Chapter 3

Pre-chirp managed amplification

Yb-doped fiber-laser systems have become the most suitable driving source for cavity-enhanced HHG due to their superior average- power scalability and excellent beam quality [76–78]. The photon flux of such an EUV source can be increased by utilizing HHG inside a femtosecond enhancement cavity driven by a high repetition-rate (in the range of 50-150 MHz) ultrafast laser [59, 76, 77]. Recent experimental results reveal that shorter laser pulses ($\leq$ 60 fs) mitigate the ionization induced enhancement limitations, allow higher intra-cavity optical intensities, and therefore increase the photon energy and EUV yield [78]. Lately we have both theoretically and experimentally demonstrated that by fine-tuning the pulse chirp prior to nonlinear amplification, high quality compressed pulses are generated in this new amplification regime —- which we refer to as pre-chirp managed amplification (PCMA) [79]. Using Yb-doped LMA fibers as the gain medium, two other groups have demonstrated > 20 W pre-chirp managed fiber amplifiers, one producing 23.5 W, 37 fs pulses (pulse energy of 287 nJ) at 82 MHz repetition rate [80] and the other producing 25 W, 55 fs pulses (pulse energy of 320 nJ) at 78 MHz repetition rate [81].

3.1 Pre-chirp managed amplification: working principle

In this section, we analyze and demonstrate direct amplification in an Yb-doped rod-type LPF producing high-quality μJ pulses that are as short as $\sim$ 60 fs after final compression. Design strategies are presented for average power levels of > 100 W at 75 MHz repetition rate. The laser system results in both high quality and high energy output pulses, hitherto not reported for direct amplification in fibers. The high quality μJ pulses are obtained by two key enabling components: (i) the large mode area of large-pitch fibers leads to intrinsically low fiber nonlinearity resulting in energy scaling; (ii) additionally, introducing a small amount of GDD (typically between -0.05 and 0.05 ps^2) prior to direct amplification results

in high output pulse quality after final compression [82]. Figure 3.1 shows a schematic of the experimental setup comprising a fiber-laser front end, a pair of diffraction gratings for pre-chirp management, a rod-type Yb-doped fiber amplifier, and a compressor.

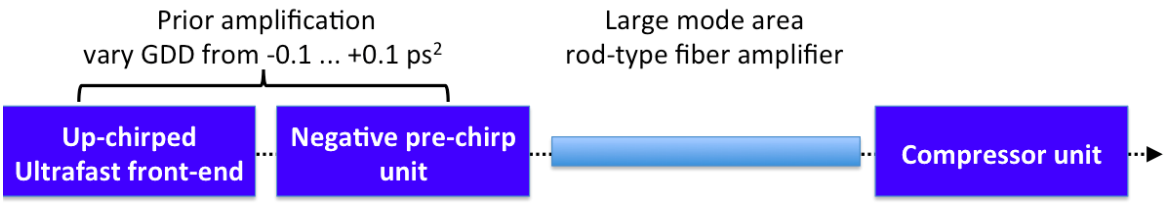

Fig. 3.1 Schematic of pre-chirp managed nonlinear amplification in fibers

The distinction of PCMA from CPA is illustrated in Fig. 3.2. In Fig. 3.2(a) pulse quality is plotted in terms of Strehl-ratio, i.e. peak-power of the compressed pulse to peak-power of the corresponding transform limited pulse, which is as a measure for residual spectral phase-shifts. Also, the pulse peak-power and the B-integral at the compressed output of the nonlinear laser system are shown in Fig. 3.2(b) and 3.2(c).

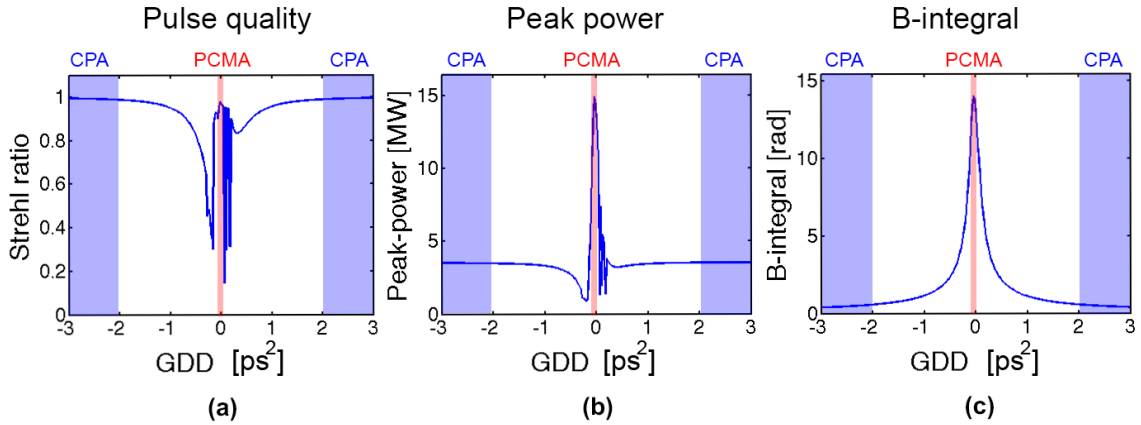

Fig. 3.2 Transition from CPA to PCMA to CPA: (a) compressed pulse quality in terms of Strehl-ratio (b) peak power of the compressed pulse and (c) accumulated nonlinear phase during amplification. The simulation assumes a transform limited 300-fs, 75-MHz input pulse train with center wavelength 1030 nm, an average power of 1 W, a YDFA small-signal peak gain of 3.8/m (corresponding to about 100 W at the fiber output).

The results in Fig. 3.2 show that for a small positive chirp there exists an optimum point at which high pulse-quality and peak-power is simultaneously possible. The CPA regime corresponds to large stretching or high GDD values, and a high pulse quality is obtained. A signature of the PCMA regime is massive spectral broadening. The larger bandwidth allows for shorter pulses as compared to the conventional CPA regime. In this case the pulse

reduction is about a factor of 8. The nonlinear nature of PCMA manifests itself in high B-integral values for the PCMA regime, another proof of the nonlinear nature of the method.

3.2 PCMA experimental results: pulse compression using diffraction gratings

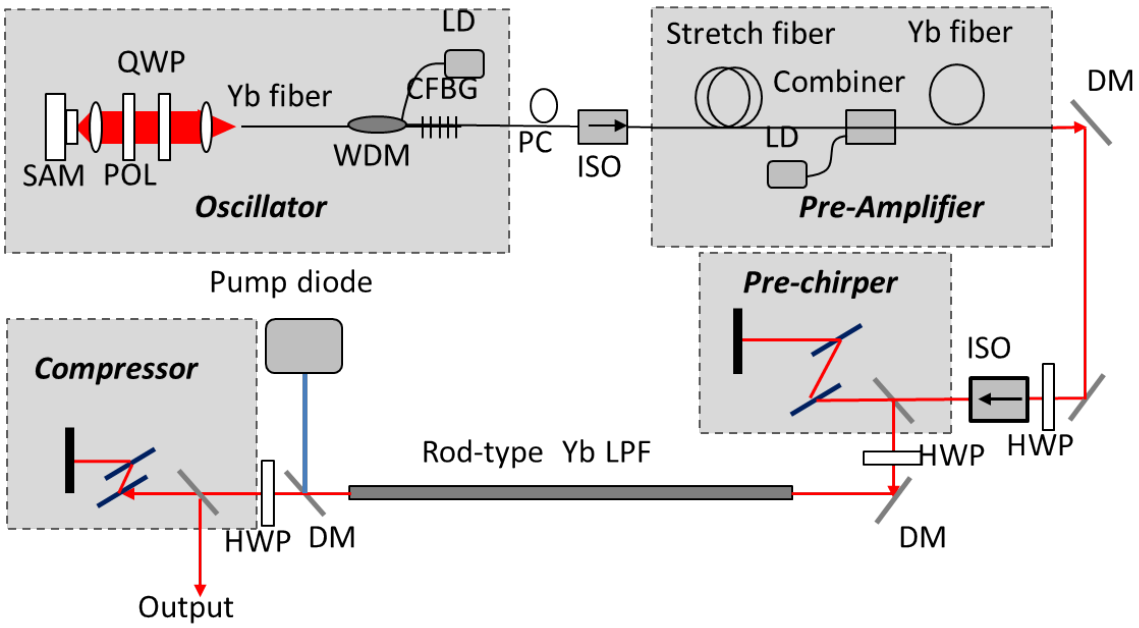

Fig. 3.3 Schematic of the pre-chirp managed amplification system. SAM: saturable absorber mirror, QWP: quarter wave plate, POL: polarizer,LD: laser diode, CFBG: chirped fiber Bragg grating, PC: polarization controller, ISO: isolator, DM: dichroic mirror, LPF: large pitch fiber

Figure 3.3 shows the schematic of the high power PCMA system. It consists of an Yb-doped fiber-laser front end, a pair of diffraction gratings for pre-chirp management, a rod-type Yb-doped fiber power amplifier, and a pulse compressor. The fiber-laser front end including a 75-MHz Yb-doped fiber oscillator (see Sec.2.2 in Chapter 2 for more detail) and an Yb-doped fiber amplifier produces positively chirped pulses with 1.75 W average power. A pair of diffraction gratings (1000 lines/mm) in a double pass configuration is employed to adjust the chirp prior to nonlinear amplification. In this way, we can vary the pre-chirp from positive to negative values. The front end can produce 300 fs pulses that are very close to the transform limit. The power amplifier is a 1.2-m Yb-doped rod-type LPF with a 90-μm diameter core and a 280-μm diameter air cladding for pumping [74]. The mode-field diameter is 80 μm and the pump absorption is 24 dB/ m. The LPF is pumped by a 976 nm

pump diode. The amplified pulses are compressed by another grating pair (1000 lines/mm) in a double pass configuration with a total efficiency of 77%.

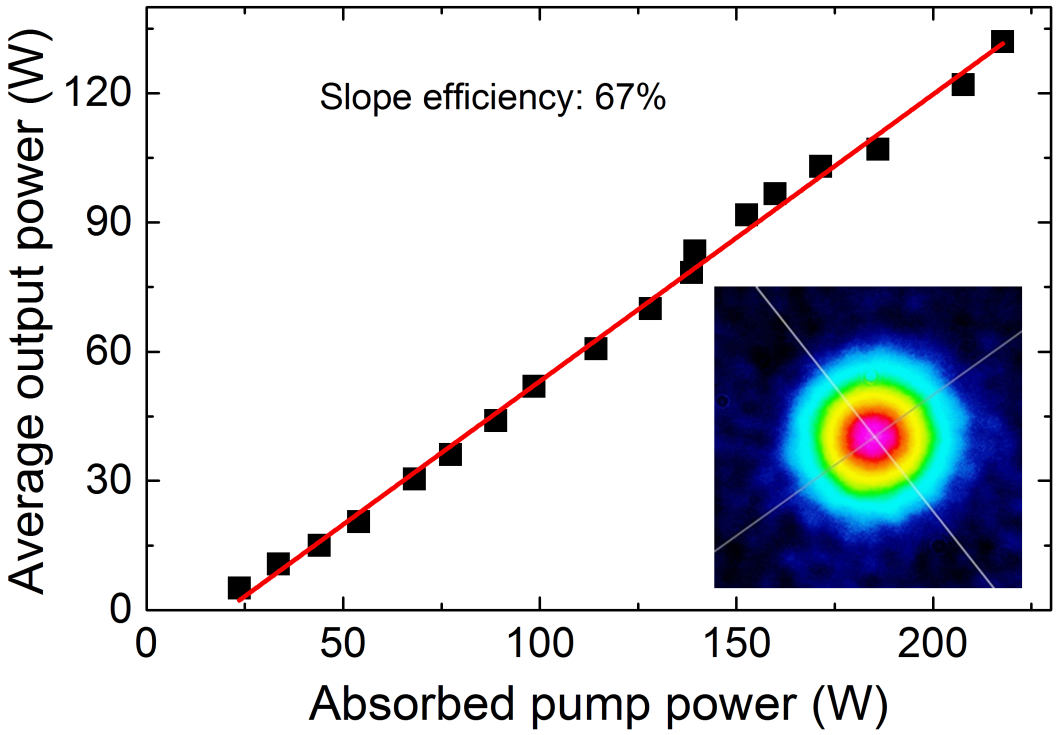

Fig. 3.4 Power amplifier output versus absorbed pump power. The inset shows the beam profile at 130 W output power (before compression)

Figure 3.4 plots the output power from the rod-type LPF amplifier versus the absorbed pump power. The seed power prior to the last amplification stage is around 1.5 W. Accounting the coupling loss to the LPF, the launched seed power is estimated to be $\sim$ 1 W. At 220-W pump power, 130-W amplified pulses are obtained. The slop efficiency is 67%, which is a reasonable number for Yb-doped fiber amplifier. The beam profile is excellent, as shown in the inset figure.

Figure 3.5 (a) shows the corresponding optical output spectrum (red curve). The significantly broadened spectrum of the amplified pulse is a characteristic of the nonlinear amplification of PCMA. Figure 3.5 (b) displays the autocorrelation trace of the amplified pulse prior to compression (blue curve) and after compression (red curve). At the system output, average power is 100 W. As shown in Fig. 3.5 (b), the compressed pulses are as short as 60 fs with high pulse quality. To optimize the compressed pulse quality in terms of residual wing structure, we adjust both the grating-pair separation prior to and after the fiber amplifier. An optimum GDD of the pre-chirp exists to achieve nearly transform-limited

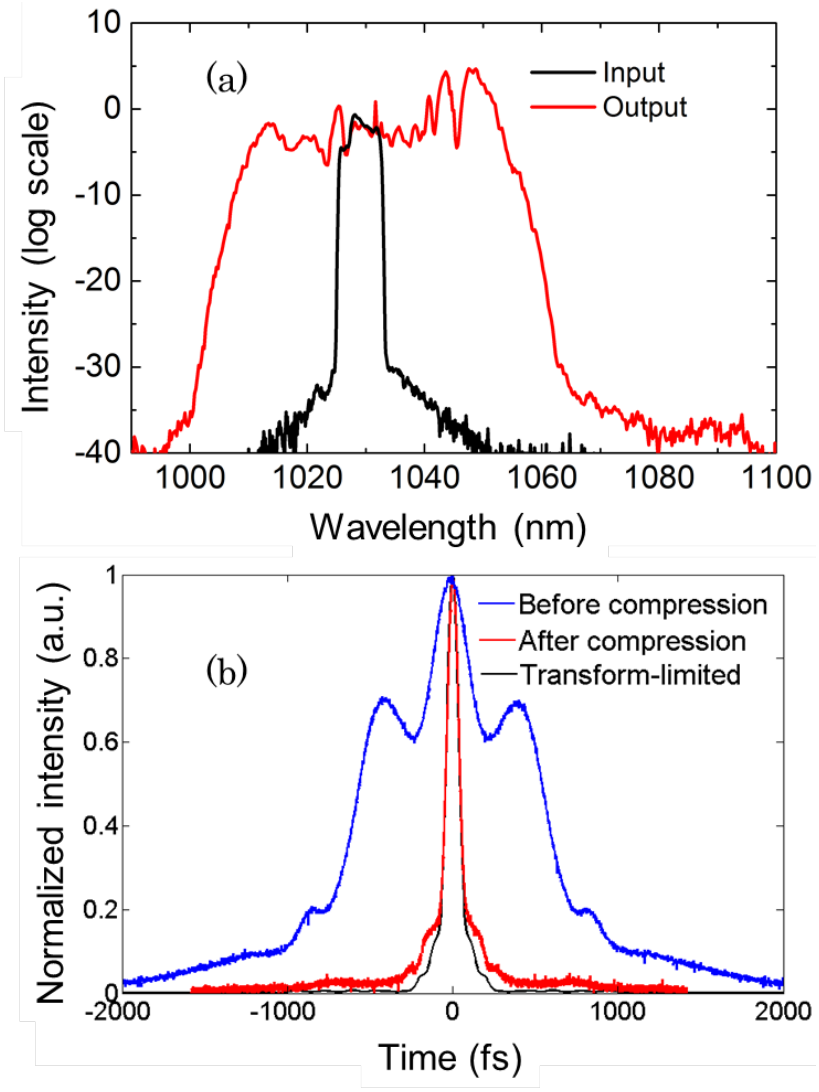

Fig. 3.5 (a) Optical spectra before (black curve) and after (red curve) the power amplifier operating at 130 W output power. (b) Autocorrelation traces of the 130 W amplified pulses (blue curve), the 100 W compressed pulses (red curve), and the corresponding transform-limited pulses (black curve).

compressed pulses with negligible pedestal. At 130 W output, the optimum pre-chirping GDD is around $26000 fs^2$ and the output pulses are de-chirped by the grating pair with only 2-3 mm separation distance. To evaluate the quality of the compression, the black curve in Fig. 3.5 (a) shows the autocorrelation trace of the corresponding transform-limited pulse that is calculated from the output spectrum, as shown in Fig. 3.5 (a).

As the concept is based on nonlinear amplification, the operation point of high-quality pulse compression depends on the power level of the amplifier. To illustrate how the pre-chirp

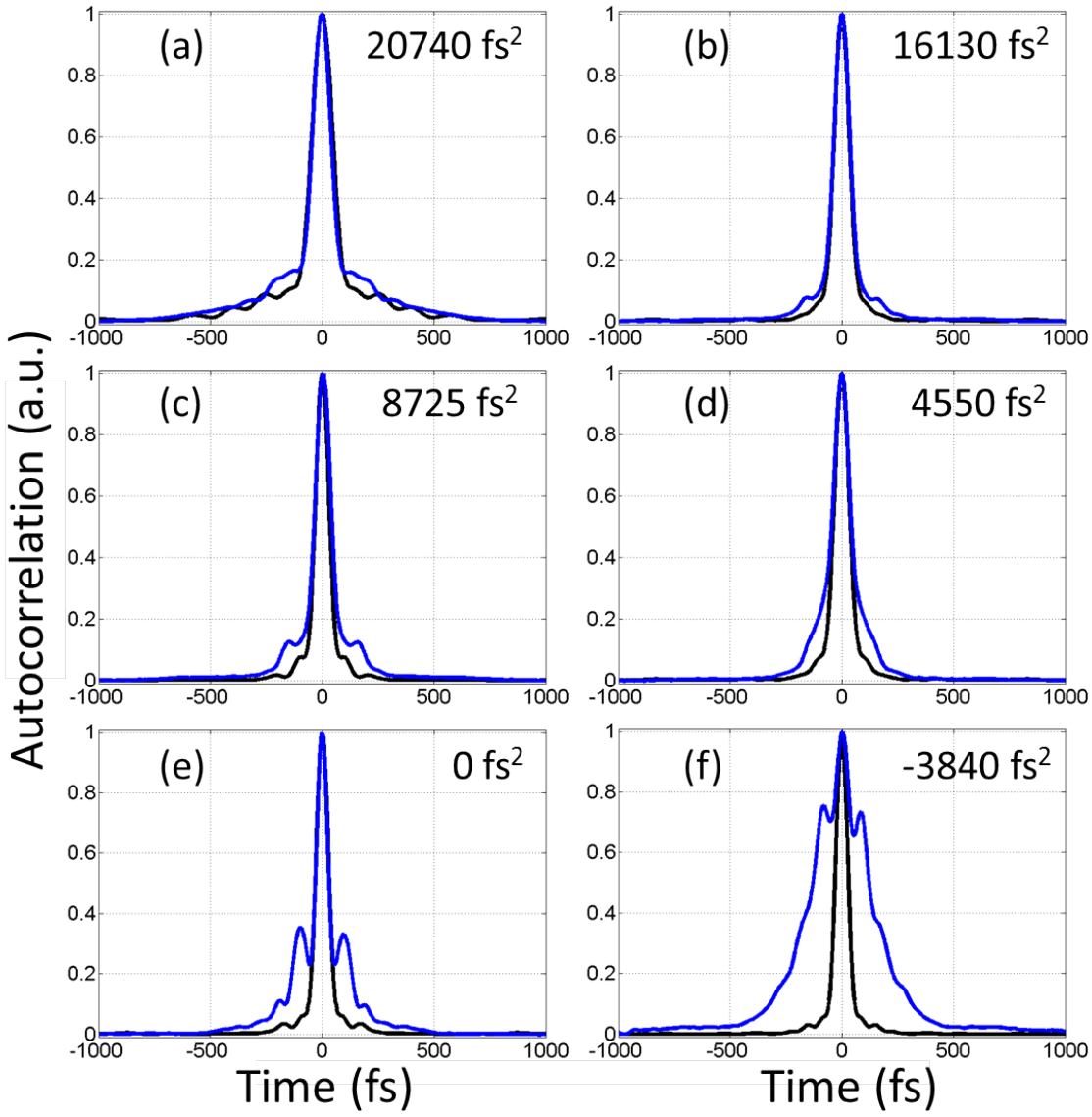

Fig. 3.6 Autocorrelation measurement (blue curves) of 75-W compressed pulses with different pre-chirp generating GDD: (a) $20740 fs^2$, (b) $16130 fs^2$, (c) $8725 fs^2$, (d) $4550 fs^2$, (e) $0 fs^2$, and (f) $-3840 fs^2$. Black curves denote the calculated autocorrelation traces of the corresponding transform-limited pulses.

affects pulse amplification and compression, for the example, we fix the compressed pulses at an average power of 75 W and vary the pre-chirp by different amount of GDD prior to amplification. Figure 3.6 shows the autocorrelation measurements (blue curves) of the 75-W compressed pulses for different pre-chirp generating GDD. Comparing them with the calculated autocorrelation traces of the corresponding transform-limit pulses clearly indicates that an optimum pre-chirping GDD exists around $16130 fs^2$. At this GDD value nearly

transform-limited compressed pulses are obtained with negligible pedestal. The optimum pre-chirp generating GDD depends on the output power of the amplifier.

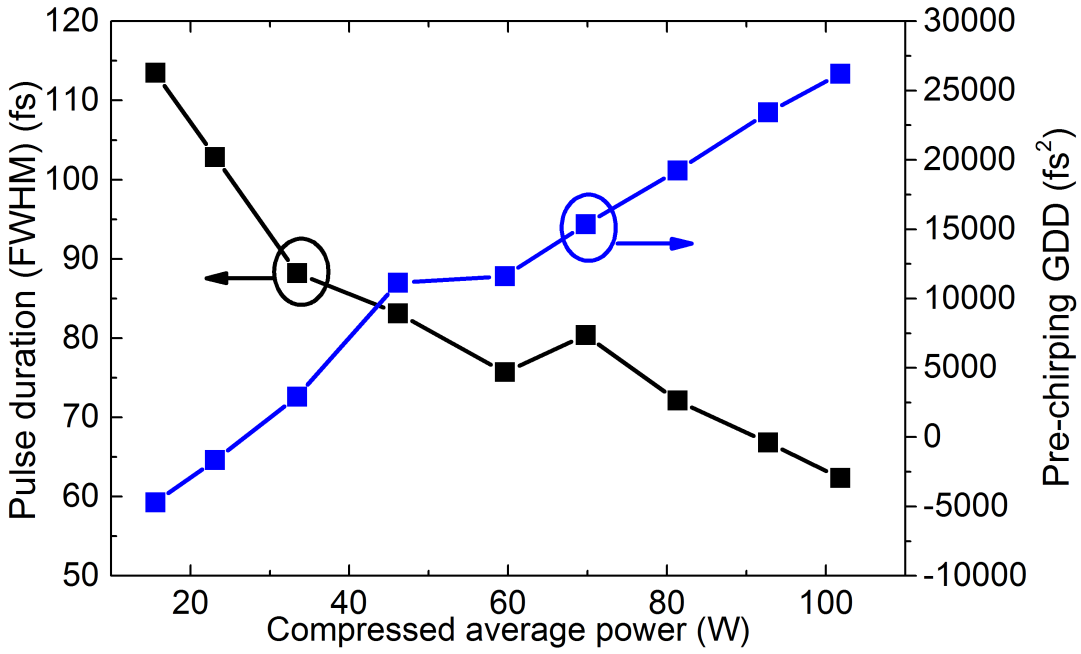

Fig. 3.7 Compressed pulse duration (black curve) and the optimum pre-chirping GDD (blue curve) versus the average power of the compressed pulses.

Figure 3.7 shows both the compressed pulse duration and the optimum pre-chirping GDD as a function of the compressed pulse average power. We find that with increasing output power the optimum pre-chirp GDD increases from negative to positive and the compressed pulses become shorter, reaching about 60 fs at around 100 W average power. These results suggest that negative (positive) pre-chirp is preferred at low (high) gain. It is noteworthy that this optimum pre-chirp depends on other parameters (e.g., input pulse duration and energy, fiber length etc.) as well. Reference [83] employed only negative pre- chirp for pulse amplification and compression of a high-power thin disk laser and achieved 55-W, 98-fs pulses at 10.6-MHz repetition rate; the system operated for around one hour before damage occurred [83]. Note that the purpose of introducing negative pre-chirp in Ref. [83] is to stretch the input pulse prior to amplification in order to avoid damage of the amplifier and self-focusing; the pre-chirp is not used for optimizing pulse amplification and compression.

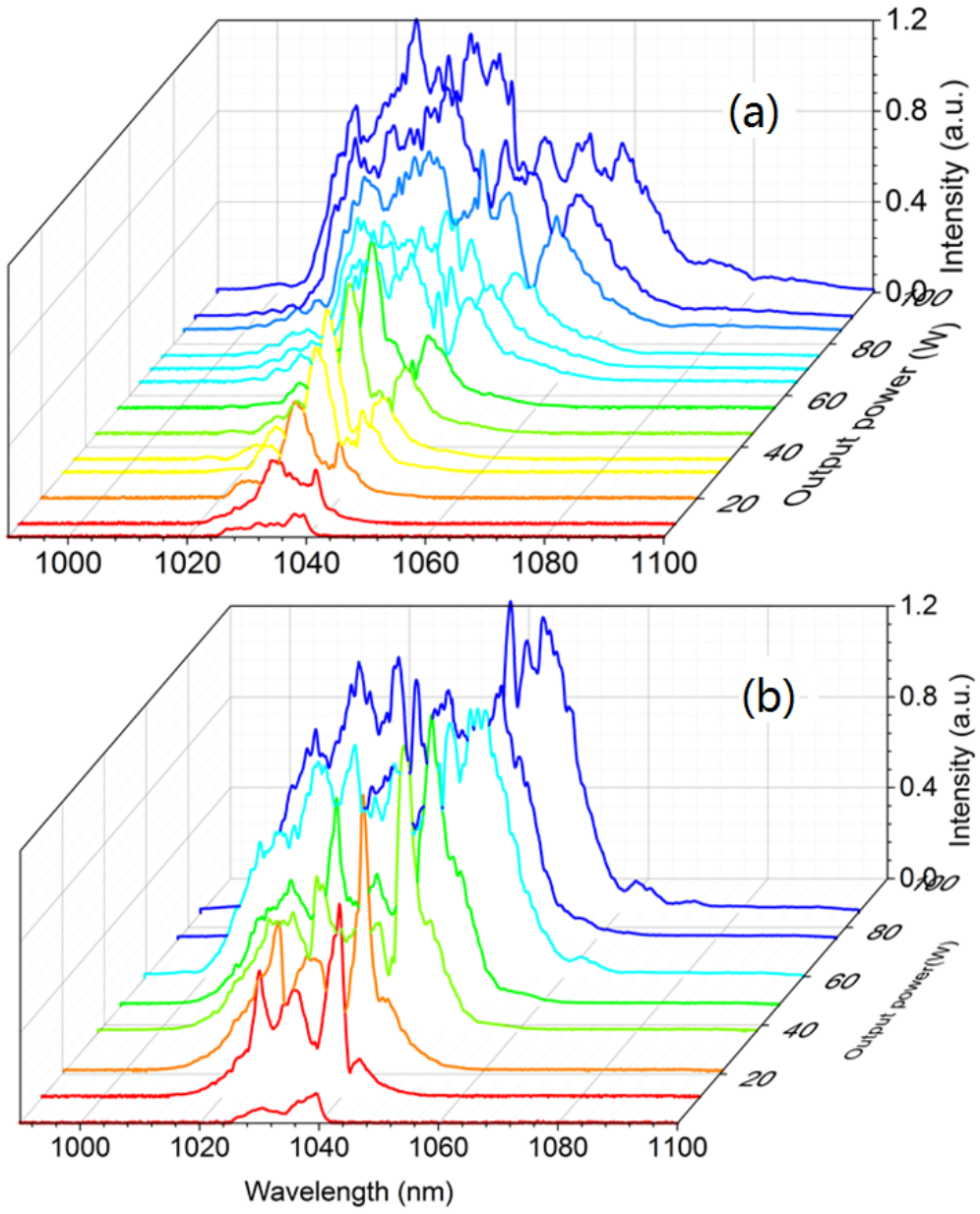

Fig. 3.8 The effect of pre-chirp on spectral evolution. (a) shows the spectral evolution versus increased power when the pre-chirping GDD was set at -11800 fs^2. (b) shows the spectral evolution versus increased power when the pre-chirping GDD was set at 22000 fs^2.

To show how the pre-chirping GDD affects the spectral evolution, we varied the pre-chirping GDD and then measured the output spectrum at different powers. Figure 3.8(a) shows the spectral evolution versus increased power when the pre-chirping GDD was set at -11800 fs^2. It can be seen that the spectrum became narrower at low powers (< 40 W) due to the spectral narrowing effect caused by a negative pre-chirp. For further increased powers,

the spectrum was broadened rapidly. As for a comparison, we changed the pre-chirping GDD to 22000 fs^2 and measured the spectrum at different powers; the results were plotted in Fig. 3.8(b). Clearly for a positive pre-chirping GDD, the spectrum narrowing phenomenon was absent and the spectrum was broadened dramatically as the power was increased from 10 W to 40 W. For the power increased from 40 W to 90 W, the spectrum continued to become broader albeit at a pace much slower than spectral broadening of the seeding pulses with negative pre-chirping GDD of -11800 fs^2.

To verify our experimental results and better understand the physics behind, we performed a detailed numerical modeling of our Yb-fiber CPA system by solving the generalized nonlinear Schrödinger equation. The pre-chirping GDD is varied between -1×10^5 fs^2 and 1×10^5 fs^2. We also vary the gain peak coefficient g_0 in the simulation, to analyze the output at different output powers (between approx. 20 and 140 W). For each of these values, the propagating through the fiber amplifier (1.2 m length, 80 μm mode-field diameter, and 25 fs^2/mm group-velocity dispersion) is calculated by the split-step Fourier method. In the simulation, we assume a gain bandwidth of 40 nm and a Gaussian input spectrum (with transform-limited pulse duration of 300 fs, center wavelength of 1030 nm, repetition rate of 75 MHz, and average input power of 1 W). The subsequent pulse compression is modeled such that maximum peak power is obtained. The simulated output pulse is analyzed in terms of the full-width at half maximum (FWHM) pulse duration and the Strehl ratio, as shown in Fig. 3.9(a) and (b), respectively. The Strehl ratio of an ultra-short pulse is the ratio of the peak power of the actual pulse to the peak power of its transform-limit. A Strehl ratio of 1 corresponds to absent residual spectral phase shifts and to the case of best pulse quality (for symmetric spectra). It can be seen that high quality pulses as short as 60 fs can be obtained for certain combinations of input chirp and power levels. The region of shortest pulse duration and highest pulse quality occurs at a narrow window of input chirps, as highlighted by the pink line in Fig. 3.9. In principle, two branches should exist for which short pulses are possible. However, as shown in Fig. 3.5, we find experimentally that only the branch of increasing GDD results in excellent pulse quality. This observation is supported by Fig. 3.9(b) showing overall better pulse quality for positive GDD. With increasing power, shortest pulses occur with increasing pre-chirp. Figure 3.9 also shows that a constant zero pre-chirp at the input would not produce high quality short pulses at high output power levels; this is in agreement with Ref. [83].

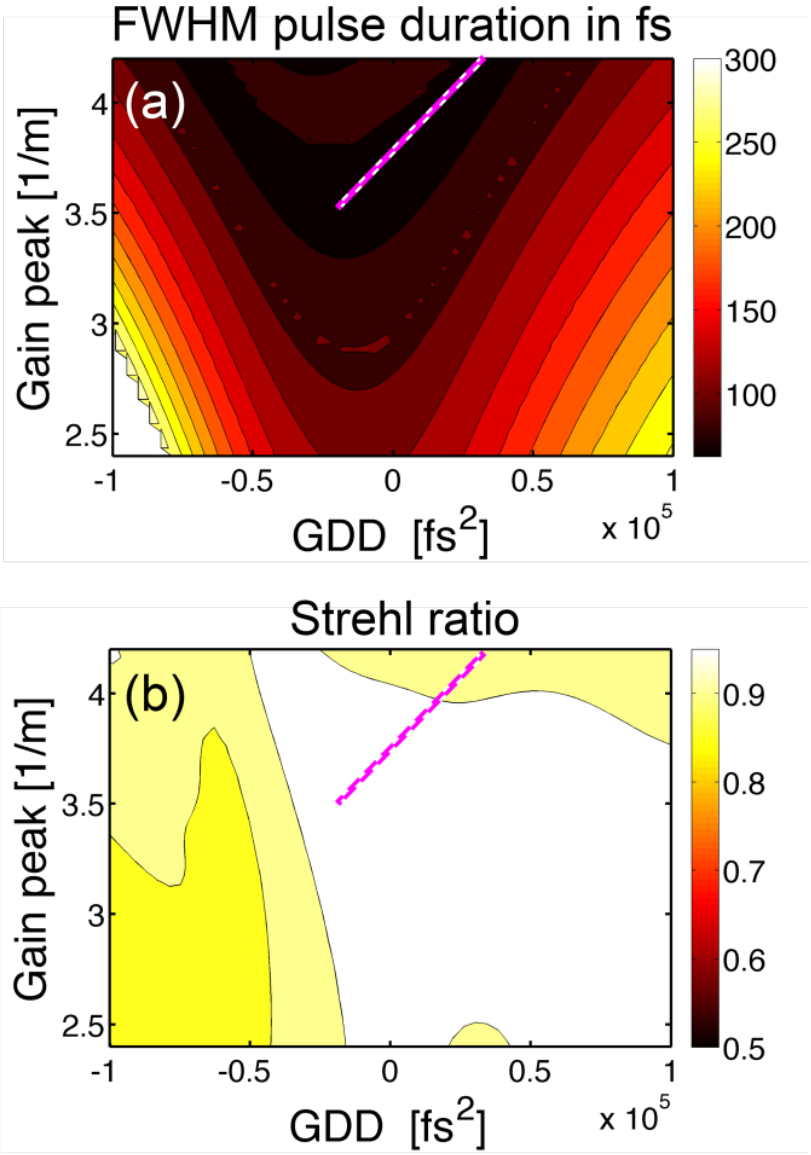

Fig. 3.9 (a) Numerical simulation of compressed pulse duration and (b) pulse quality in terms of Strehl ratio as a function of pre-chirping GDD and gain peak of an assumed Lorentzian spectral gain profile with bandwidth of 40 nm. The pink line in both figures highlights the region of interest for operation with 60 fs pulse duration.

3.3 PCMA experimental results: pulse compression using chirped mirrors

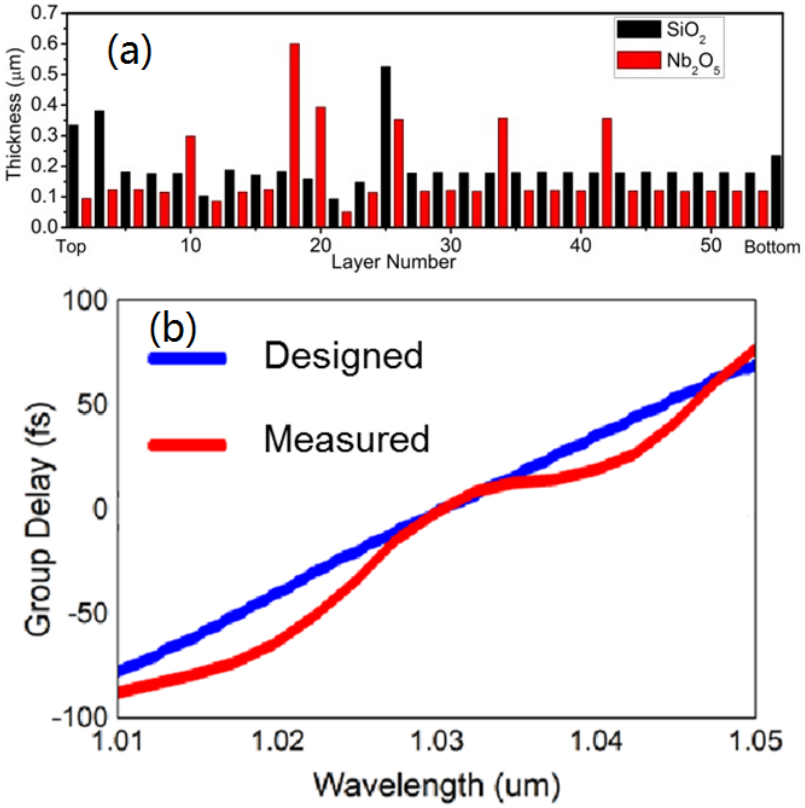

Fig. 3.10 (a) Designed structure of highly dispersive mirrors. (b) Designed (blue curve) and measured (red curve) group delay of the in-house designed highly dispersive mirrors.

Given the small chirp of the amplified pulses, highly dispersive mirrors (HDMs) can be applied instead of a grating pair for pulse compression. In addition to increasing the throughput efficiency and improving the beam-quality, the use of a HDM compressor simplifies the experimental setup. Figure 3.3.10 (a) shows the coating structure of such a in-house designed HDM, including 55 alternating layers of Nb_2O_5 and SiO_2. The dispersive behavior of this HDM is shown in Fig. 3.3.10 (b): each bounce provides a dispersion of $-2000fs^2$, four times larger than the dispersion from typical commercially available chirped mirrors.

To find the best-compressed pulse using HDMs, we adjust the bounces on the mirrors. Figure 3.11(a) illustrates the compressed pulse duration as a function of number of bounces at different output power levels. At 120 W, the pulse can be compressed down to $\sim$ 70 fs using 6 bounces on the HDMs. Figure 3.11(b) shows the autocorrelation traces before and after compression with the HDMs as well as the compression with the diffraction grating pair.

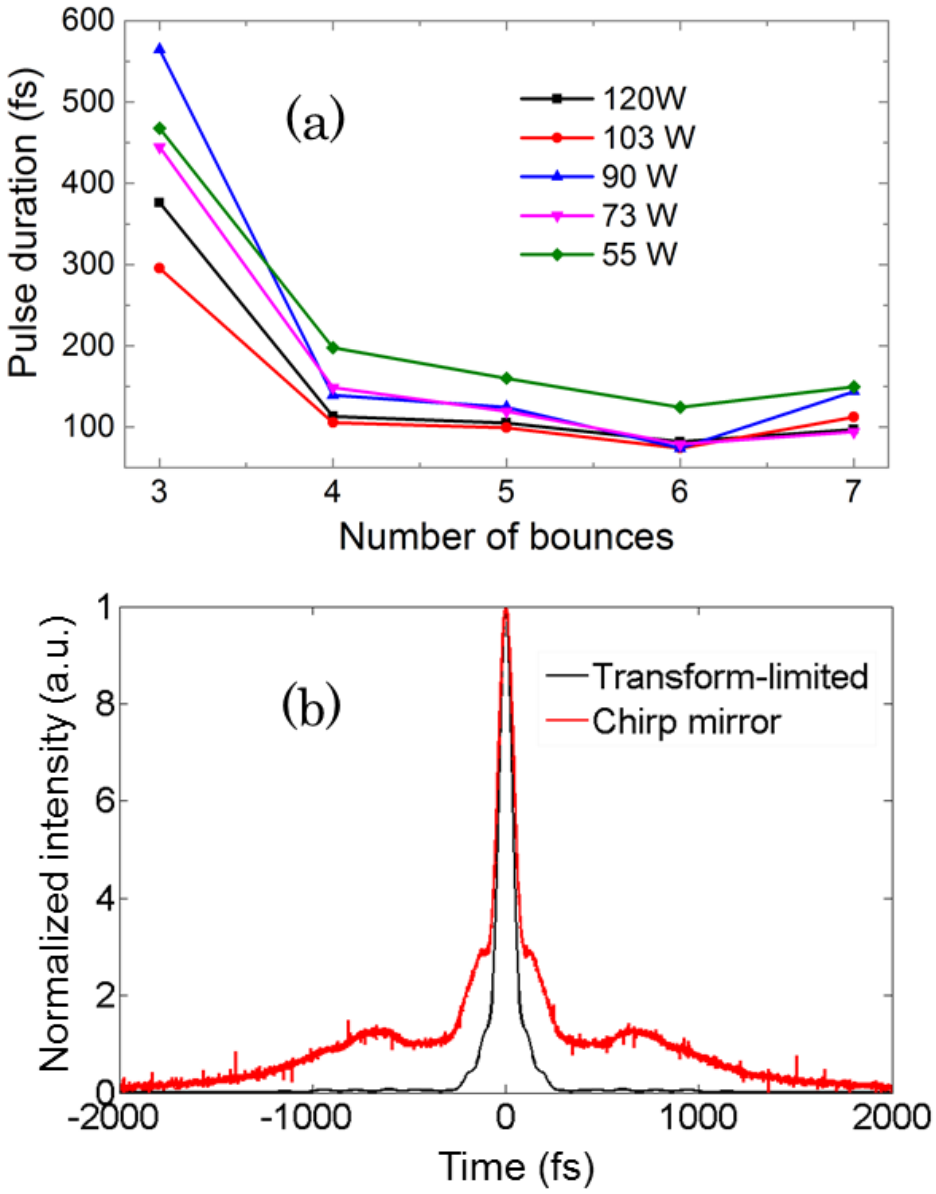

Fig. 3.11 (a) Compressed pulse duration by HDMs as a function of number of bounces for different output power: 120 W (black curve), 103 W (red curve), 90 W (blue curve), 73 W (pink curve), and 55 W (green curve). (b) Comparison of compressed pulse by HDMs and transform limited pulse.

Compared with the diffraction grating compressor, the pulse compressed with the HDMs (red curve in Fig. 3.11(b)) shows a wing structure mainly caused by uncompensated higher-order dispersion. An accurate characterization of the spectral phase for the amplified pulses allows precisely designing the dispersion of HDMs to improve pulse compression. Dispersion

compensating wedges can be employed as well to achieve continuous GDD compensation to remove the residual pedestals in the compressed pulses.

The pulse compressed with the HDMs (red curve in Fig. 3.11(b)) shows a wing structure mainly caused by uncompensated higher-order dispersion. An accurate characterization of the spectral phase for the amplified pulses allows precisely designing the dispersion of HDMs to improve pulse compression. Dispersion compensating wedges can be employed as well to achieve continuous GDD compensation to remove the residual pedestals in the compressed pulses.

3.4 PCMA experimental results: high-power second-harmonic generation

Recent investigations of the EUV power scaling show that shorter driving wavelengths yield higher conversion efficiencies. Pumping an enhancement cavity by 5-W, 155-fs pulses at 518 nm has demonstrated a significant improvement of HHG average power [84]. To show applicability of the PCMA system for shorter wavelength generation, we use a 0.5 mm long BBO crystal to perform a frequency doubling experiment.

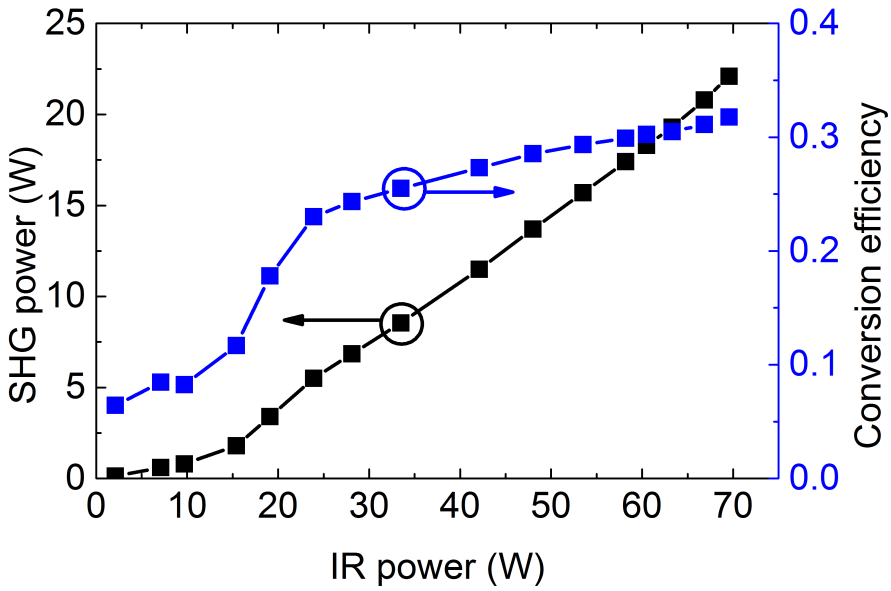

Fig. 3.12 Second harmonic generation (SHG) output power and conversion efficiency for different IR power at 60 fs pulse duration.

Figure 3.12 shows the second-harmonic generation (SHG) output power and conversion efficiency for different IR power at 60 fs pulse duration (compression with a grating pair). For IR power levels below 30 W, the conversion efficiency increases dramatically. At 71 W pump power the conversion efficiency reaches 32% and we obtain 21 W of SHG. To prevent BBO crystal damaging, we limit the maximum IR power at 71 W; at this power level, the conversion efficiency is far from saturation. The pulse duration of the SHG is estimated to be around 40-50 fs. Figure 3.13 shows a picture of the experimental setup achieving high power SHG.

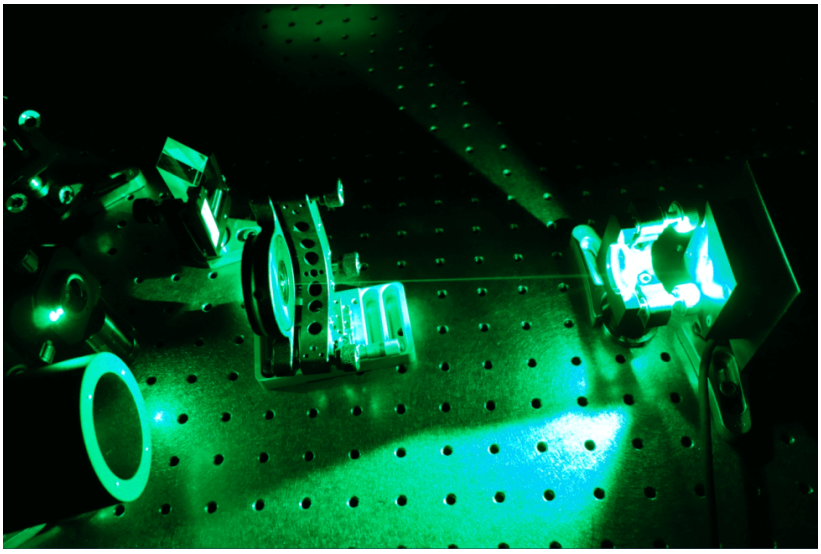

Fig. 3.13 Picture of high power SHG

3.5 Discussion and conclusion

3.5.1 Self-focusing limitation of PCMA

In PCMA, SPM due to Kerr nonlinearity is utilized to broaden the spectrum that can support shorter output pulses. However, the same Kerr nonlinearity may cause self-focusing that places limitations on the peak power for single pulse amplification. Arising from Kerr nonlinearity with positive $\chi^{(3)}$, the higher optical intensities on the beam axis, as compared with the wings of the spatial intensity distribution, cause an effectively increased refractive index for the central part of the beam. This modified refractive index distribution then acts like a focusing lens. Consequently an intense optical pulse propagating in a nonlinear medium can experience nonlinear self-focusing; that is, the beam diameter decreases compared with that of a weak pulse. When the pulse peak power exceeds a certain critical power, self-focusing

leads to a catastrophic collapse of the optical and results in high optical intensities, which can easily destroy the optical medium. Such a critical power is given by [85, 86]

$$P_{crit} = \frac{0.148\lambda^2}{n \cdot n_2}, \tag{3.1}$$

where n_2 is the nonlinear index coefficient, λ the vacuum wavelength, and n the linear refractive index.

Note that the critical power does NOT depend on the original beam size. For silica optical fibers, the critical power given by above equation is about 4 MW in the $1\mu m$ wavelength region. No method is known for increasing the self-focusing limit of optical fibers beyond that value. Self-focusing is the fundamental physical limitation of PCMA technique. At the output of our pre-chirp managed fiber amplifier, the amplified pulses are $\sim$ 1 ps in duration. At 130 W output power, the pulse energy is around 1.7 μJ, corresponding to a peak power close to 2 MW, half of the critical power. This implies that the self-focusing limited pulse energy is about 4 μJ for a PCMA system using pre-chirped pulse of $\sim$ 1 ps duration.

Such a self-focusing limitation can be alleviated by seeding PCMA with circularly (rather than linearly) polarized pulses because the nonlinear refraction coefficient for circularly polarized light is 2/3 of that for linearly polarized light. This fact has been used to reduce detrimental impact of Kerr-nonlinearity in a fiber CPA system [87]. Fiber PCMA-system with circularly polarized pulses will generate amplified pulses with 6 μJ pulse energy.

3.5.2 Energy scaling in combination of PCMA and divided pulse amplification

To further energy scaling beyond $\sim$ 6 μJ pulse energy level, PCMA can be combined with divided-pulse amplification [88–91]; that is, the pulse to be amplified is temporally split into multi-copies before the amplification and then recombined to one single pulse right after the amplifier. However this method is hard to be combined with CPA because the long stretched pulse in a CPA system requires a huge delay for the temporal splitting. Such a drawback is prevented in a PCMA system, in which the amplified pulses are $\sim$ 1 ps in duration; therefore, it becomes possible to incorporate divided pulse amplification in a PCMA system. If we divide the seed pulse into N replicas (e.g. 2, 4, 8, 16...), and each replica reaches its self-focusing limit during PCMA, the total pulse energy is N times the self-focusing limited pulse energy. The schematic of the divided-pulse amplification is shown in Fig. 3.14. The seed pulse is divided into two orthogonally-polarized replicas and some time-delay added

between them prevents their temporal overlap. With more replicas, the system could emit tens of μJ pulse energy, while the pulse duration is below 60 fs.

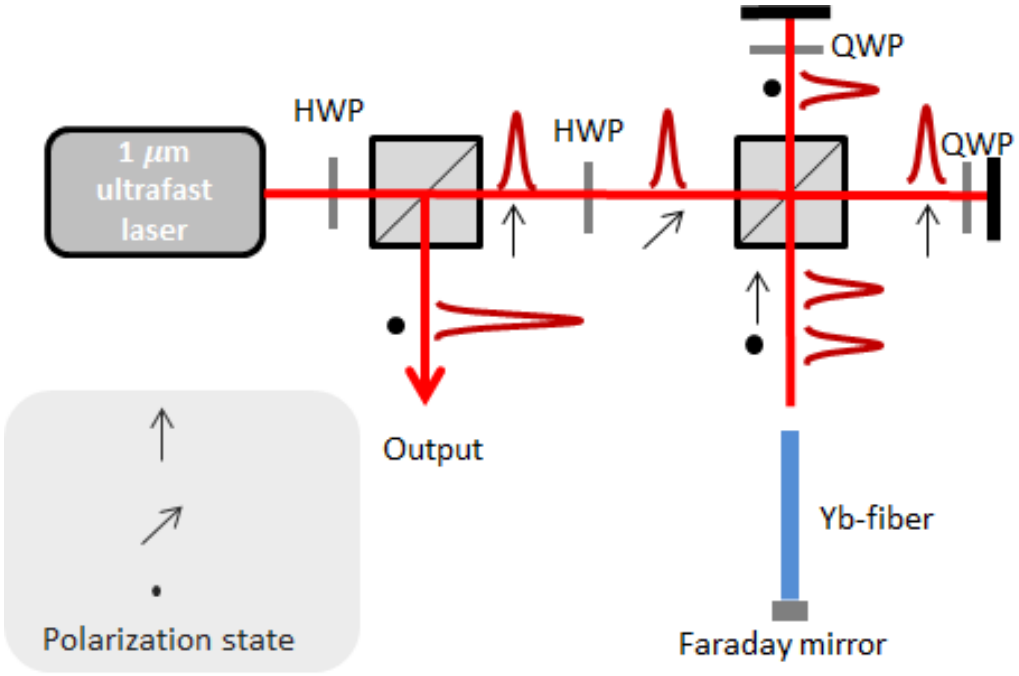

Fig. 3.14 Proposed technique of combing divided-pulse amplification and pre-chirp management for high energy pulses generation. HWP: half-wave plate; QWP: quarter-wave plate.

3.5.3 Comparison of CPA and PCMA

The advantages and disadvantages of both the CPA and PCMA techniques are summarized in Table 3.1. The objectivity of this summary is supported by the use of both techniques in the identical Yb-doped LPF amplifier.

For pulse energy at several μJ level, PCMA shows much better performance than CPA in terms of compactness, complexity, and cost. Especially the small amount of amplified-pulse chirp in a PCMA system makes the compressor much smaller; indeed, such a compact free-space compressor may be replaced by a hollow-core Kagome PCF. Figure 3.15 compares the large dimension and expensive grating pair required by the CPA system described in Chapter 2 and the much smaller and cheaper grating pair for the PCMA system demonstrated in this chapter.

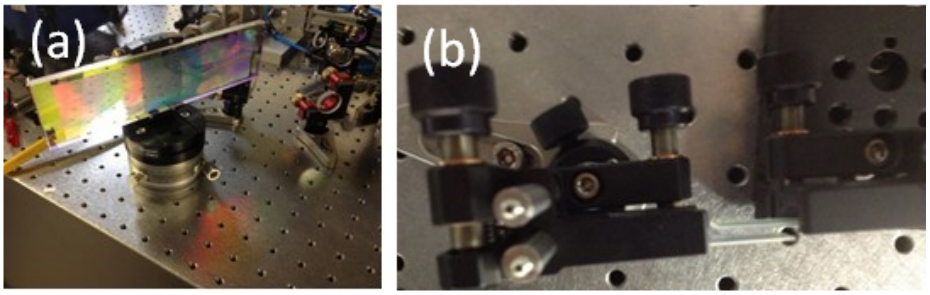

Fig. 3.15 (a) Large dimension and expensive grating pair required by the CPA system and (b) small dimension and cheap grating pair required by PCMA system.

Table 3.1 Comparison between CPA and PCMA

CPA	PCMA
- limited gain bandwidth	+ extended spectra bandwidth by nonlinearity
- pulse duration typically >200 fs	+ pulse duration < 60 fs
- stretching pulse duration up to 300 ps	+ pre-chirp to ~ 1 ps
- large high order dispersion	+ negligible high order dispersion
- large dimension compression grating pair	+ small dimension compression grating pair or chirp mirrors
- spatial chirp induced by misalignment of compressor	+ spatial chirp could be eliminated by chirp mirror compressor
- free space	+ all fiber configuration could be realized if replace the compressor with hollow-core fiber
- expensive	+ cheap
- complicated setup	+ compact
+ pulse energy could reach up to mJ	- several uJ pulse energy limited by self-focusing
+ linear amplification	- different output power requires the re-set of pre-chirp and compressor

3.5.4 Conclusion of chapter 3

We report on PCMA that is a distinct from the conventional CPA technique. By optimizing the input pulse chirp prior to nonlinear amplification, pedestal-free compressed pulses at various output power levels can be produced. PCMA allows for highly nonlinear amplifier operation producing high-quality pulses at the output until the self-focusing limit. LMA fibers enable μJ pulses as short as 60 fs at output powers >100 W. The PCMA approach is compact due to operation with moderate stretching and compression. The small amount of GDD required for the desired pre-chirp and final compression can be easily implemented with chirped mirrors. Further energy scaling can be achieved by combining PCMA with circular polarization amplification and divided-pulse amplification; $\sim$ 20-μJ amplified pulse energy is expected. Such a high repetition-rate PCMA system constitutes a simple and suitable laser source for several applications, in particular, driving extreme nonlinear optics in femtosecond enhancement cavities.

Chapter 4

SPM-enabled, wavelength-tunable ultrafast fiber laser sources: theory

4.1 Introduction

Implemented using various imaging contrast mechanisms, MPM enables optical sectioning and deeper penetration in biomedical imaging with submicron resolution [46]. For the last two decades, Ti:sapphire femtosecond lasers have been the typical MPM driving source largely because their center wavelength can be widely tuned in 700-1000 nm. Recent advances in MPM, however, reveal that shifting to longer (>1000 nm) driving wavelength causes less potential photo-damage and offers deeper penetration, which has spurred tremendous research efforts in developing Yb-fiber laser based MPM driving sources [92–99]. In contrast to bulky, expensive Ti:sapphire lasers—which are equipped in specialized laboratories, Yb-fiber lasers operate at about 1030 nm and can be constructed using all polarization-maintaining fibers without any free-space elements [100–102]. The resulting reliable, cost-effective, and compact Yb-fiber lasers will undoubtedly offer advantages for deploying MPM systems in rugged environments for in vivo imaging and clinical applications.

Due to limited gain bandwidth, ultrafast Yb-fiber lasers typically emit femtosecond pulses in 1020-1060 nm, a wavelength tuning range one order of magnitude less than that offered by Ti:sapphire lasers. Fortunately such a drawback can be overcome using nonlinear fiber-optic means to further expand the wavelength coverage. By imaging of human skin based on SHG, M. Balu et al. compared the performance of a Ti:sapphire laser operating at 800 nm and an Yb-fiber laser at 1060 nm. They found that use of the Yb-fiber laser improved the SHG imaging depth by 80% compared with the Ti:sapphire laser [96]. It is therefore expected that

shifting a MPM driving source towards longer (>1060 nm) wavelength will further improve the imaging penetration depth.

Continuously wavelength shifting output pulses from an ultrafast Yb-fiber laser can be readily achieved using soliton self-frequency shift (SSFS) inside an optical fiber—a phenomenon that originates from stimulated Raman scattering (SRS) [103]. SSFS requires negative GVD and can be realized in standard SMFs if the center wavelengths of input pulses are larger than 1300 nm—the typical zero dispersion wavelength for the fundamental mode [104]. In order to achieve SSFS for the excitation wavelengths below 1300 nm, PCFs are usually employed because their dispersion can be flexibly engineered [105–118]. When suitable PCFs are pumped by an Yb-fiber laser, SSFS can lead to a soliton pulse with the center wavelength shifted beyond 1300 nm, even reaching 1700 nm [111, 112, 116]. However, due to strong nonlinearity in these PCFs, the resulting wavelength-converted pulses are limited to <1 nJ in pulse energy; in the wavelength range of 1070-1200 nm, the pulse energies are typically less than 0.2 nJ, making these SSFS-based sources unsuitable for driving MPM systems. SSFS in higher-order mode fibers pumped by Yb-fiber lasers can result in >1 nJ pulse energies; however the generated soliton pulses are propagating in the higher-order mode. Mode converting them back to the fundamental mode—a necessary beam profile for most MPM systems—is challenging [117, 118].

In this chapter and next chapter we propose and demonstrate a new method of producing wavelength widely tunable femtosecond pulses for MPM. The method employs fiber-optic nonlinearities (dominated by SPM) to broaden an input optical spectrum, followed by optical bandpass filters to select the leftmost or rightmost spectral lobes. The filtered spectral lobes correspond to nearly transform-limited pulses with $\sim$100 fs pulse duration. In this chapter, we present a detailed numerical modeling of the method and discuss the effects of dispersion and nonlinearities.

4.2 Generalized nonlinear Schrödinger equation (GNLSE) for modeling fiber-optic spectral broadening

Nonlinear spectral broadening of ultrashort pulses in an optical fiber can be precisely modeled by the well-known GNLSE [104]:

$$\frac{\partial A}{\partial z}+\left(\sum_{n=2}\beta_n\frac{i^{n-1}}{n!}\frac{\partial^n}{\partial T^n}\right)A=i\gamma\left(1+\frac{i}{\omega_0}\frac{\partial}{\partial T}\right)\left(A(z,T)\int_{-\infty}^{+\infty}R(t')\left|A(z,T-t')\right|^2dt'\right) \tag{4.1}$$

where $A(z,t)$ denotes the pulse's amplitude envelope. β_n accounts for the n-th order fiber dispersion. Nonlinear parameter γ is defined as $\gamma=\omega_0 n_2/(cA_{eff})$, where ω_0 is the pulse center frequency, n_2 the nonlinear-index coefficient of fused silica with a typical value of $2.4\times10^{-20}m^2W^{-1}$, c the light speed in vacuum, and A_{eff} the mode-field area. A_{eff} is connected to mode-field diameter d by$A_{eff}=\pi(d/2)^2$. $R(t)$ describes both the instantaneous electronic and delayed molecular responses (i.e., SRS) of fused silica, and is defined as

$$R(t)=(1-f_R)\delta(t)+f_R(\tau_1^2+\tau_2^2)/(\tau_1\tau_2^2)\exp(-t/\tau_2)\sin(t/\tau_1) \tag{4.2}$$

where typical values of f_R, τ_1, and τ_2 are 0.18, 12.2 fs, and 32 fs, respectively [104]. Taking into account dispersion, SPM, self-steepening (SS), and SRS, Eq. 4.1 has been widely used to study nonlinear propagation of ultrashort optical pulses inside an optical fiber. Such a nonlinear propagation can significantly broaden the optical spectrum and, under certain conditions, lead to supercontinuum generation.

To gain physical insight, we first neglect dispersion and investigate the role of each nonlinear effect—namely SPM, SS, and SRS—in Section 4.1 and 4.2. In Section 4.3, we include dispersion in the simulation and show how dispersion affects the nonlinear spectral broadening.

4.3 Pure SPM

We first consider only SPM and neglect dispersion, self-steepening, and SRS. Consequently Eq. 4.1 is simplified as

$$\frac{\partial A}{\partial z}=i\gamma|A|^2A \tag{4.3}$$

Equation 4.3 has an analytical solution:

$$A(z,t)=A(0,t)\exp(i\gamma|A|^2z) \tag{4.4}$$

Using this solution, we simulate a 200-fs hyperbolic secant-squared pulse (central wavelength at 1.03 μm with 50-nJ pulse energy) propagating inside an optical fiber with a mode-field diameter of 6 μm; the simulation results are summarized in Fig. 4.1.

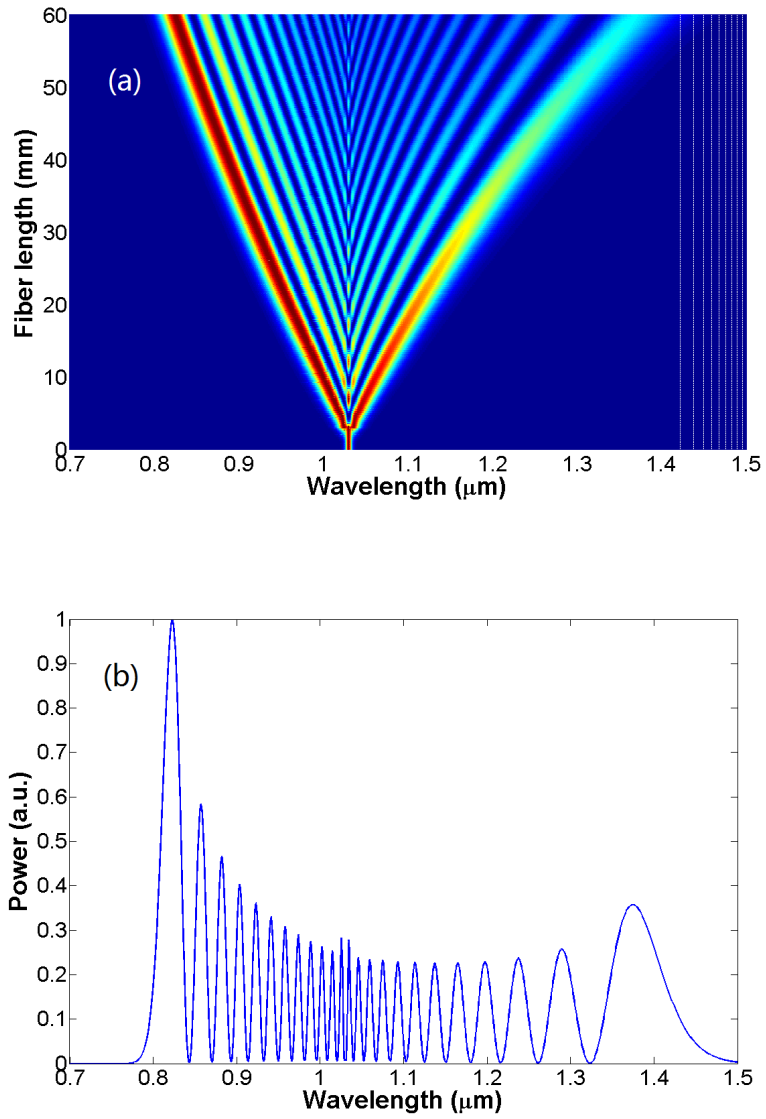

Fig. 4.1 Propagation of a 50-nJ, 200-fs pulse inside an optical fiber with a mode-field diameter of 6 μm. In the simulation, only SPM is considered. (a) Spectrum evolution versus fiber length. (b) Optical spectrum after propagating 6 cm in the fiber.

Figure 4.1(a) shows that the optical spectrum broadens dramatically along the fiber length and is composed of isolated spectral lobes; the number of these spectral lobes is linearly proportional to the fiber length—a unique feature of SPM-broadened spectrum. For example,

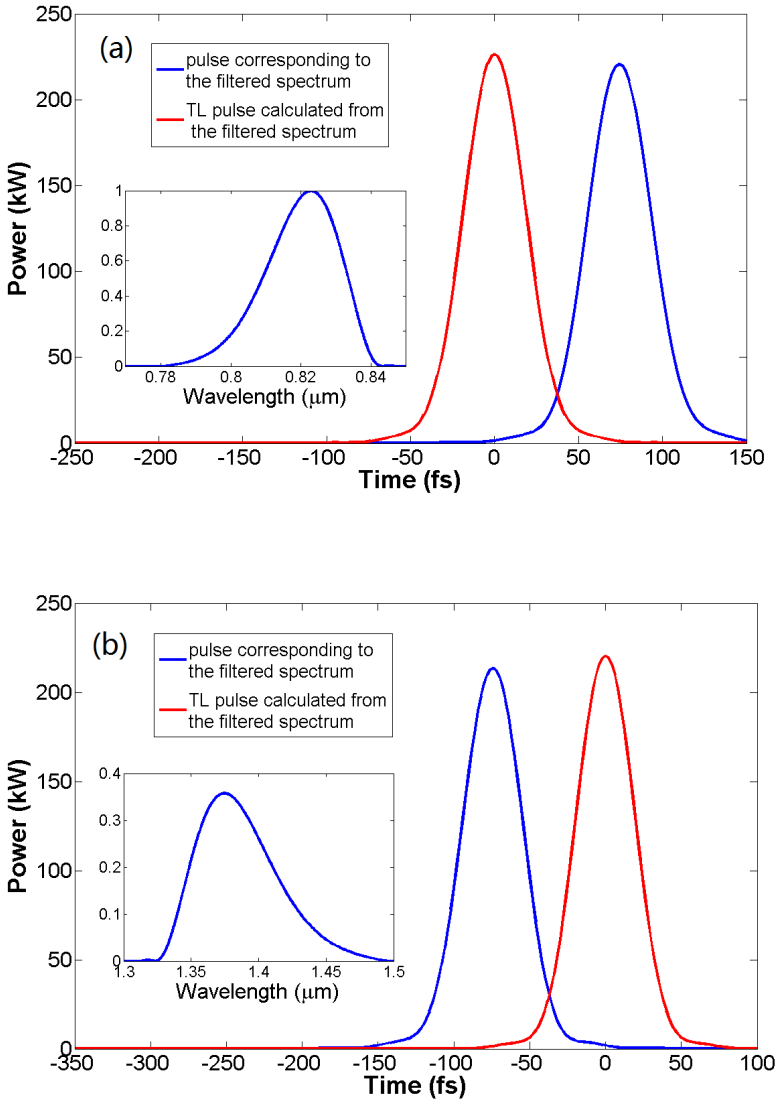

Fig. 4.2 Propagation of a 50-nJ, 200-fs pulse inside an optical fiber with a mode-field diameter of 6 μm. In the simulation, only SPM is considered. The corresponding optical pulse (blue curve) and the calculated transform-limited pulse (red curve) from the filtered spectral are shown in (a) for the leftmost lobe and in (b) for the rightmost lobe. Insets: filtered optical spectra. TL: transform-limited.

after propagating 6-cm distance (Fig. 4.1(b)) the optical spectrum develops 24 spectral lobes and covers the spectral range between 800 nm and 1.4 μm—a spectral range highly desired for MPM imaging.

We numerically filter both the leftmost and the rightmost spectral lobes, and plot them as the insets of Figs. 4.2(a) and 4.2(b), respectively. The blue curves in these figures are

the optical pulses corresponding to the filtered spectra; as a comparison, we also plot in these figures the transform-limited pulses (red curves) calculated from the filtered spectra. Clearly, both optical pulses are nearly transform-limited with the same pulse duration of 44 fs. Another intriguing feature of the SPM-broadened spectrum is that the leftmost and rightmost spectral lobes are the strongest; these two spectral lobes have a total energy of 21 nJ (10.5 nJ for each), accounting for $>40\%$ of the total energy. Note that other spectral lobes in Fig. 4.1(b) can also be filtered; however these intermediate spectra possess much less pulse energies compared with the leftmost/rightmost spectral lobes. In the rest of this Chapter, we restrict our discussion on these leftmost/rightmost spectral lobes.

Simulation results in Fig. 4.1 suggest a novel method to implement a multi-color ultrafast source. The filtered two spectral lobes plus the original laser wavelength enable the laser system producing ultrashort pulses at three different center-wavelengths. More important, the center wavelength of these filtered spectral lobes can be continuously tuned by adjusting the power coupled into the fiber for a fixed fiber length.

4.4 Effect of SS and SRS

The results in Fig. 4.1, though informative and impressive, are unpractical since only SPM is considered. Other nonlinear effects such as SS and SRS take place as well. To investigate their role in spectral broadening, we redo the simulation in Section 4.3 by further including SS or both SS and SRS; the resulting spectra after propagating 6 cm are plotted in Fig. 4.3(a). The spectrum broadened due to SPM and SS (blue curve in Fig. 4.3(a)) is significantly blue shifted compared with the SPM-broadened spectrum (Fig. 4.1(b)). When SRS is also included, the resulting spectrum (red curve in Fig. 4.3(a)) becomes slightly narrower due to the small red shift of those spectral lobes on the left side; the corresponding pulse of this spectrum is shown as the inset. Nearly maintaining its initial pulse duration of 200 fs, the optical pulse exhibits a much steeper trailing edge because of SS. It is the SS-induced steep trailing edge that extends the overall spectrum more into the shorter wavelength range.

We filter the leftmost and rightmost spectral lobes in the spectrum broadened by SPM together with SS and SRS (red curve in Fig. 4.3(a)), and plot the corresponding optical pulses in Fig. 4.3(b). The filtered spectral lobes are shown as insets in Fig. 4.3(b). The filtered pulse centered at 0.7 μm has a duration of 19 fs with 5.6-nJ pulse energy; the other pulse centers at 1.23 μm with 67-fs duration and 13.2-nJ energy. Both pulses are nearly transform limited (off by <0.5 fs). We also calculate the peak wavelength and energy conversion efficiency as a function of propagation distance for the leftmost and right most spectral lobes, respectively; the simulation results are summarized in Fig. 4.4(a) for the leftmost lobe and Fig. 4.4(b) for

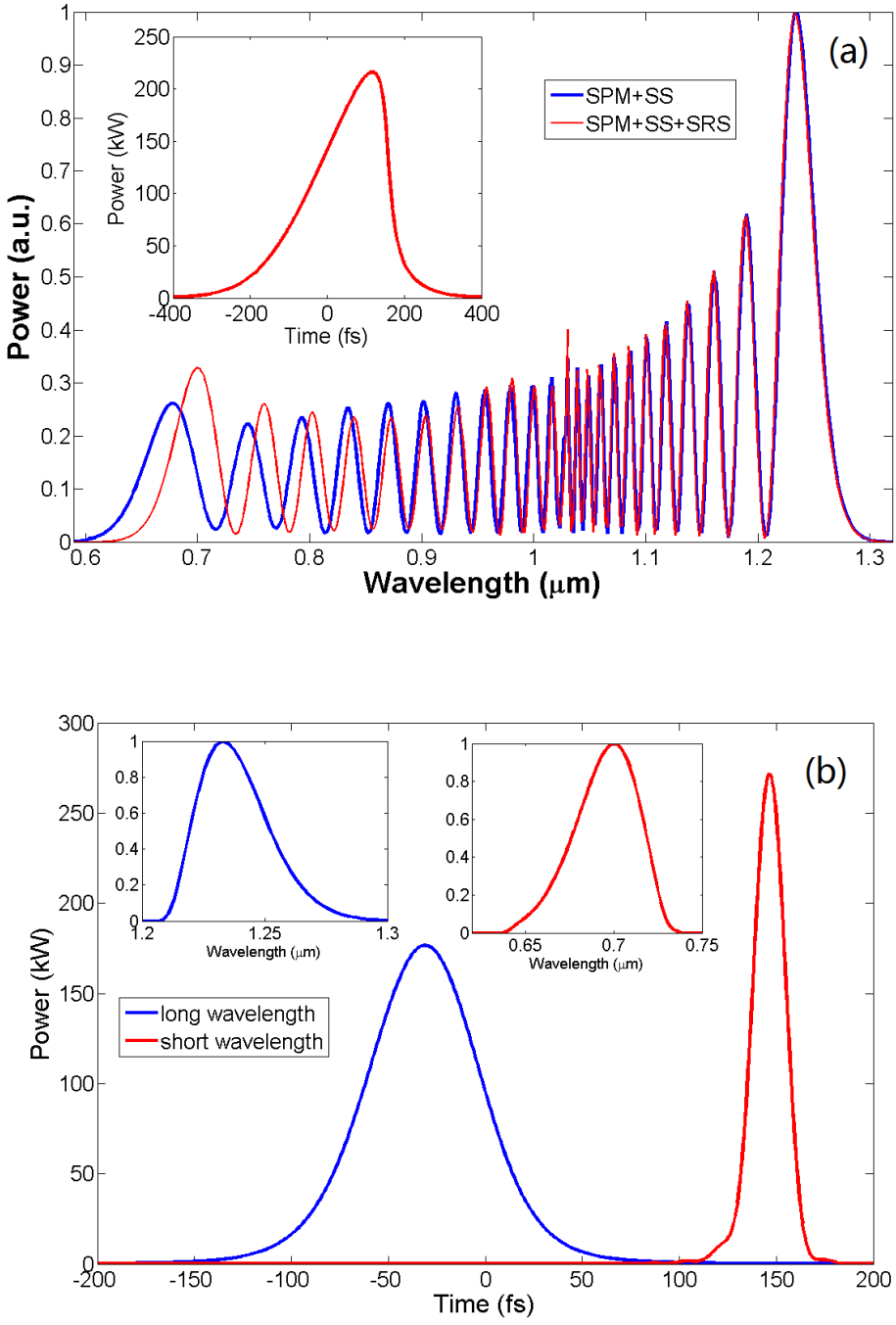

Fig. 4.3 Propagation of a 50-nJ, 200-fs pulse through 6-cm optical fiber with a mode-field diameter of 6 μm. (a) Optical spectra for simulations including SPM and SS (blue curve) or including SPM, SS, and SRS (red curve). Inset: optical pulse at the fiber output when the simulation includes SPM, SS, and SRS. (b) Leftmost and rightmost spectral lobes are filtered, respectively.

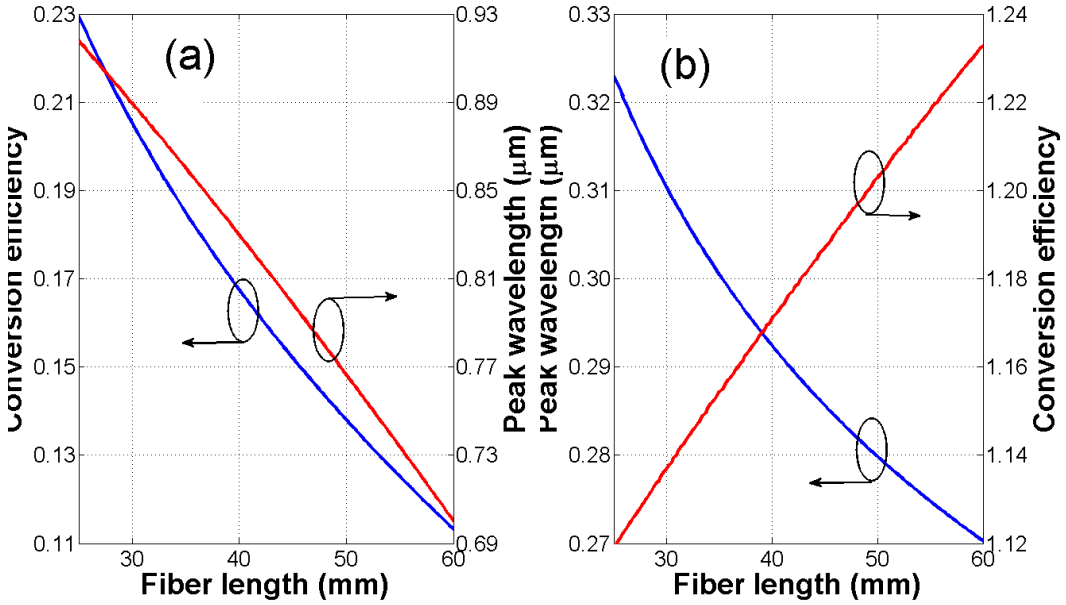

Fig. 4.4 The calculated peak wavelength and energy conversion efficiency as a function of propagation distance for the leftmost (a) and right most spectral lobes (b), respectively

the rightmost lobe. The peak wavelengths for both lobes shift linearly with respect to the fiber length. Meanwhile, the conversion efficiency continuously drops from 23% to 11% for the leftmost spectral lobe as the fiber length increases from 2.5 cm to 6 cm. As a contrast, the conversion efficiency for the rightmost spectral lobe exhibits a slight decrease, from 32% to 27%. The simulation results in this section reveal the following effects exerted by SS and SRS on spectral broadening and energy conversion to the leftmost/rightmost spectral lobes:

1. SS extends the broadened spectrum more towards the shorter wavelength.
2. For SPM-broadened spectrum, the leftmost and rightmost spectral lobes share the same energy. When SS and SRS are included, more energy is converted into the rightmost spectral lobe, though total conversion efficiency into these two spectral lobes is comparable for the two cases—40% for SPM-broadened spectrum and 38% if SS and SRS are considered as well.
3. The effect of SRS is minimal compared with SS.

4.5 Effect of dispersion

The simulation in Section 4.4 takes into account all the nonlinear effects and serves the purpose of understanding the physical mechanism underlying the spectral broadening; however, neglecting GVD makes the simulation inaccurate in predicting experimental results.

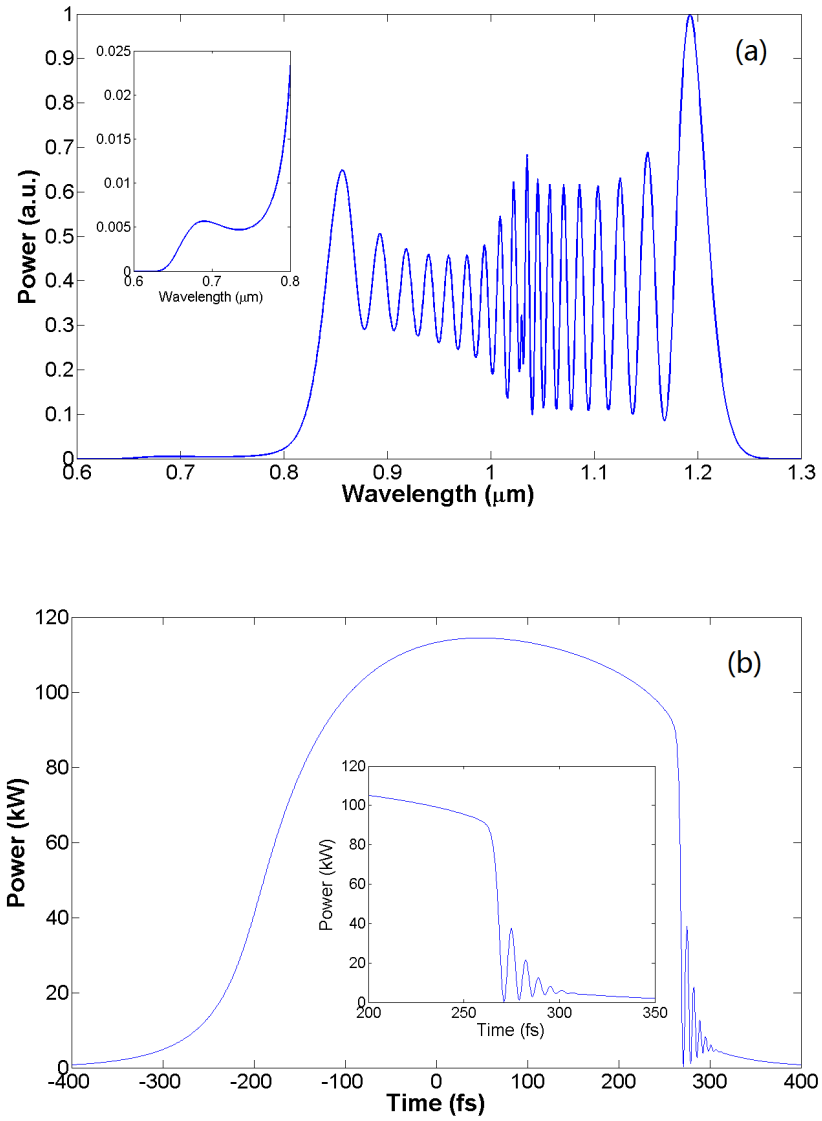

Fig. 4.5 Propagation of a 50-nJ, 200-fs pulse through 6-cm optical fiber with a mode-field diameter of 6 μm. (a) Optical spectra for simulations including SPM, SS, SRS, and GVD (5 fs^2/mm). Inset: close-up of the spectral range from 600-800 nm. (b) Corresponding optical pulse. Inset: close-up of the pulse envelope in the temporal range of 250-300 fs.

GVD undoubtedly plays an important role in nonlinear fiber optics, and can be flexibly engineered in a broad range [119]. Various fascinating nonlinear phenomena arise from the nonlinear pulse propagation inside a fiber with negative GVD, such as modulation instability, soliton formation, soliton fission, dispersive wave generation, and Raman soliton, to name a few. Due to complicated nonlinear interaction taking place inside a negative-GVD fiber, the resulting broadened spectrum features fine structures with reduced phase coherence; generation of nearly transform-limited pulse from a filtered spectrum becomes challenging and suffers from poor conversion efficiency. In contrast, spectral broadening in a positive-GVD fiber avoids involving above mentioned nonlinear phenomena and generates much smoother optical spectrum. Therefore we restrict our discussion in the context of positive GVD.

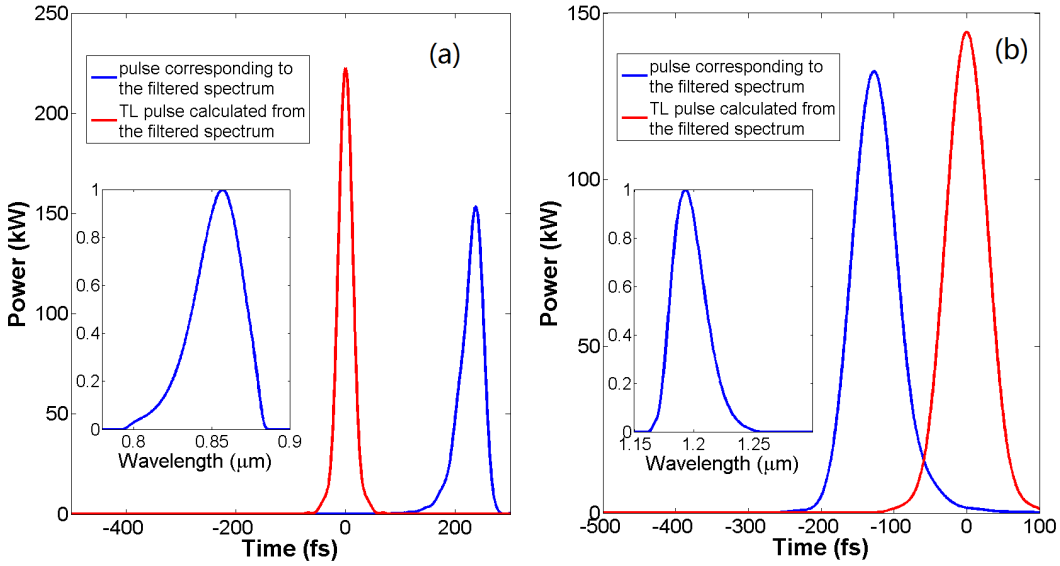

Fig. 4.6 The calculated peak wavelength and energy conversion efficiency as a function of propagation distance for the leftmost (a) and right most spectral lobes (b), respectively

We redo the simulation in Section 4.4 by further including a GVD of 5 fs^2/mm for the fiber with all other parameters unchanged. Figures 4.5(a) and 4.5(b) plot the optical spectrum and the pulse after 6-cm propagation distance. Due to the positive GVD, the initial 200-fs pulse increases its duration along the propagation, leading to a reduced nonlinearity and thus a narrower broadened-spectrum. As Fig. 4.5(b) shows, the pulse at 6-cm propagation distance has a duration of $\sim$ 400 fs. Rapid oscillation (inset of Fig. 4.5(b)) appears at the pulse's steep trailing edge, indicating onset of optical wave breaking [104], which in the spectral domain manifests as a pedestal extending to < 650 nm (inset of Fig. 4.5(a)).

Comparison of Fig. 4.5(a) and Fig. 4.4(a) suggests that positive GVD tends to wash out the lobe structures in the optical spectrum; that is, the spectral valleys between two adjacent peaks become shallower when positive GVD is included. We numerically use super-Gaussian shaped bandpass filters to select the leftmost and the rightmost spectral lobes, and plot them as the insets of Figs. 4.6(a) and 4.6(b), respectively. Similar to Figs. 4.2(a) and 4.2(b), the blue curves in these figures are the optical pulses corresponding to the filtered spectra, and red curves are the transform-limited pulses calculated from the filtered spectra. The filtered

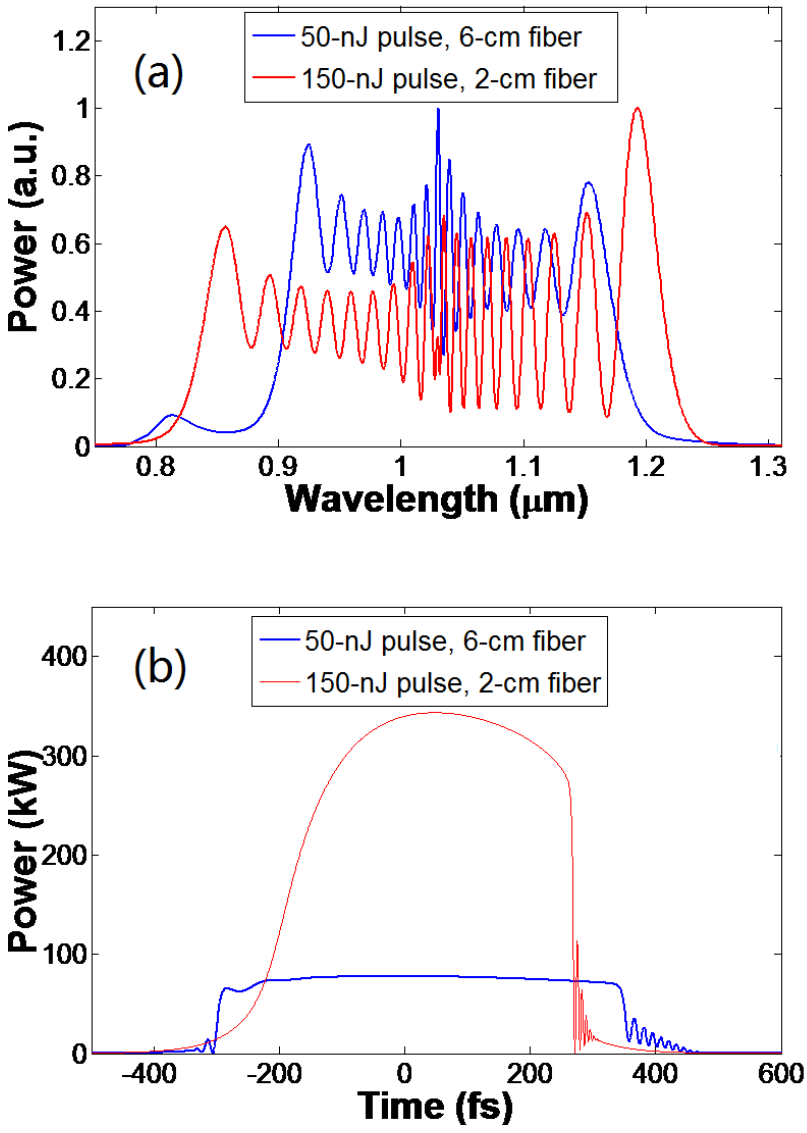

Fig. 4.7 The evolution of 50 nJ pulses propagating in 6-cm fiber and the evolution of 150 nJ pulses propagating in 2-cm fiber. (a) spectra evolution. (b) temporal evolution

spectral lobes peak at $\sim$ 855 nm and $\sim$ 1195 nm, corresponding to a 42-fs, 7.4-nJ pulse and a 71-fs, 10.3-nJ pulse, respectively. The transform-limited pulses calculated from the filtered spectra are 30 fs and 67 fs in duration, respectively, showing that the filtered pulses are slightly chirped.

To better understand the effect of GVD, we perform another simulation with the GVD increased from $5fs^2/mm$ to $15fs^2/mm$ with all other parameters unchanged. As the blue curve in Fig. 4.7(a) shows, the resulting optical spectrum becomes much narrower and its lobe structures tend to wash out. Due to larger GVD, optical wave breaking occurs at the leading edge of the pulse as well and becomes stronger at the trailing edge (blue curve in Fig. 4.7(b)), manifesting in the spectral domain as pedestals emerging at both the short- and long-wavelength edges (blue curve in Fig. 4.7(a)).

Fortunately, the detrimental effects caused by GVD can be prevented by increasing the input pulse energy and reducing the fiber length. Indeed, Eq. 4.1 remains unchanged if $A(z,t)$, β_n, and z are replaced by $\sqrt{N}A(z,t)$, $N\beta_n$, and z/N, where N is a positive number. Such a scaling property suggests that increasing the input pulse energy and shortening the propagation distance can cancel out the unfavorable effects of an increased GVD. To confirm this scaling property, we numerically propagate a 150-nJ pulse through 2-cm fiber with $15fs^2/mm$ GVD and plot the results as the red curves in Fig. 4.7. As expected, the resulting spectrum (red curve in Fig. 4.7(a)) and pulse (red curve in Fig. 4.7(b)) share exactly the same profile as their counterparts shown in Figs. 4.3(a) and 4.3(b) that are obtained from propagating 50-nJ pulse through 6-cm fiber with $5fs^2/mm$ GVD. The filtered spectra and pulses from the red curve in Fig. 4.7(a) are also the same in profile as those in Figs. 4.6(a) and 4.6(b), but possess 3 times more energy. More specific, the filtered pulses have 22.2 nJ (30.9 nJ) pulse energy for the filtered spectral lobe at $\sim$855 nm ($\sim$1195 nm). These results suggest an energy scalable approach in implementing wavelength tunable ultrafast sources: increase input pulse energy and shorten fiber length to minimize the GVD effect such that fiber nonlinearities (mainly SPM) dominate the spectral broadening process.

4.6 Conclusion of Chapter 4

We propose and demonstrate a new method of producing widely tunable femtosecond pulses. The method employs fiber-optic nonlinearities to broaden an input optical spectrum, followed by optical bandpass filters to select the leftmost or rightmost spectral lobes. The simulation results show that the filtered spectral lobes correspond to nearly transform-limited pulses with $\sim$ 100 fs pulse duration. Fiber dispersion causes optical wave breaking, which slows down the shift of the leftmost/rightmost spectral lobes and ultimately limits the wavelength

tuning range of the filtered spectra. A detailed numerical simulation verified by subsequent experimental results reveal that such a dispersion-induced limitation can be overcome by shortening the fiber length while increasing the input pulse energy. The benefits are twofold: (1) optical wave breaking is alleviated leading to larger spectral shift and (2) the filtered spectral lobes have higher power, indicating a practical approach of power scaling. We believe that our proposed source represents a cost-effective substitute of the conventional MPM driving source, i.e., a combination of Ti:sapphire laser plus a solid-state OPO. With the possibility of implementing our ultrafast source in an all-fiber format (Yb-fiber laser plus fiber-optic spectral broadening), this energy scalable approach paves an avenue to operate MPM in rugged environments outside research labs.

Chapter 5

SPM-enabled, wavelength-tunable ultrafast fiber laser sources: experiment

5.1 Introduction

In Chapter 4, we proposed a new method of producing wavelength widely tunable femtosecond pulses for driving MPM. The method employs fiber-optic nonlinearities (dominated by SPM) to broaden an input optical spectrum, followed by optical bandpass filters to select the leftmost or rightmost spectral lobes. The filtered spectral lobes correspond to nearly transform-limited pulses with 100 fs pulse duration. Optical wave breaking caused by fiber dispersion slows down the spectral broadening and ultimately limits the wavelength tuning range of the filtered spectra. Such a dispersion- induced limitation can be overcome by shortening the fiber length while increasing the input pulse energy. The resulting benefits are twofold: (1) optical wave breaking is alleviated leading to larger spectral shift and (2) the filtered spectral lobes have higher power, indicating a practical approach of energy scaling.

In this chapter, we verify the theoretical prediction in Chapter 4 by presenting detailed experimental results. In particular, we demonstrate that energy scaling of this method can be achieved by using shorter, LMA fibers for SPM-enabled spectral broadening. In Section 5.2, we present the details of constructing an ultrafast Yb-fiber CPA system of moderate power level (<10 W) serving as the driving source for SPM-enabled spectral broadening. Section 5.3 and 5.4 describe experimental results using low-dispersion PCFs and LMA fibers, respectively. We then use such a source for MPM imaging and present the preliminary results in Section 5.5. Section 5.6 concludes this chapter.

5.2 Ultrafast Yb-fiber CPA system of moderate power level (<10 W)

The 1 μm laser system producing the ultrashort pulses for our SPM-enabled wavelength-tunable source was designed and built using the CPA architecture similar as the laser system described in Chapter 2, but at a substantially lower power level. We call this laser system as "mini-CPA" in the following discussion.

5.2.1 Setup of Yb-fiber mini-CPA system

Figure 5.1 depicts the schematic of our mini-CPA system. A home-built Yb-fiber oscillator based on nonlinear polarization evolution produces 55-MHz ultrashort pulses centered at 1033 nm with 70-mW average power. These pulses were first stretched to $\sim$ 20 ps in a fiber-based stretcher, and then amplified in a two-stage fiber amplifier using polarization-maintaining Yb-doped fibers. The first stage was constructed with single- clad gain fiber (PM Yb-501 from Coractive) and pumped with a 500 mW single-mode butterfly pump diode. The second stage was built using double-clad Yb-doped fiber (Yb1200-PM from nLight) and pumped by a 20-W multimode pump diode. The central wavelength of the two pump lasers was both at 975 nm. After an optical isolator, a compressor including two identical fused-silica transmission diffraction-gratings (1000 lines/mm groove density) de-chirped the amplified pulses.

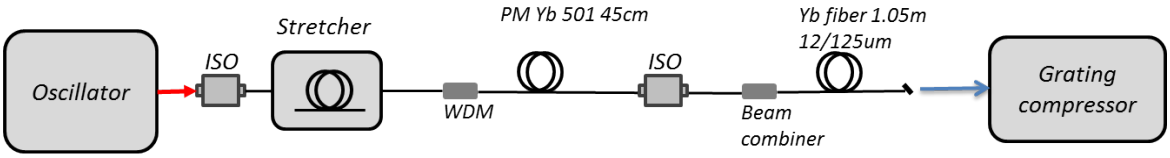

Fig. 5.1 Schematic of Yb-fiber mini CPA system used for SPM-enabled spectral broadening.

5.2.2 Experimental results

Figure 5.2 demonstrates the output power from the main amplifier and the compressed output average power depending on the absorbed pump power. The slope efficiency is as high as 74%, which is a typical number for Yb-doped fiber amplifier. With about 14-W absorbed pump power, we obtained >10 W output power, corresponding to $\sim$200-nJ output pulse energy. After the transmission grating pair, the maximum output power is 8 W, corresponding to 170 nJ compressed pulse energy. The compression efficiency is $\sim$80%.

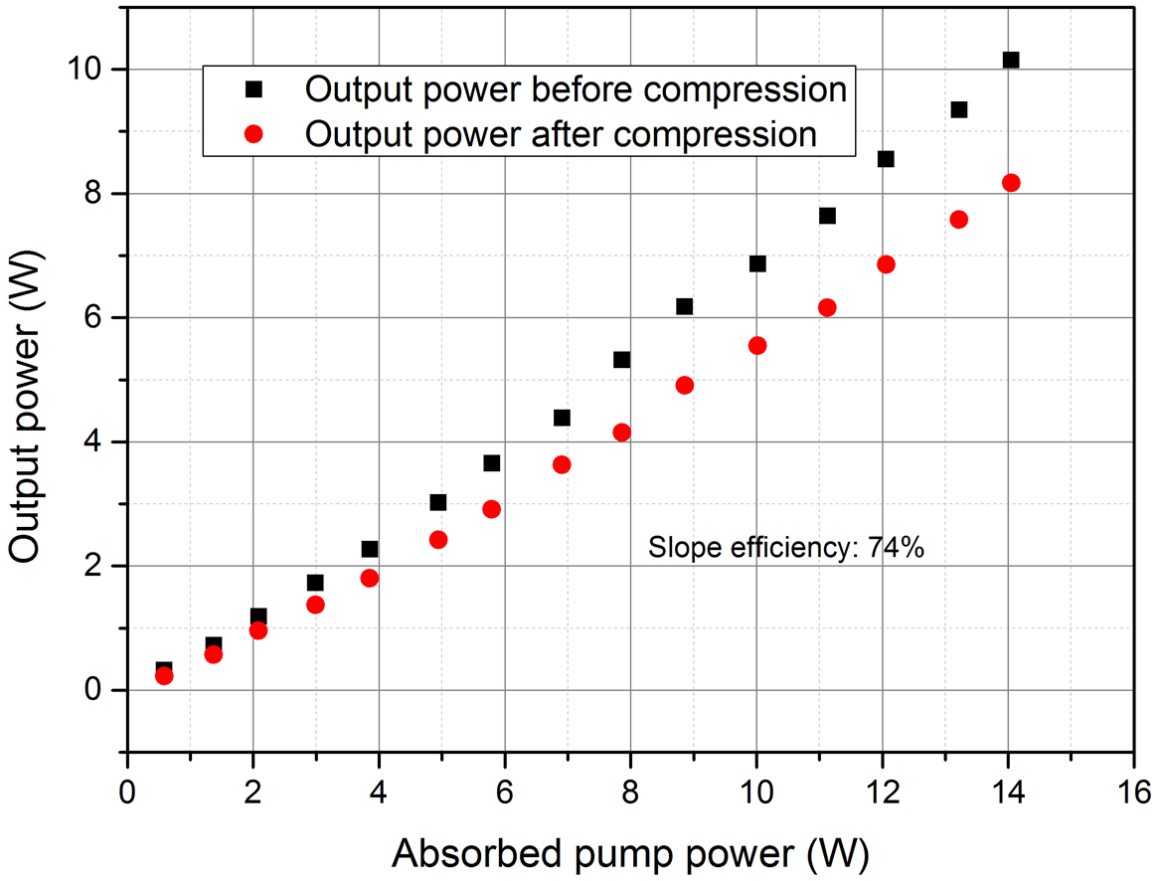

Fig. 5.2 Laser output power and compressed output power versus absorbed pump power.

By varying the distance between the two compressor gratings and changing the length of fiber stretcher for higher-order dispersion compensation, the output pulse duration can be de-chirped to the close-to-transform-limited value of 190 fs. Figure 5.3 and Fig. 5.4 show the optimization process for pulse compression by cutting back the stretcher fiber. Using 32 meters of SMF (PM 980) and 2.6 meters of stretcher fiber (customized from OFS), the GDD of the system can be well compensated by the diffraction-grating pair. With such a combination, the pedestal of autocorrelation trace caused by higher-order dispersion was substantially suppressed. The detailed dispersion of the OFS stretcher fiber can be found in Chapter 2 (Sec. 2.3).

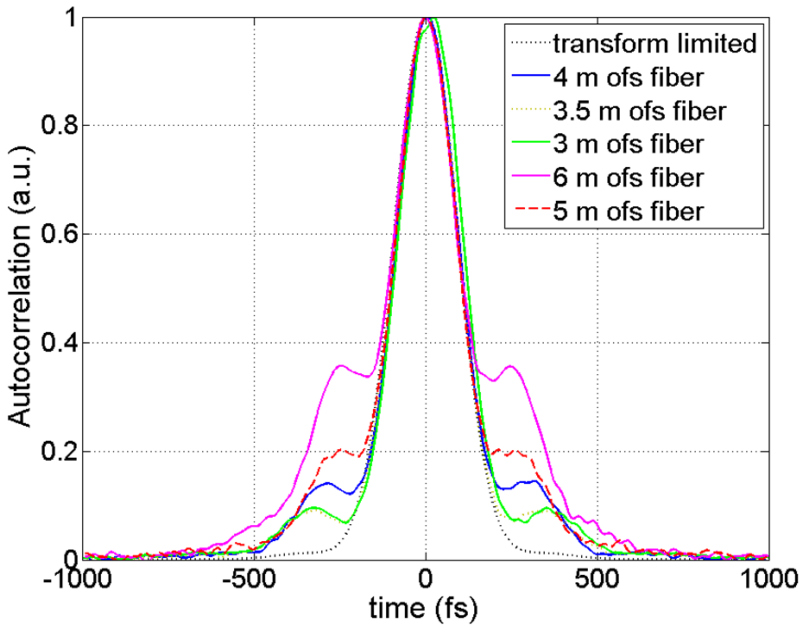

Fig. 5.3 Compressed pulses from mini-CPA system, optimized by cutting-back the OFS stretcher fiber (rough tuning).

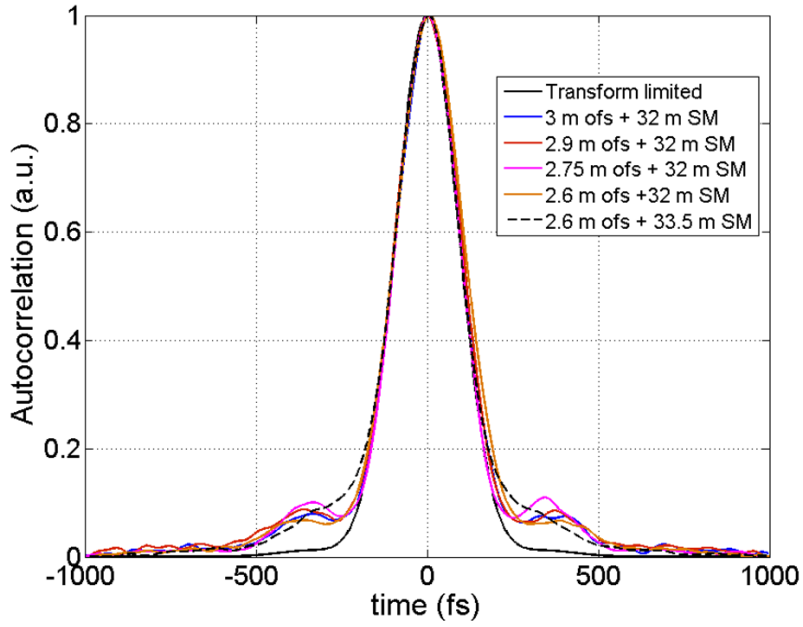

Fig. 5.4 Compressed pulses from mini-CPA system, optimized by cutting-back the OFS stretcher fiber (fine tuning).

5.2.3 Potential for all-fiber format

Yb-doped fiber lasers exhibit superior performance (such as high optical- to-optical efficiency, broad gain bandwidth and outstanding thermo-optical behavior, and simplicity of operation) and have established themselves as one of the most promising candidate for application in harsh environment. Thanks to the rapid progress in novel fiber fabrication, an all-fiber configuration CPA system with moderate pulse energy (hundreds of nJ) is possible. For example, with specific fiber design, a fused-silica fiber can exhibit negative TOD and therefore can be used to replace the traditional grating stretcher. As for the compressor, the situation becomes more challenging due to the high peak power obtained in the amplifier. Since the pulse energy for MPM application is at the level of hundreds of nJ, pulse compression in a hollow-core (HC) photonic band-gap fiber (PBGF) is an ideal replacement for diffraction gratings. Such a HC PBGF possesses anomalous dispersion with a significantly reduced nonlinearity because light propagates inside the air core.

It is noteworthy that commercially available HC PBGFs have considerable transmission loss, and thus the compression fiber should be short, which limits the stretched pulse duration.

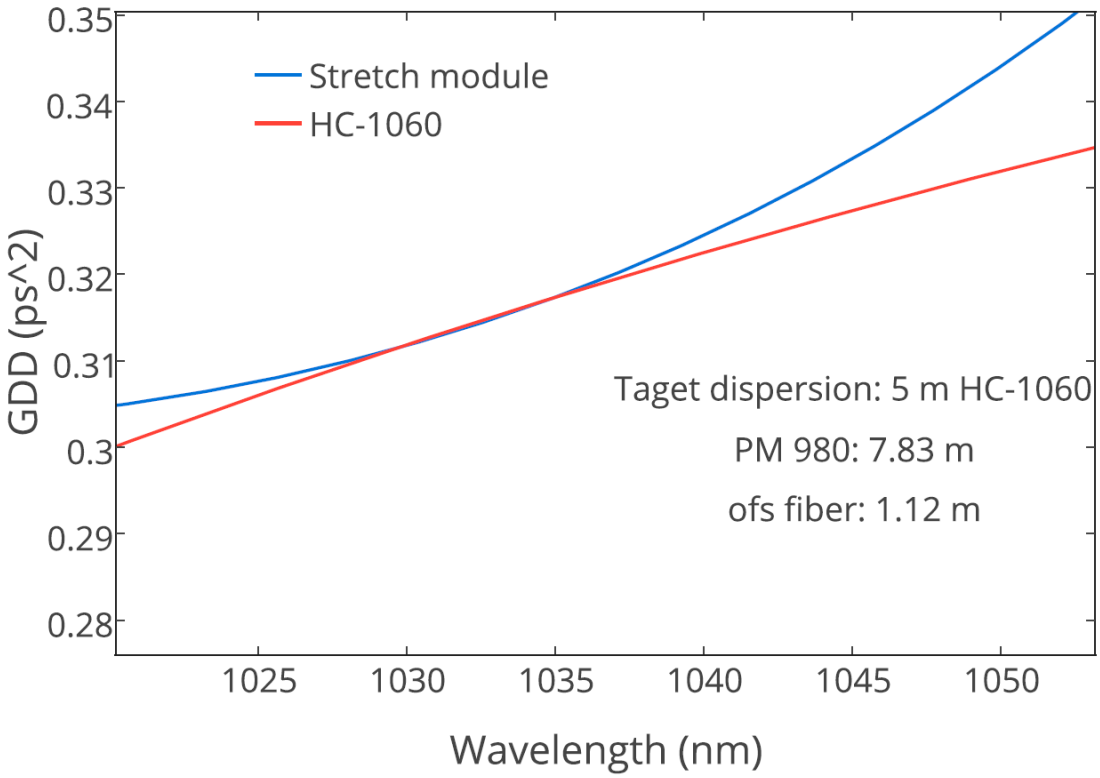

Fig. 5.5 Proposed routine for using HC-PCF to replacing diffraction grating pair to realize all fiber CPA system.

To suppress the accumulated nonlinear phase we could use the gain fiber with larger mode area.

Figure 5.5 shows a proposed design of replacing the diffraction grating compressor with commercially available HC PBGF (HC-1060-2 from NKT). To mitigate the detrimental nonlinear effects, we need to double the mode-field diameter of current gain fiber such that only 5 meters of HC-1060-2 are required to compress the amplified pulses.

5.3 SPM-enabled tunable source based on low-dispersion PCFs

To confirm the simulation results in Chapter 4, we carry out a detailed experimental study. The setup is depicted in Fig. 5.6. The compressed pulses from the mini-CPA system were coupled into a nonlinear fiber for SPM-enabled spectral broadening followed by optical bandpass filters to select the rightmost spectral lobe. A half-wave plate and a polarization beam splitter were used to adjust the powered coupled into the nonlinear fiber. Finally, as a proof-of-principle, we employed the filtered femtosecond source to drive a laser scanning microscope to perform MPM imaging of cancer cells and skin samples. The optical spectrum and the measured autocorrelation trace of the pulse train are shown in Fig. 5.7. As the simulation predicts, use of low-dispersion fibers facilitates SPM-dominated spectral broadening, leading to further shift for the leftmost and rightmost spectral lobes. As a proof-of-principle

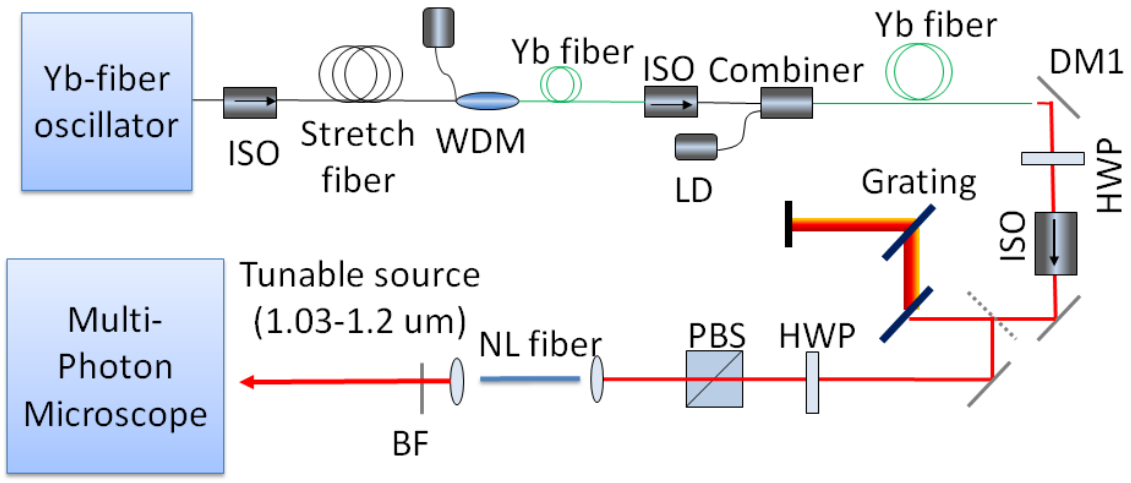

Fig. 5.6 Schematic setup of the fiber-based SPM-enabled tunable source.ISO: isolator, WDM: wavelength division multiplexer, LD: laser diode, DM: dichroic mirror, HWP: half-wave plate, PBS: polarization beam splitter, NL fiber: nonlinear fiber, BP: optical bandpass filter

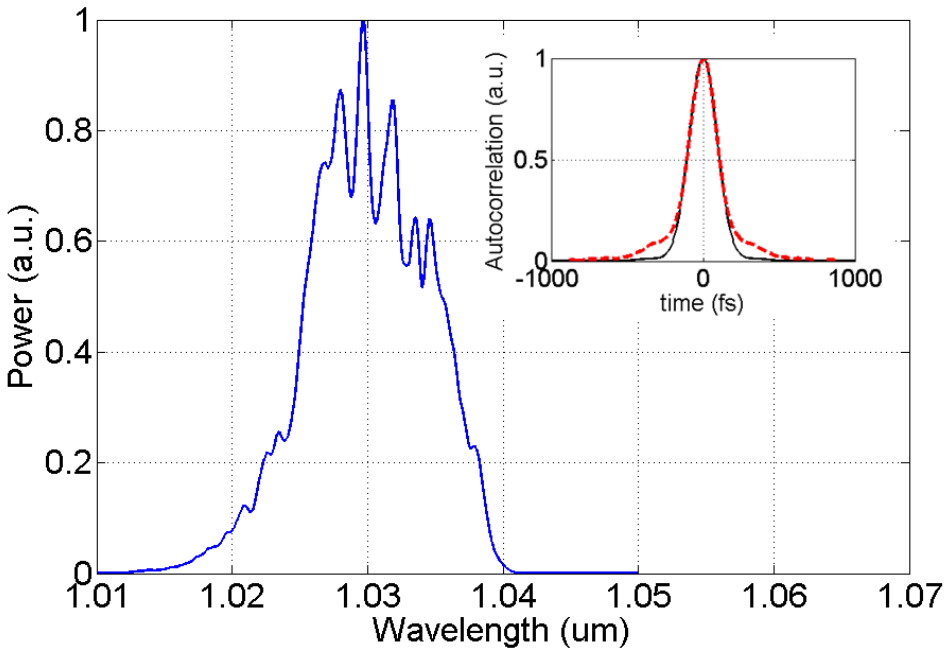

Fig. 5.7 Measured laser output spectrum and autocorrelation trace at maximum output power (10 W).

demonstration, we choose two PCFs commercially available from NKT Photonics: NL-1050-ZERO-2 and NL-1050-NEG-1, both featuring low and flat dispersion in the wavelength range of 850-1250 nm. Their dispersion curves are plotted in Fig. 5.8; also plotted in the same figure for comparison is the dispersion curve of fiber HI1060—a popular SMF fabricated by Corning. Indeed, these two PCFs (NL-1050-ZERO-2 and NL-1050-NEG-1) have been widely used in nonlinear spectral broadening for supercontinuum generation [120–125] and generation of femtosecond pulses in the 1.3-μm spectral region [126–129].

Figure 5.9 records the rapid broadening of the output spectra generated from PCF NL-1050-ZERO-2 and NL-1050-NEG-1 for different input pulse energies of 1 nJ (Fig. 5.9(a)), 3 nJ (Fig. 5.9(b)), 5 nJ (Fig. 5.9(c)), and 7 nJ (Fig. 5.9(d)). Both fibers are 80 mm in length. Clearly, for a fixed fiber length, the spectrum broadens with increased pulse energy. Take PCF NL-1050-ZERO-2 (blue solid curves in Fig. 5.9) as the example: as we increase the coupled pulse energy from 1 nJ to 5 nJ, SPM dominates the spectral broadening and the rightmost spectral lobe red-shifts linearly with the increased energy. With 5-nJ pulse energy coupled into the fiber, optical wave breaking occurs at the pulse's trailing edge and generates a noticeable spectral bump at the short-wavelength side peaking at 790 nm (blue solid curve in Fig. 5.9(c)). Further increasing pulse energy to 7 nJ leads to stronger optical wave breaking and thus a blue-shifted spectral pedestal reaching 700 nm; meanwhile, a small spectral bump

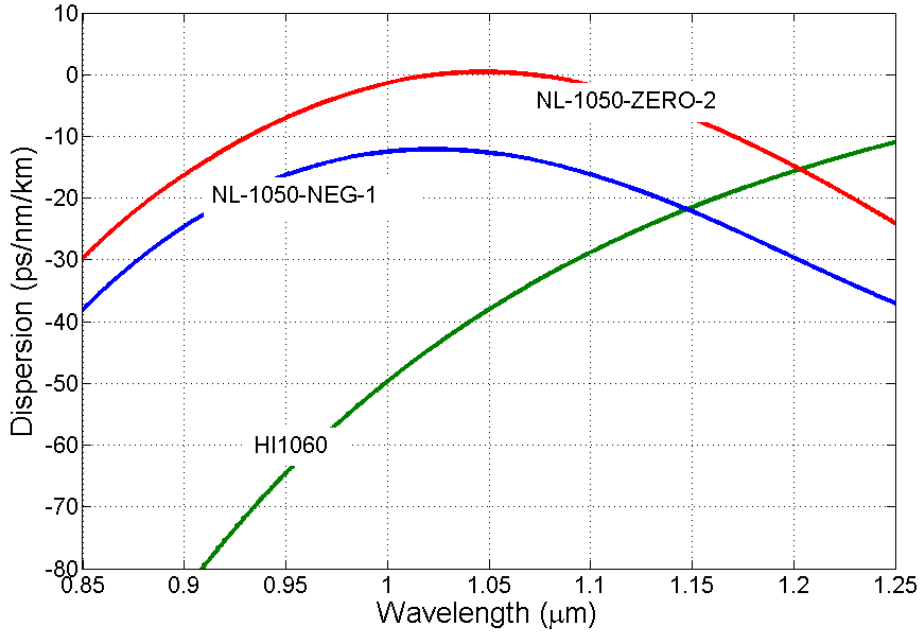

Fig. 5.8 Dispersion curves for PCF NL-1050-ZERO-2 (red), NL-1050-NEG-1 (blue), and SMF HI1060 (green).

emerges at the long-wavelength side peaking at 1300 nm due to the optical wave breaking taking place at the pulse's leading edge (blue solid curve in Fig. 5.9(d)). Onset of optical wave breaking slows down and eventually stops the red-shift (blue-shift) of the rightmost (leftmost) spectral lobe. Similar features can be found for the optical spectra (red dotted curves) generated by 80-mm PCF NL-1050-NEG-1.

It is noteworthy that these two PCFs have nearly identical mode-field diameter (MFD) of 2.2 μm (corresponding to nonlinear coefficient of 37 $W^{-1}km^{-1}$ at 1064 nm). The huge difference between the two spectra generated from these two fibers at the same input pulse energy is thus caused by dispersion. The results in Fig. 5.9 clearly show that PCF NL-1050-ZERO-2 produces a broader spectrum than PCF NL-1050-NEG-1 at the same pulse energy because the former fiber exhibits less dispersion than the latter one (Fig. 5.8). Furthermore, simulation results in Sec. 4.3 suggest that positive GVD tends to wash out the lobe structures in the optical spectrum and the spectral valleys between two adjacent peaks become shallower. This is experimentally verified by comparing the five optical spectra obtained from 80-mm PCF NL-1050-ZERO-2. As we broaden the spectrum by increasing the input pulse energy form 1 nJ to 5 nJ, both the left and right spectral edges of the broadened spectrum experience more positive GVD due to the parabolic shape of the dispersion curve. Consequently, the spectral lobes become less pronounced. The optical spectra generated by 80-mm PCF NL-

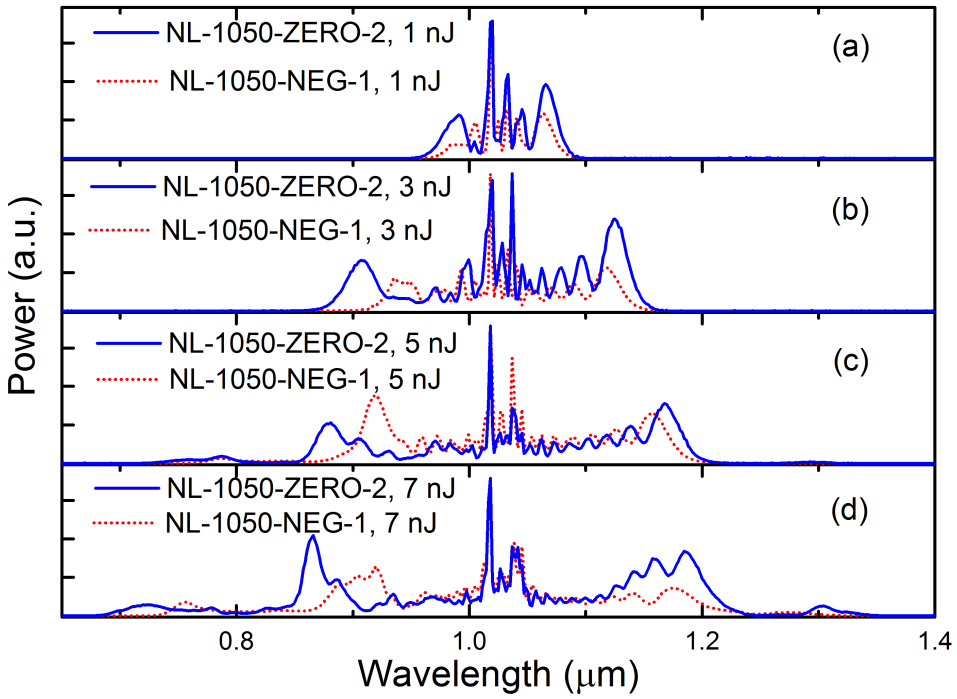

Fig. 5.9 Output spectra from PCF NL-1050-ZERO-2 (blue solid curves) and NL-1050-NEG-1 (red dotted curves) with different input pulse energies of 1 nJ (Fig. 6(a)), 3 nJ (Fig. 6(b)), 5 nJ (Fig. 6(c)), and 7 nJ (Fig. 6(d)). Both fibers are 80 mm long.

1050-NEG-1 share similar features with even shallower spectral valleys due to the larger dispersion than PCF NL-1050-ZERO-2.

To investigate the energy scaling property offered by shortening the fiber length, we prepare another 40-mm long PCF NL-1050-ZERO-2 and adjust the coupled pulse energy such that the resulting rightmost spectral lobes peak at the same wavelength as those obtained from the 80-mm PCF. Figure 5.10 records the output spectra generated from both fibers at different input pulse energies. A comparison between the experimental results from 80-mm (blue solid curves) and 40-mm (red dotted curves) PCFs reveal the following interesting facts:

1. In order to generate the rightmost spectral lobe peaking at a certain wavelength, using shorter PCF requires more pulse energy.

2. Results in Figs. 5.10(a)-5.10(c) indicate that, before optical wave breaking becomes notable, reducing the fiber length by a factor of two (80 mm vs. 40 mm) demands nearly twice much energy (1 nJ vs. 2.1 nJ, 3 nJ vs. 6 nJ, and 5 nJ vs. 9.8 nJ) to overlap

the rightmost spectral lobes. It can be expected that if we use proper optical bandpass filters to select the rightmost spectral lobes, the resulting filtered spectra from the 40-mm PCF have twice power/energy compared with those obtained from the 80-mm PCF. This proves the power/energy scalability of our proposed method.

3. With 7-nJ pulse energy (Fig. 5.10(d)) coupled into the 80-mm PCF, onset of optical wave breaking at the pulse's leading edge slows down the red shift of the rightmost spectral lobe. As the pulse energy is increased from 5 nJ to 7 nJ, the rightmost spectral lobe shifts only 15 nm from 1.17 μm to 1.185 μm. For the 40-mm PCF, optical wave breaking at the pulse's leading edge is nearly absent due to less accumulated dispersion; as a result, only 11.1-nJ (rather than $\sim$ 14 nJ) pulse energy is required to generate the rightmost spectral lobe peaking at 1.185 μm.

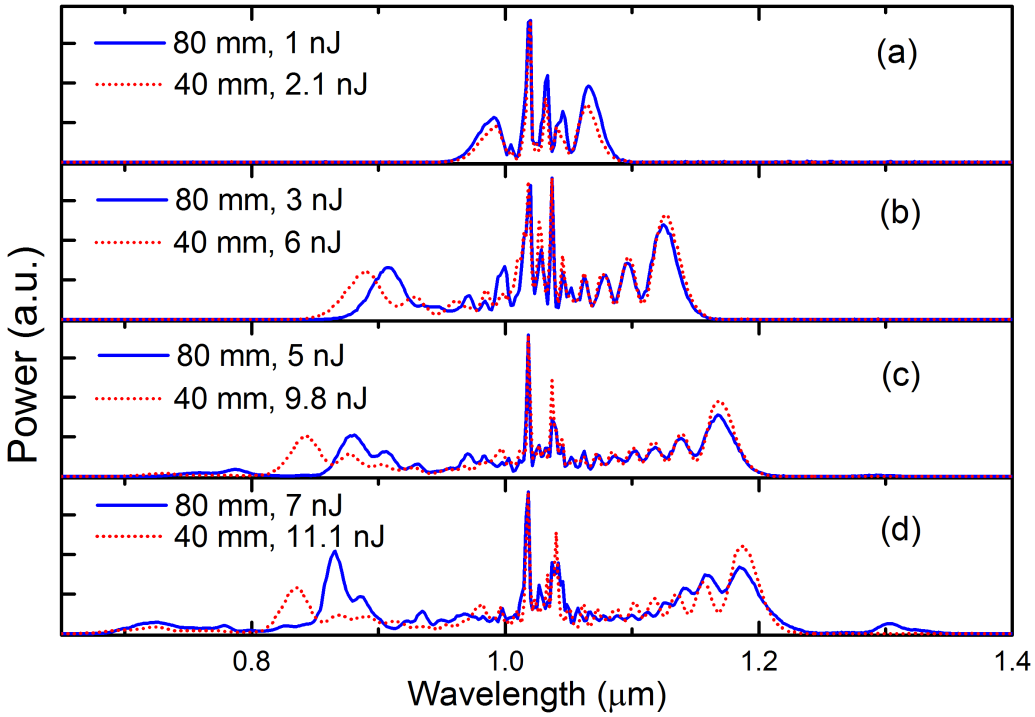

Fig. 5.10 Output spectra from PCF NL-1050-ZERO-2 at different fiber lengths (80 mm versus 40 mm) and input pulse energies. Blue solid curves and red dotted curves represent optical spectral generated from 80-mm PCF and 40-mm PCF, respectively. We adjust the input pulse energies such that the spectra generated by both fibers have their rightmost spectral lobes peaking at 1.07 μm (Fig. (a)), 1.12 μm (Fig. (b)), 1.17 μm (Fig. (c)), 1.185 μm (Fig. (d)), and 1.20 μm (Fig. (e)). Coupled pulse energies for each fiber are presented in each figure as well.

4. Optical wave breaking arises from the interaction between SPM and positive GVD. Using a shorter PCF reduces the overall positive GVD and consequently mitigates the effect of optical wave breaking. This is evidenced by the results shown in Figs. 5.10(c)-5.10(d) the spectral bumps become less noteworthy for the spectra obtained using 40-mm PCF, whereas the leftmost lobes in these spectra experience a larger blue-shift. For example, the leftmost spectral lobe peaks at 0.83 μm when 11.1-nJ pulse energy is coupled into the 40-mm PCF. In contrast, this spectral lobe peaks at 0.86 μm for the 80-mm PCF with 7-nJ input pulse energy.

To demonstrate a wavelength-tunable ultrafast source with >1 nJ pulse energy, we further shorten PCF NL-1050-ZERO-2 to 20 mm. We vary the average power coupled into the fiber and use a series of optical bandpass filters to select the leftmost or the rightmost spectral lobes. The corresponding optical pulses are characterized by an autocorrelator. With average powers at 820 mW, 605 mW, 550 mW, 760 mW, and 900 mW, we obtain five representative filtered spectra (left column in Fig. 5.11) peaking at 825 nm, 875 nm, 1100 nm, 1150 nm, and 1210 nm with average powers of 60 mW, 56 mW, 154 mW, 167 mW, and 180 mW, respectively. At a repetition-rate of 55 MHz, all the filtered spectra exhibit >1 nJ pulse energies. The measured autocorrelation traces of the optical pulses corresponding to these filtered spectra are shown as red curves in the right column of Fig. 5.11. Also plotted in the right column are the calculated autocorrelation traces of the transform-limited pulses allowed by the filtered spectra. Clearly these pulses are slightly chirped; the FWHM duration of their autocorrelation traces is in the range of 96-164 fs. The corresponding pulse duration is estimated to be 70-120 fs, assuming a deconvolution factor of 1.4.

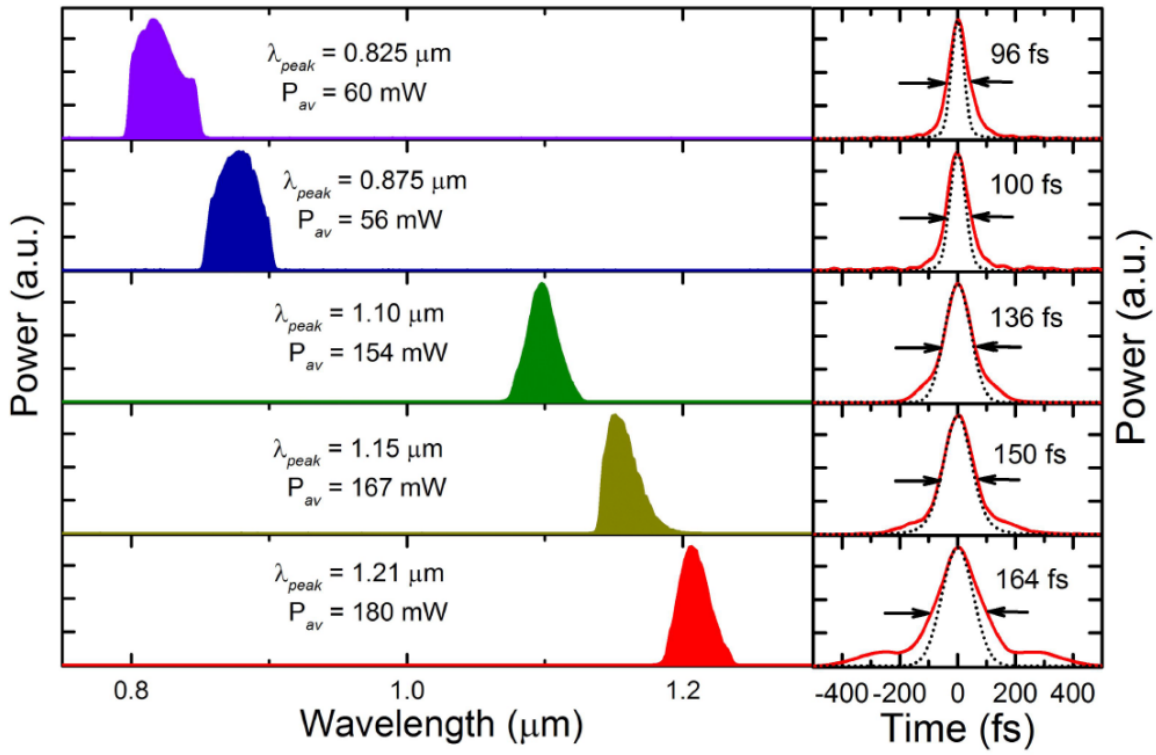

Fig. 5.11 (left column) Filtered optical spectra from 20-mm PCF NL-1050-ZERO-2; their peak wavelength and average power are labeled in the figure. (right column) Measured autocorrelation traces (red solid curves) and autocorrelation traces calculated from the transform-limited pulses allowed by the filtered spectra (black dotted curves).

The experimental results show that we can implement a femtosecond (70-120 fs) source with the peak wavelength tunable from 825 nm to 1210 nm with > 1 nJ pulse energy (repetition rate of our laser: 55 MHz). Both the wavelength tuning range and pulse energy can be improved by further shortening the fiber.

5.4 SPM-enabled tunable source based on LMA fibers

In the previous work, the SPM-broadened spectra were obtained inside PCFs with a MFD of 2.2 μm. We expect that use of optical fibers with larger MFDs will lead to much stronger filtered pulses. In this work, we tested three different commercially available fibers: LMA-8, HI-1060, and LMA-5; see Table 5.1 for information about these fibers. Their MFDs are 7.5 μm (LMA-8), 5.8 μm (HI-1060), and 4.7 μm (LMA-5); the corresponding GVDs at 1030 nm are -21, -42 and -5 $ps/km/nm$, respectively. The strength of fiber-optic nonlinearity can be quantified by the well-known nonlinear parameter γ, which is defined as parameter

$\gamma = 2\pi n_2/(\lambda A_{eff})$. n_2 is the nonlinear-index coefficient of fused silica with a typical value of $2.3 \times 10^{-20} m^2/W$. λ denotes the wavelength and A_{eff} the mode-field area. The last column of Table 5.1 lists the calculated nonlinear parameter for these three optical fibers. Apparently fiber LMA-8 has the smallest nonlinear parameter ($3.2\ W^{-1}km^{-1}$) due to the largest MFD while fiber LMA-5 has the largest nonlinear parameter ($8.1\ W^{-1}km^{-1}$) due to the smallest MFD.

Table 5.1 Properties of optical fibers used for spectra broadening

Type	λ_{ZDW} nm	D@1030 nm $ps/(km\,nm)$	MFD @ 1030 nm µm	γ @ 1030 nm $W^{-1}km^{-1}$
LMA-8	1160	-21	7.5	3.2
HI-1060	1310	-42	5.8	5.3
LMA-5	1050	-5	4.7	8.1

For a fair comparison of their energy scalability, all the three fibers under test are 70 mm long. We varied the coupling power into each fiber such that the rightmost spectral lobe peaks at 1100 nm. Figures 5.12(a-c) show the entire broadened spectra from these three fibers. Also labeled in these figures are the coupled powers into these fibers: 1.46 W for LMA-8, 1.36 W for HI-1060, and 0.4 W for LMA-5. Clearly because fiber LMA-8 has the smallest nonlinear parameter, it requires more coupled power such that the generated rightmost spectral lobe peaks at 1100 nm. We then use a 50-nm optical bandpass filter centered at 1100 nm to filter the rightmost spectral lobes of these spectra and record them in Fig. 5.12(d). Clearly, the filtered spectrum generated from fiber LMA-8 corresponds to the highest average power of 340 mW (6.2-nJ pulse energy) largely because it has a smaller nonlinear parameter due to a larger MFD than the other two fibers. Furthermore, a larger MFD allows fiber LMA-8 to handle higher coupled power than fiber HI-1060 and LMA-5 before surface damages take place. Therefore fiber LMA-8 shows an overall better scaling performance and we carried out further detailed experimental investigation of this fiber.

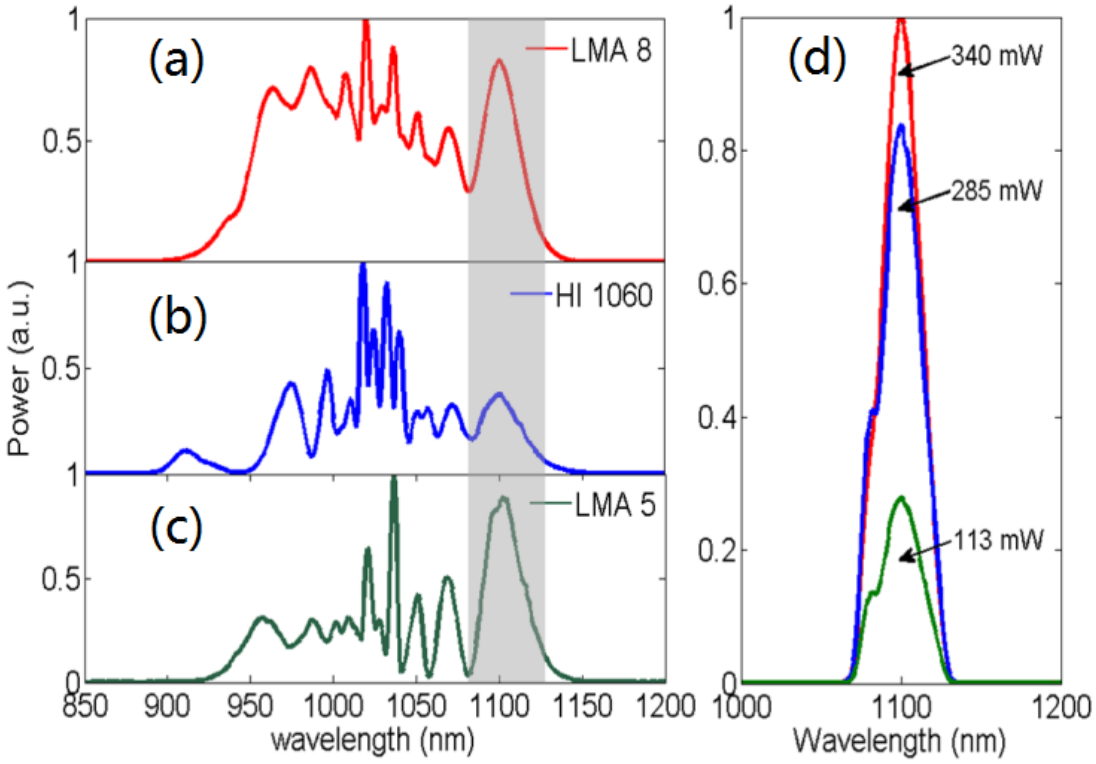

Fig. 5.12 (a-c) SPM-broadened spectra in three different types of optical fibers: (a) fiber LMA-8, (b) fiber HI-1060, and (c) fiber LMA-5. All the fibers are 70 mm in length. The coupled powers into each fiber are also given in each figure. (d) Power comparison of the rightmost spectral lobes filtered from the spectra shown in (a-c). The optical bandpass filter peaks at 1100 nm with 50-nm bandwidth.

To demonstrate the wavelength tunability, we varied the coupled average power into 70-mm fiber LMA-8; the resulting spectral evolution versus coupled average power is shown in Fig. 5.13(a). The optical spectrum becomes broader with more coupled power into the fiber. At 4-W coupled power, the enter spectrum spans from 870 nm to 1220 nm, and the resulting rightmost spectral lobe redshifts from 1050 nm to 1220 nm. We then used a set of optical bandpass filters to filter the rightmost spectral lobes and recorded seven typical filtered spectra in Fig. 5.13(b), with their center wavelength varying in 1080-1200 nm. Figure 5.13(c) plots the measured autocorrelation traces (red curves) for the filtered spectra at 1080 nm, 1140 nm, and 1220 nm. We also plot in the same figure the calculated autocorrelation traces of the transform-limited pulses allowed by the filtered spectra. Clearly these pulses are slightly chirped; the full-width-half-maximum duration of their autocorrelation traces is in the range of 68-90 fs. The corresponding pulse duration is estimated to be 50-65 fs, assuming a deconvolution factor of 1.4.

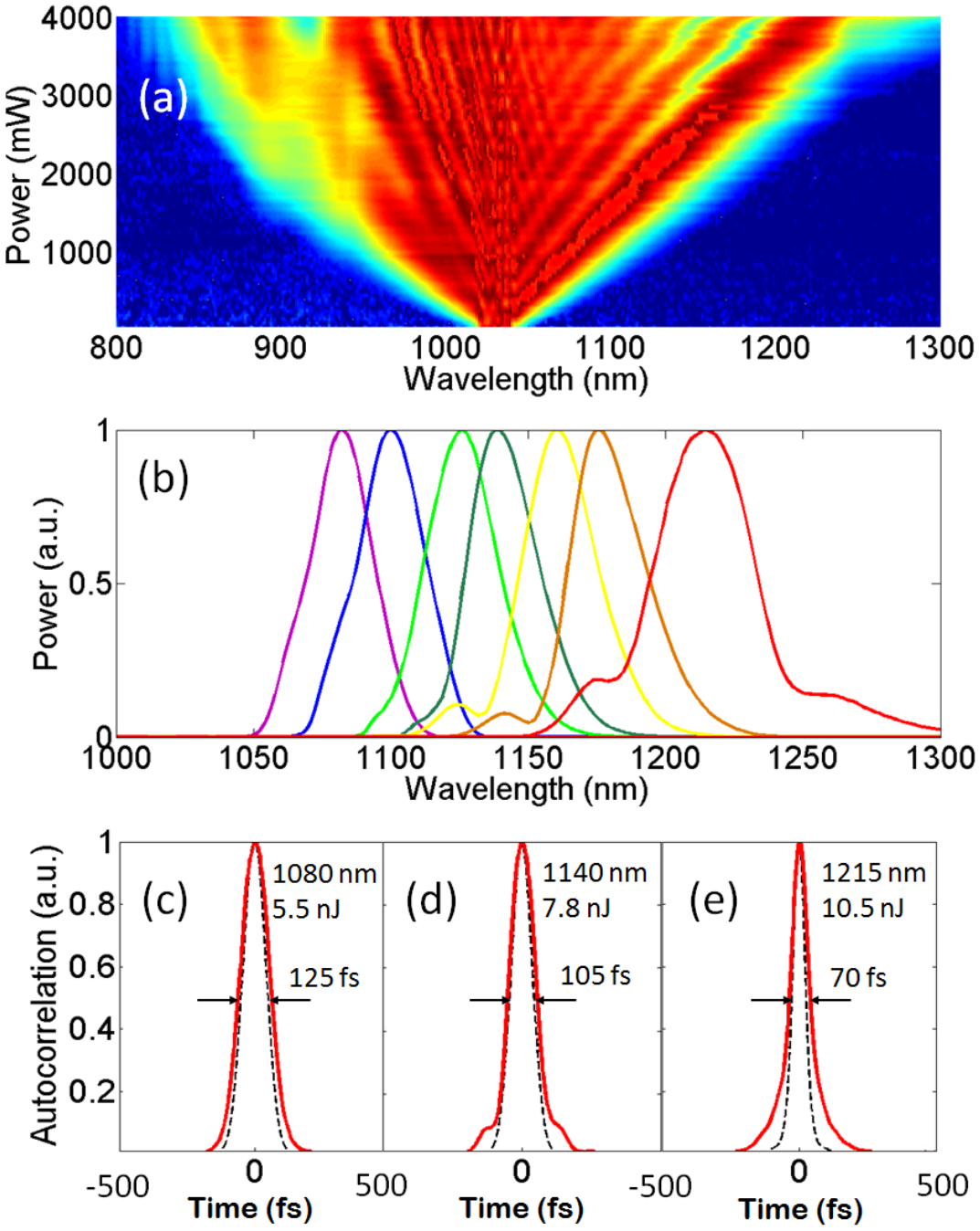

Fig. 5.13 SPM-enabled femtosecond sources using 70-mm fiber LMA-8. (a) Optical spectral evolution as a function of coupled power. (b) Filtered rightmost spectral lobes for different coupled powers. (c) Measured autocorrelation traces of the filtered lobes at 1080 nm, 1140 nm, and 1220 nm. The calculated autocorrelation traces of the transform-limited pulses allowed by the filtered spectra are shown as black dotted curve.

In addition to managing nonlinearity using fibers with different MFDs, fiber length is another degree of freedom. To show how fiber length affects fiber-optic spectral broadening, we coupled 3 W pulses into fiber LMA-8 of four different lengths: 20 mm, 30 mm, 50 mm, and 70 mm. Figure 5.14 shows the resulting broadened spectra from these fibers. Cleary the distinct, rightmost spectral lobe red shifts with the increased fiber length. The rightmost spectral lobe peaks at 1080 nm (1170 nm) for 20-mm (70-mm) LMA-8. Apparently much more powers need to be coupled into the 20-mm fiber LMA-8 such that the resulting rightmost spectral lobe will be shifted to 1170 nm; in this scenario, the filtered spectrum at 1170 nm should result in much higher pulse energy than can be generated by filtering the rightmost spectral lobe generated by the 70-mm LMA-8. This constitutes another powerful energy-scaling means—using shorter fibers for SPM-enabled spectral broadening. We varied the coupled power into these fibers to generate the filtered spectra at different wavelengths. Figure 5.15 summarizes the pulse energies given by the filtered spectra peaking at different wavelengths corresponding to different fiber lengths. As expected, the filtered spectra from shorter fibers exhibit higher pulse energies at the same peaking wavelength. For example, the filtered spectrum at 1100 nm has a pulse energy of 6.5 nJ, 8.5 nJ, 14.5 nJ, and 22 nJ for the fiber length of 70 mm, 50 mm, 30 mm, and 20 mm, respectively. However, due to the available power from our fiber laser system, using shorter fibers reduces the wavelength-shift range; that is, the farthest reaching wavelengths are 1215 nm, 1200 nm, 1140 nm, and 1110

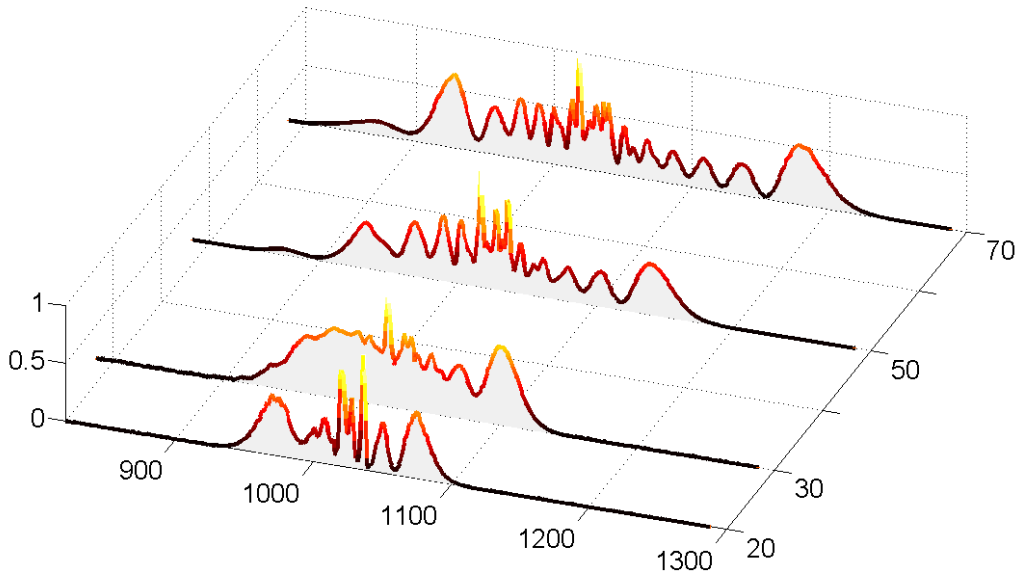

Fig. 5.14 The spectrum broadening of LMA-8 with four different lengths: 20 mm, 30 mm, 50 mm, and 70 mm. The coupled power is fixed at 3W.

nm for the fiber LMA-8 length at 70 mm, 50 mm, 30 mm, and 20 mm, respectively. Using a more powerful fiber laser source can increase the farthest reaching wavelength. Numerical simulation shows that, if 11-W average power (200-nJ pulse energy) is coupled into the 20-mm LMA-8, the rightmost spectral lobe peaks at 1200 nm and the filtered spectrum will exhibit >40 nJ pulse energy, corresponding to >2.2-W average power.

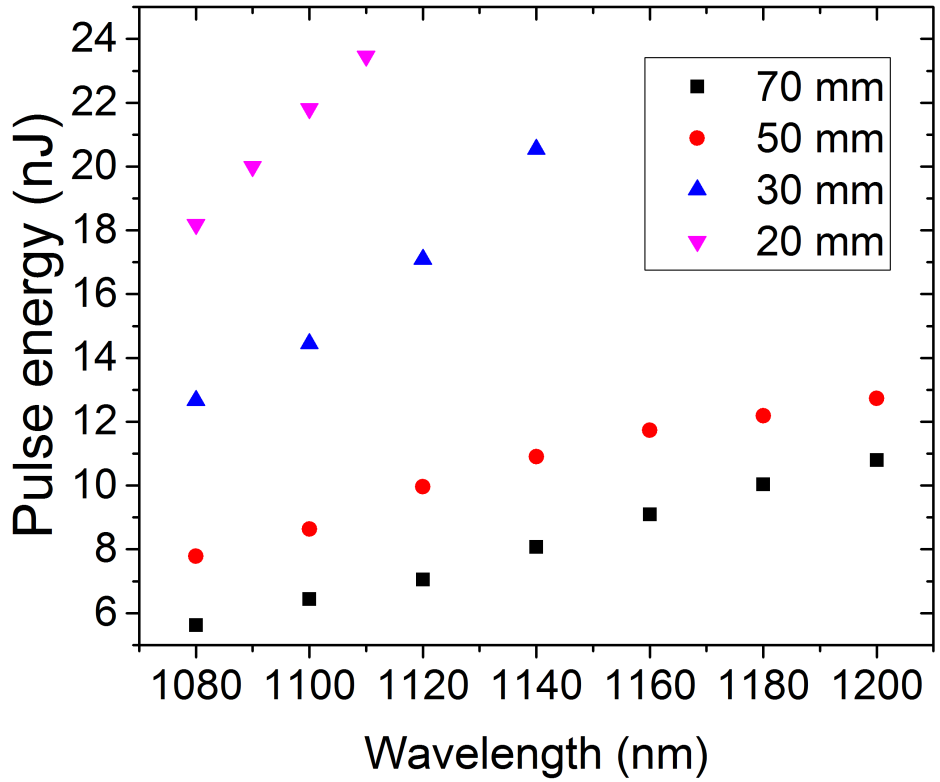

Fig. 5.15 Pulse energy of the filtered rightmost spectral lobes at different central wavelengths corresponding to different fiber lengths of 70 mm, 50 mm, 30 mm, and 20 mm.

5.5 MPM bio-imaging using SPM-enabled ultrafast sources

To show that our SPM-enabled ultrafast fiber laser source is well suited for MPM, we use this source to drive a laser scanning microscope to perform MPM imaging.

First example is to use this energy-scalable femtosecond source in a two-photon excited fluorescence microscope to study cancer cells. The cancer cells are labeled with green fluorescence proteins, which can be two-photon excited by the filtered spectrum at 920 nm

with 1.4 nJ pulse energy and 85 fs pulse duration. Figure 5.16 shows a typical fluorescence image.

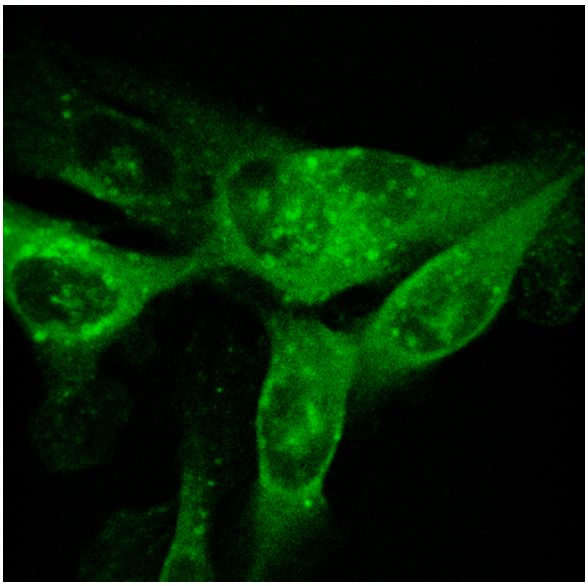

Fig. 5.16 Two-photon excited fluorescence imaging of cancer cells labelled with green fluorescence proteins.

The second example is to use the filtered 1100-nm source to perform MPM imaging of a human skin sample. We use SHG and THG as the image contrast. Figure 5.17 shows the MPM images at different penetration depth; SHG of collagen is colored in green and THG of basal cell in purple.

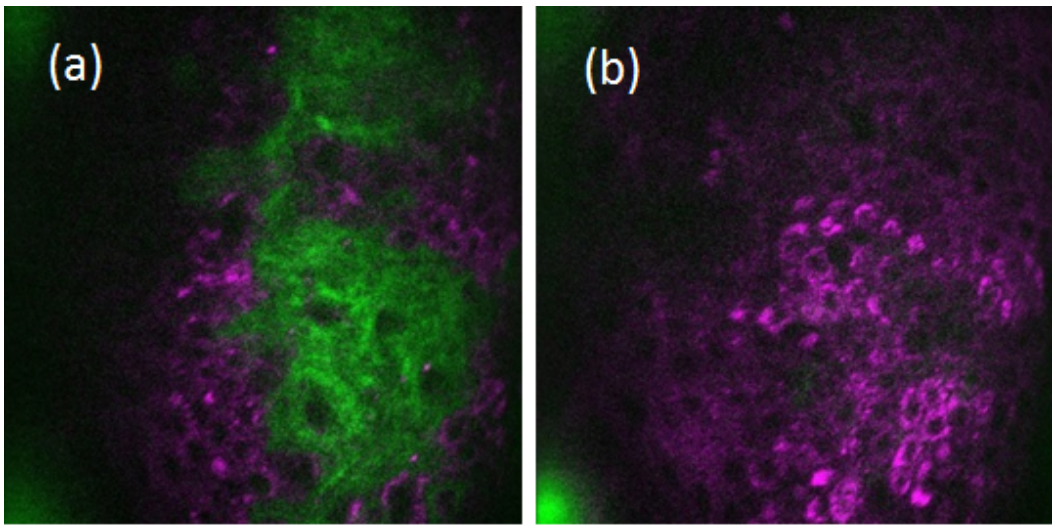

Fig. 5.17 MPM imaging of a human skin sample driven by the filtered out spectra lobes.

5.6 Conclusion of Chapter 5

We experimentally demonstrated a new type of fiber-laser based femtosecond source, which employs SPM in an optical fiber as the dominant spectral-broadening mechanism. Using 20-mm commercially available PCF to achieve spectral broadening and several optical bandpass filters to select the leftmost/rightmost spectral lobes, we implemented a femtosecond (70-120 fs) source with wavelength tunable from 825 nm to 1210 nm with >1 nJ pulse energy.

The obtained pulse energy can be further increased using LMA fibers for spectral broadening. LMA fibers with proper dispersion allow us to scale up the pulse energies up to 20 nJ in the wavelength range of 1070-1220 nm. Such a powerful source is well suited for deep tissue MPM imaging. A proof-of-principle study of a human skin sample using multiple imaging modalities demonstrates that such an ultrafast source has the potential for virtual skin biopsy.

Chapter 6

Conclusion and outlook

In recent years, high–power ultrafast fiber laser systems have become the main workhorse in many fields in industry and medical applications as well as for scientific research, due to their main advantages of excellent heat dissipation capability, high single-pass gain, robustness, compactness and simplicity of operations. Finding new avenues to improve two essential properties of such laser systems–energy scaling capability and wavelength tunability–is currently a topic of important research efforts.

High average power ultrafast Yb-fiber laser system driving an enhancement cavity is one of the most promising methods for HHG with high photon flux. This method relies on the coherent superposition of ultrashort pulses inside a high-finesse cavity resulting in an enhancement of peak intensity by a factor of more than 100. In Chapter 2, we have constructed from scratch a high-power Yb-fiber MOPA system, consisting of a monolithic Yb-fiber oscillator, an all-fiber stretcher, a pre-amplifier chain, a LPF-based main amplifier, and a diffraction-grating based compressor. The monlithic Yb-fiber oscillator was carefully designed with near-zero net-cavity dispersion compensated by CFBG, to reach the lowest noise state of mode-locking. The oscillator has two locking interfaces to allow the laser system easily locked together with the enhancement cavity. In particular, high-order dispersion compensation by special fiber with negative TOD was carefully described in Chapter 2.

To increase the conversion efficiency to high-energy photons by HHG, it is highly desirable to obtain the ultrafast pulses with duration as short as possible. Due to the limited gain bandwidth ($\sim$ 40 nm) of Yb-doped fiber, the pulse generated from traditional CPA system (as described in Chapter 2) normally has more than 150 fs pulse duration. Consequently, pulse-shortening techniques play a pivotal role for efficient high-power HHG. In Chapter 3, we demonstrate a pre-chirp managed nonlinear Yb-fiber amplifier that outputs 75-MHz spectrally broadened pulses with >130-W average power. The amplified pulses are compressed to $\sim$60-fs pulses with 100-W average power, constituting a suitable driving

source for cavity-enhanced HHG. The key enabling technique employed in this Yb-fiber laser system is pre-chirp management; that is, fine tuning chirp of the pulses before seeding into a nonlinear Yb-fiber amplifier. We have both theoretically and experimentally demonstrated that such a pre-chirp management method ensures high-quality compression of the amplified and spectrally broadened pulses. Here we show that, by using an Yb-doped rod-type LPF as the power amplifier, the pulse energy can be scaled to the μJ-level without the need for conventional CPA technique. In particular, due to the small GDD of the output put pulses, we could apply high-dispersion mirrors to compress the pulses, further reducing the complexities and shrinking the size of the whole system compared with CPA technology.

In Chapter 4, we propose a new type of fiber-laser based femtosecond source, which employs SPM in an optical fiber as the dominant spectral-broadening mechanism. This source is energy scalable and has a potential to cover the entire wavelength-tunable range of 800-1300 nm in an all-in-one unit. This chapter presents an in-depth theoretical analysis of the effects of dispersion, self-steepening and SRS on the novel mechanism. As the simulation results predict, the resulting filtered spectra correspond to slightly chirped, femtosecond (70-120 fs) pulses, which can be easily compressed to the transform-limited duration. The proposed source represents a cost-effective substitute of the conventional MPM driving source, i.e., a combination of Ti:sapphire laser plus a solid-state OPO. With the possibility of implementing our ultrafast source in an all-fiber format (Yb-fiber laser plus fiber-optic spectral broadening), this energy scalable approach paves an avenue to operate MPM in rugged environments outside research labs.

In Chapter 5, according to the simulation in the last chapter, we experimentally demonstrated the new method of producing wavelength widely tunable femtosecond pulses for MPM. The method employs fiber-optic nonlinearities (dominated by SPM) to broaden an input optical spectrum, followed by optical bandpass filters to select the leftmost or rightmost spectral lobes. The filtered spectral lobes correspond to nearly transform-limited pulses with $\sim$ 100 fs pulse duration. Using 20-mm commercially available PCF, we can implement a femtosecond (70-120 fs) source tunable in 825-1210 nm with >1 nJ pulse energy. More specific, we obtained $\sim$ 3 nJ pulse energies in the wavelength range of 1100-1210 nm. Although these results already represent an order of magnitude improvement in pulse energies compared with SSFS-based soliton sources in PCFs, higher pulse energies will open more applications. We present another energy scaling method—using LMA fibers for spectral broadening, which allows us to scale the pulse energies up to 20 nJ in the wavelength range of 1080-1220 nm, enabling nonlinear light excitation even for THG in human skin.

References

[1] Tim A Birks, Jonathan C Knight, and P St J Russell. Endlessly single-mode photonic crystal fiber. *Optics letters*, 22(13):961–963, 1997.

[2] JC Knight, TA Birks, RF Cregan, P St J Russell, and JP De Sandro. Large mode area photonic crystal fibre. *Electronics Letters*, 34(13):1347–1348, 1998.

[3] RF Cregan, BJ Mangan, JC Knight, TA Birks, P St J Russell, PJ Roberts, and DC Allan. Single-mode photonic band gap guidance of light in air. *science*, 285(5433):1537–1539, 1999.

[4] JC Knight, J Arriaga, TA Birks, A Ortigosa-Blanch, WJ Wadsworth, and P St J Russell. Anomalous dispersion in photonic crystal fiber. *IEEE photonics technology letters*, 12(7):807–809, 2000.

[5] Rüdiger Paschotta. *Encyclopedia of laser physics and technology*, volume 1. Wiley-vch Berlin, 2008.

[6] Frank W Wise, Andy Chong, and William H Renninger. High-energy femtosecond fiber lasers based on pulse propagation at normal dispersion. *Laser & Photonics Reviews*, 2(1-2):58–73, 2008.

[7] ME Fermann, ML Stock, MJ Andrejco, and Y Silberberg. Passive mode locking by using nonlinear polarization evolution in a polarization-maintaining erbium-doped fiber. *Optics letters*, 18(11):894–896, 1993.

[8] K Tamura, EP Ippen, HA Haus, and LE Nelson. 77-fs pulse generation from a stretched-pulse mode-locked all-fiber ring laser. *Optics letters*, 18(13):1080–1082, 1993.

[9] MJ Guy, DU Noske, and JR Taylor. Generation of femtosecond soliton pulses by passive mode locking of an ytterbium-erbium figure-of-eight fiber laser. *Optics letters*, 18(17):1447–1449, 1993.

[10] YS Fedotov, AV Ivanenko, SM Kobtsev, and SV Smirnov. High average power mode-locked figure-eight yb fibre master oscillator. *Optics express*, 22(25):31379–31386, 2014.

[11] Daniele Brida, Günther Krauss, Alexander Sell, and Alfred Leitenstorfer. Ultrabroadband Er: fiber lasers. *Laser & Photonics Reviews*, 8(3):409–428, 2014.

[12] Robert W Boyd. *Nonlinear optics*. Academic press, 2003.

[13] Jean Toulouse. Optical nonlinearities in fibers: review, recent examples, and systems applications. *Journal of Lightwave Technology*, 23(11):3625–3641, 2005.

[14] Robert Hellwarth, Joel Cherlow, and Tien-Tsai Yang. Origin and frequency dependence of nonlinear optical susceptibilities of glasses. *Physical Review B*, 11(2):964, 1975.

[15] RW Hellwarth. Third-order optical susceptibilities of liquids and solids. *Progress in Quantum Electronics*, 5:1–68, 1977.

[16] Stephen Jacobs, Murray Sargent III, James F Scott, and Marlan O Scully. Laser applications to optics and spectroscopy. *Laser Applications to Optics and Spectroscopy*, 1, 1975.

[17] Akira Ozawa, Jens Rauschenberger, Ch Gohle, Maximilian Herrmann, David R Walker, Volodymyr Pervak, Alma Fernandez, Roswitha Graf, A Apolonski, Ronald Holzwarth, et al. High harmonic frequency combs for high resolution spectroscopy. *Physical review letters*, 100(25):253901, 2008.

[18] Ioachim Pupeza, Tino Eidam, Jens Rauschenberger, Birgitta Bernhardt, Akira Ozawa, Ernst Fill, Alexander Apolonski, Thomas Udem, Jens Limpert, Zeyad A Alahmed, et al. Power scaling of a high-repetition-rate enhancement cavity. *Optics letters*, 35(12):2052–2054, 2010.

[19] DJ Richardson, J Nilsson, and WA Clarkson. High power fiber lasers: current status and future perspectives [invited]. *JOSA B*, 27(11):B63–B92, 2010.

[20] Chia-Ming Chen and Paul L Kelley. Nonlinear pulse compression in optical fibers: scaling laws and numerical analysis. *JOSA B*, 19(9):1961–1967, 2002.

[21] T Südmeyer, F Brunner, E Innerhofer, R Paschotta, K Furusawa, JC Baggett, TM Monro, DJ Richardson, and U Keller. Nonlinear femtosecond pulse compression at high average power levels by use of a large-mode-area holey fiber. *Optics letters*, 28(20):1951–1953, 2003.

[22] B Schenkel, J Biegert, U Keller, C Vozzi, M Nisoli, G Sansone, S Stagira, S De Silvestri, and O Svelto. Generation of 3.8-fs pulses from adaptive compression of a cascaded hollow fiber supercontinuum. *Optics letters*, 28(20):1987–1989, 2003.

[23] G Steinmeyer and G Stibenz. Generation of sub-4-fs pulses via compression of a white-light continuum using only chirped mirrors. *Applied Physics B*, 82(2):175–181, 2006.

[24] Steffen Hädrich, Jan Rothhardt, Tino Eidam, Jens Limpert, and Andreas Tünnermann. High energy ultrashort pulses via hollow fiber compression of a fiber chirped pulse amplification system. *Optics express*, 17(5):3913–3922, 2009.

[25] Oliver D Mücke, Skirmantas Ališauskas, Aart J Verhoef, Audrius Pugžlys, Andrius Baltuška, Valerijus Smilgevičius, Jonas Pocius, Linas Giniūnas, Romualdas Danielius, and Nicolas Forget. Self-compression of millijoule 1.5 μm pulses. *Optics letters*, 34(16):2498–2500, 2009.

[26] KF Mak, JC Travers, NY Joly, A Abdolvand, and P St J Russell. Two techniques for temporal pulse compression in gas-filled hollow-core kagomé photonic crystal fiber. *Optics letters*, 38(18):3592–3595, 2013.

[27] AA Amorim, MV Tognetti, P Oliveira, JL Silva, LM Bernardo, FX Kärtner, and HM Crespo. Sub-two-cycle pulses by soliton self-compression in highly nonlinear photonic crystal fibers. *Optics letters*, 34(24):3851–3853, 2009.

[28] Jesper Lægsgaard and Peter John Roberts. Dispersive pulse compression in hollow-core photonic bandgap fibers. *Optics express*, 16(13):9628–9644, 2008.

[29] P St J Russell, P Hölzer, Wonkeun Chang, A Abdolvand, and JC Travers. Hollow-core photonic crystal fibres for gas-based nonlinear optics. *Nat. Photonics*, 8(4):278–286, 2014.

[30] T Balciunas, C Fourcade-Dutin, G Fan, T Witting, AA Voronin, AM Zheltikov, Frédéric Gerome, GG Paulus, A Baltuska, and F Benabid. A strong-field driver in the single-cycle regime based on self-compression in a kagome fibre. *Nature communications*, 6, 2015.

[31] KF Mak, Marcus Seidel, O Pronin, MH Frosz, A Abdolvand, V Pervak, A Apolonski, Ferenc Krausz, JC Travers, and P St J Russell. Compressing μj-level pulses from 250 fs to sub-10 fs at 38-mhz repetition rate using two gas-filled hollow-core photonic crystal fiber stages. *Optics letters*, 40(7):1238–1241, 2015.

[32] Ka Fai Mak, Marcus Seidel, Oleg Pronin, Michael Frosz, Vladimir Pervak, Alexander Apolonskiy, Ferenc Krausz, John Travers, and Philip Russell. Compression of μj-level pulses from 250 fs to sub-10 fs at 38 mhz repetition rate using two gas-filled hollow-core kagomé-pcf stages. In *Advanced Solid State Lasers*, pages AF4A–4. Optical Society of America, 2014.

[33] K Murari, GJ Stein, H Cankaya, Benoît Debord, Frédéric Gérôme, G Cirmi, OD Mücke, P Li, A Ruehl, I Hartl, et al. Kagome-fiber-based pulse compression of mid-infrared picosecond pulses from a ho: Ylf amplifier. *Optica*, 3(8):816–822, 2016.

[34] RE Kennedy, AB Rulkov, SV Popov, and JR Taylor. High-peak-power femtosecond pulse compression with polarization-maintaining ytterbium-doped fiber amplification. *Optics letters*, 32(10):1199–1201, 2007.

[35] ME Fermann, VI Kruglov, BC Thomsen, JM Dudley, and JD Harvey. Self-similar propagation and amplification of parabolic pulses in optical fibers. *Physical Review Letters*, 84(26):6010, 2000.

[36] JM Dudley, Christophe Finot, DJ Richardson, and Guy Millot. Self-similarity and scaling phenomena in nonlinear ultrafast optics. *Nature Physics*, 15(24):15824–15835, 2007.

[37] Thomas Schreiber, Carsten K Nielsen, Bülend Ortac, Jens Limpert, and Andreas Tünnermann. Microjoule-level all-polarization-maintaining femtosecond fiber source. *Optics letters*, 31(5):574–576, 2006.

[38] VI Kruglov, AC Peacock, JD Harvey, and JM Dudley. Self-similar propagation of parabolic pulses in normal-dispersion fiber amplifiers. *JOSA B*, 19(3):461–469, 2002.

[39] Jens Limpert, T Schreiber, T Clausnitzer, K Zöllner, H Fuchs, E Kley, H Zellmer, and A Tünnermann. High-power femtosecond yb-doped fiber amplifier. *Optics Express*, 10(14):628–638, 2002.

[40] Yujun Deng, Ching-Yuan Chien, Bernard G Fidric, and James D Kafka. Generation of sub-50 fs pulses from a high-power yb-doped fiber amplifier. *Optics letters*, 34(22):3469–3471, 2009.

[41] Dimitris N Papadopoulos, Yoann Zaouter, Marc Hanna, Frédéric Druon, Eric Mottay, Eric Cormier, and Patrick Georges. Generation of 63 fs 4.1 mw peak power pulses from a parabolic fiber amplifier operated beyond the gain bandwidth limit. *Optics letters*, 32(17):2520–2522, 2007.

[42] Guoqing Chang, Almantas Galvanauskas, Herbert G Winful, and Theodore B Norris. Dependence of parabolic pulse amplification on stimulated raman scattering and gain bandwidth. *Optics letters*, 29(22):2647–2649, 2004.

[43] Daniel B Soh, Johan Nilsson, and Anatoly B Grudinin. Efficient femtosecond pulse generation using a parabolic amplifier combined with a pulse compressor. i. stimulated raman-scattering effects. *JOSA B*, 23(1):1–9, 2006.

[44] Daniel B Soh, Johan Nilsson, and Anatoly B Grudinin. Efficient femtosecond pulse generation using a parabolic amplifier combined with a pulse compressor. ii. finite gain-bandwidth effect. *JOSA B*, 23(1):10–19, 2006.

[45] Yoann Zaouter, Dimitris N Papadopoulos, Marc Hanna, J Boullet, L Huang, C Aguergaray, Frédéric Druon, Eric Mottay, Patrick Georges, and Eric Cormier. Stretcher-free high energy nonlinear amplification of femtosecond pulses in rod-type fibers. *Optics letters*, 33(2):107–109, 2008.

[46] Warren R Zipfel, Rebecca M Williams, and Watt W Webb. Nonlinear magic: multiphoton microscopy in the biosciences. *Nature biotechnology*, 21(11):1369–1377, 2003.

[47] Demirhan Kobat, Michael E Durst, Nozomi Nishimura, Angela W Wong, Chris B Schaffer, and Chris Xu. Deep tissue multiphoton microscopy using longer wavelength excitation. *Optics express*, 17(16):13354–13364, 2009.

[48] C Xu and FW Wise. Recent advances in fibre lasers for nonlinear microscopy. *Nature photonics*, 7(11):875–882, 2013.

[49] Ke Wang, Nicholas G Horton, Kriti Charan, and Chris Xu. Advanced fiber soliton sources for nonlinear deep tissue imaging in biophotonics. *IEEE Journal of Selected Topics in Quantum Electronics*, 20(2):50–60, 2014.

[50] Xiang Gao, Weijian Zong, Bingying Chen, Jian Zhang, Chen Li, Yizhou Liu, Aimin Wang, Yanrong Song, and Zhigang Zhang. Core-pumped femtosecond nd: fiber laser at 910 and 935 nm. *Optics letters*, 39(15):4404–4407, 2014.

[51] Hung-Wen Chen, Zia Haider, JinKang Lim, Shanhui Xu, Zhongmin Yang, Franz X Kärtner, and Guoqing Chang. 3 ghz, yb-fiber laser-based, few-cycle ultrafast source at the Ti: Sapphire laser wavelength. *Optics letters*, 38(22):4927–4930, 2013.

[52] Ming-Che Chan, Chi-Hsiang Lien, Jyan-Yo Lu, and Bo-Han Lyu. High power nir fiber-optic femtosecond cherenkov radiation and its application on nonlinear light microscopy. *Optics express*, 22(8):9498–9507, 2014.

[53] H Lim, J Buckley, A Chong, and FW Wise. Fibre-based source of femtosecond pulses tunable from 1.0 to 1.3 μm. *Electronics Letters*, 40(24):1523–1525, 2004.

[54] Jinkang Lim, Hung-Wen Chen, Shanhui Xu, Zhongmin Yang, Guoqing Chang, and Franz X Kärtner. 3 ghz, watt-level femtosecond raman soliton source. *Optics letters*, 39(7):2060–2063, 2014.

[55] Yuan Liu, Haohua Tu, Wladimir A Benalcazar, Eric J Chaney, and Stephen A Boppart. Multimodal nonlinear microscopy by shaping a fiber supercontinuum from 900 to 1160 nm. *IEEE Journal of Selected Topics in Quantum Electronics*, 18(3):1209–1214, 2012.

[56] Thomas Gottschall, Tobias Meyer, Michael Schmitt, Jürgen Popp, Jens Limpert, and Andreas Tünnermann. Four-wave-mixing-based optical parametric oscillator delivering energetic, tunable, chirped femtosecond pulses for non-linear biomedical applications. *Optics express*, 23(18):23968–23977, 2015.

[57] Tino Eidam, Stefan Hanf, Enrico Seise, Thomas V Andersen, Thomas Gabler, Christian Wirth, Thomas Schreiber, Jens Limpert, and Andreas Tünnermann. Femtosecond fiber cpa system emitting 830 w average output power. *Optics letters*, 35(2):94–96, 2010.

[58] Andrew J Benedick, Guoqing Chang, Jonathan R Birge, Li-Jin Chen, Alexander G Glenday, Chih-Hao Li, David F Phillips, Andrew Szentgyorgyi, Sylvain Korzennik, Gabor Furesz, et al. Visible wavelength astro-comb. *Optics express*, 18(18):19175–19184, 2010.

[59] R Jason Jones, Kevin D Moll, Michael J Thorpe, and Jun Ye. Phase-coherent frequency combs in the vacuum ultraviolet via high-harmonic generation inside a femtosecond enhancement cavity. *Physical Review Letters*, 94(19):193201, 2005.

[60] Dylan C Yost, Thomas R Schibli, and Jun Ye. Microwatt-level xuv frequency comb via intracavity high harmonic generation. In *Advanced Solid-State Photonics*, page WA1. Optical Society of America, 2009.

[61] Johan Boullet, Yoann Zaouter, Jens Limpert, Stéphane Petit, Yann Mairesse, Baptiste Fabre, Julien Higuet, Eric Mével, Eric Constant, and Eric Cormier. High-order harmonic generation at a megahertz-level repetition rate directly driven by an ytterbium-doped-fiber chirped-pulse amplification system. *Optics letters*, 34(9):1489–1491, 2009.

[62] F Tavella, A Willner, J Rothhardt, S Hädrich, E Seise, S Düsterer, T Tschentscher, H Schlarb, J Feldhaus, J Limpert, et al. Fiber-amplifier pumped high average power few-cycle pulse non-collinear opcpa. *Optics express*, 18(5):4689–4694, 2010.

[63] Axel Ruehl, Andrius Marcinkevicius, Martin E Fermann, and Ingmar Hartl. 80 W, 120 fs yb-fiber frequency comb. *Optics letters*, 35(18):3015–3017, 2010.

[64] A Fernández, K Jespersen, L Zhu, L Grüner-Nielsen, A Baltuška, A Galvanauskas, and AJ Verhoef. High-fidelity, 160 fs, 5 μj pulses from an integrated yb-fiber laser system with a fiber stretcher matching a simple grating compressor. *Optics letters*, 37(5):927–929, 2012.

[65] Cesar Jauregui, Jens Limpert, and Andreas Tünnermann. High-power fibre lasers. *Nature photonics*, 7(11):861–867, 2013.

[66] Fabian Stutzki, Florian Jansen, Hans-Jürgen Otto, Cesar Jauregui, Jens Limpert, and Andreas Tünnermann. Designing advanced very-large-mode-area fibers for power scaling of fiber-laser systems. *Optica*, 1(4):233–242, 2014.

[67] Fabian Stutzki, Christian Gaida, Martin Gebhardt, Florian Jansen, Cesar Jauregui, Jens Limpert, and Andreas Tünnermann. Tm-based fiber-laser system with more than 200 mw peak power. *Optics letters*, 40(1):9–12, 2015.

[68] M Leich, W He, S Grimm, J Kobelke, Y Zhu, B Müller, J Bierlich, H Bartelt, and M Jäger. High peak power amplification in large-core all-solid yb fibers with an index-elevated pump clad and a low numerical aperture core. In *SPIE LASE*, pages 93440T–93440T. International Society for Optics and Photonics, 2015.

[69] Lora Nugent-Glandorf, Todd A Johnson, Yohei Kobayashi, and Scott A Diddams. Impact of dispersion on amplitude and frequency noise in a yb-fiber laser comb. *Optics letters*, 36(9):1578–1580, 2011.

[70] WH Knox. In situ measurement of complete intracavity dispersion in an operating Ti: Sapphire femtosecond laser. *Optics letters*, 17(7):514–516, 1992.

[71] Jean-Claude Diels and Wolfgang Rudolph. *Ultrashort laser pulse phenomena*. Academic press, 2006.

[72] Travis C Briles, Dylan C Yost, Arman Cingöz, Jun Ye, and Thomas R Schibli. Simple piezoelectric-actuated mirror with 180 kHz servo bandwidth. *Optics express*, 18(10):9739–9746, 2010.

[73] Lars Grüner-Nielsen, Dan Jakobsen, Kim G Jespersen, and Bera Pálsdóttir. A stretcher fiber for use in fs chirped pulse yb amplifiers. *Optics express*, 18(4):3768–3773, 2010.

[74] Jens Limpert, Fabian Stutzki, Florian Jansen, Hans-Jürgen Otto, Tino Eidam, Cesar Jauregui, and Andreas Tünnermann. Yb-doped large-pitch fibres: effective single-mode operation based on higher-order mode delocalisation. *Light: Science & Applications*, 1(4):e8, 2012.

[75] J Limpert, O Schmidt, J Rothhardt, F Röser, T Schreiber, A Tünnermann, S Ermeneux, P Yvernault, and F Salin. Extended single-mode photonic crystal fiber lasers. *Optics Express*, 14(7):2715–2720, 2006.

[76] Christoph Gohle, Thomas Udem, Maximilian Herrmann, Jens Rauschenberger, Ronald Holzwarth, Hans A Schuessler, Ferenc Krausz, and Theodor W Hänsch. A frequency comb in the extreme ultraviolet. *Nature*, 436(7048):234–237, 2005.

[77] Arman Cingöz, Dylan C Yost, Thomas K Allison, Axel Ruehl, Martin E Fermann, Ingmar Hartl, and Jun Ye. Direct frequency comb spectroscopy in the extreme ultraviolet. *Nature*, 482(7383):68–71, 2012.

[78] Ioachim Pupeza, Simon Holzberger, T Eidam, Henning Carstens, D Esser, J Weitenberg, P Rußbüldt, Jens Rauschenberger, J Limpert, Th Udem, et al. Compact high-repetition-rate source of coherent 100 ev radiation. *Nature Photonics*, 7(8):608–612, 2013.

[79] Hung-Wen Chen, JinKang Lim, Shu-Wei Huang, Damian N Schimpf, Franz X Kärtner, and Guoqing Chang. Optimization of femtosecond yb-doped fiber amplifiers for high-quality pulse compression. *Optics express*, 20(27):28672–28682, 2012.

[80] Sijia Wang, Bowen Liu, Minglie Hu, Lu Chai, and Chingyue Wang. Generation of sub-40fs pulses from a spectral-breathing self-similar fiber amplifier. In *Conference on Lasers and Electro-Optics/Pacific Rim*, page WA1_3. Optical Society of America, 2013.

[81] Tsung-Han Wu, David Carlson, and R Jason Jones. A high-power fiber laser system for dual-comb spectroscopy in the vacuum-ultraviolet. *Frontiers in Optics*, pages FTu2A–4, 2013.

[82] Wei Liu, Damian N Schimpf, Tino Eidam, Jens Limpert, Andreas Tünnermann, Franz X Kärtner, and Guoqing Chang. Pre-chirp managed nonlinear amplification in fibers delivering 100 w, 60 fs pulses. *Optics letters*, 40(2):151–154, 2015.

[83] CJ Saraceno, OH Heckl, CRE Baer, T Südmeyer, and U Keller. Pulse compression of a high-power thin disk laser using rod-type fiber amplifiers. *Optics express*, 19(2):1395–1407, 2011.

[84] Birgitta Bernhardt, Akira Ozawa, Andreas Vernaleken, Ioachim Pupeza, Jan Kaster, Yohei Kobayashi, Ronald Holzwarth, Ernst Fill, Ferenc Krausz, Theodor W Hänsch, et al. Vacuum ultraviolet frequency combs generated by a femtosecond enhancement cavity in the visible. *Optics letters*, 37(4):503–505, 2012.

[85] Yuen-ron Shen. Self-focusing: experimental. *Progress in quantum electronics*, 4:1–34, 1975.

[86] JH Marburger. Self-focusing: theory. *Progress in Quantum Electronics*, 4:35–110, 1975.

[87] Damian N Schimpf, Tino Eidam, Enrico Seise, Steffen Hädrich, Jens Limpert, and Andreas Tünnermann. Circular versus linear polarization in laser-amplifiers with kerr-nonlinearity. *Optics express*, 17(21):18774–18781, 2009.

[88] Qiang Hao, Qingshan Zhang, Tingting Sun, Jie Chen, Zhanhua Guo, Yuqing Wang, Zhengru Guo, Kangwen Yang, and Heping Zeng. Divided-pulse nonlinear amplification and simultaneous compression. *Applied Physics Letters*, 106(10):101103, 2015.

[89] Fabien Lesparre, Jean Thomas Gomes, Xavier Délen, Igor Martial, Julien Didierjean, Wolfgang Pallmann, Bojan Resan, Frederic Druon, François Balembois, and Patrick Georges. Yb:YAG single-crystal fiber amplifiers for picosecond lasers using the divided pulse amplification technique. *Optics letters*, 41(7):1628–1631, 2016.

[90] Benjamin Webb, Ahmad Azim, Nathan Bodnar, Michael Chini, Lawrence Shah, and Martin Richardson. Divided-pulse amplification to the joule level. *Optics Letters*, 41(13):3106–3109, 2016.

[91] LJ Kong, LM Zhao, S Lefrancois, DG Ouzounov, CX Yang, and FW Wise. Generation of megawatt peak power picosecond pulses from a divided-pulse fiber amplifier. *Optics letters*, 37(2):253–255, 2012.

[92] Shuo Tang, Jian Liu, Tatiana B Krasieva, Zhongping Chen, and Bruce J Tromberg. Developing compact multiphoton systems using femtosecond fiber lasers. *Journal of biomedical optics*, 14(3):030508–030508, 2009.

[93] Gangjun Liu, Khanh Kieu, Frank W Wise, and Zhongping Chen. Multiphoton microscopy system with a compact fiber-based femtosecond-pulse laser and handheld probe. *Journal of biophotonics*, 4(1-2):34–39, 2011.

[94] Dong Uk Kim, Hoseong Song, Woosub Song, Hyuk-Sang Kwon, Miae Sung, and Dug Young Kim. Two-photon microscopy using an yb 3+-doped fiber laser with variable pulse widths. *Optics express*, 20(11):12341–12349, 2012.

[95] Bai Nie, Ilyas Saytashev, Andy Chong, Hui Liu, Sergey N Arkhipov, Frank W Wise, and Marcos Dantus. Multimodal microscopy with sub-30 fs yb fiber laser oscillator. *Biomedical optics express*, 3(7):1750–1756, 2012.

[96] Mihaela Balu, Ilyas Saytashev, Jue Hou, Marcos Dantus, and Bruce J Tromberg. Sub-40 fs, 1060-nm yb-fiber laser enhances penetration depth in nonlinear optical microscopy of human skin. *Journal of biomedical optics*, 20(12):120501–120501, 2015.

[97] Carsten Tischbirek, Antje Birkner, Hongbo Jia, Bert Sakmann, and Arthur Konnerth. Deep two-photon brain imaging with a red-shifted fluorometric ca^{2+} indicator. *Proceedings of the National Academy of Sciences*, 112(36):11377–11382, 2015.

[98] Erin S Lamb and Frank W Wise. Multimodal fiber source for nonlinear microscopy based on a dissipative soliton laser. *Biomedical optics express*, 6(9):3248–3255, 2015.

[99] Evan P Perillo, Justin E McCracken, Daniel C Fernée, John R Goldak, Flor A Medina, David R Miller, Hsin-Chih Yeh, and Andrew K Dunn. Deep in vivo two-photon microscopy with a low cost custom built mode-locked 1060 nm fiber laser. *Biomedical optics express*, 7(2):324–334, 2016.

[100] Miro Erkintalo, Claude Aguergaray, Antoine Runge, and Neil GR Broderick. Environmentally stable all-PM all-fiber giant chirp oscillator. *Optics express*, 20(20):22669–22674, 2012.

[101] Claude Aguergaray, Ryan Hawker, Antoine FJ Runge, Miro Erkintalo, and Neil GR Broderick. 120 fs, 4.2 nJ pulses from an all-normal-dispersion, polarization-maintaining, fiber laser. *Applied Physics Letters*, 103(12):121111, 2013.

[102] Jan Szczepanek, Tomasz M Kardaś, Maria Michalska, Czesław Radzewicz, and Yuriy Stepanenko. Simple all-PM-fiber laser mode-locked with a nonlinear loop mirror. *Optics letters*, 40(15):3500–3503, 2015.

[103] Fedor M Mitschke and Linn F Mollenauer. Discovery of the soliton self-frequency shift. *Optics letters*, 11(10):659–661, 1986.

[104] Govind P Agrawal. *Nonlinear fiber optics*. Academic press, 2007.

[105] Wei Liu, Chen Li, Zhigang Zhang, Franz X Kärtner, and Guoqing Chang. Self-phase modulation enabled, wavelength-tunable ultrafast fiber laser sources: an energy scalable approach. *Optics Express*, 24(14):15328–15340, 2016.

[106] Xiang Liu, C Xu, WH Knox, JK Chandalia, BJ Eggleton, SG Kosinski, and RS Windeler. Soliton self-frequency shift in a short tapered air–silica microstructure fiber. *Optics Letters*, 26(6):358–360, 2001.

[107] BR Washburn, SE Ralph, PA Lacourt, JM Dudley, WT Rhodes, RS Windeler, and S Coen. Tunable near-infrared femtosecond soliton generation in photonic crystal fibres. *Electronics Letters*, 37(25):1, 2001.

[108] IG Cormack, DT Reid, WJ Wadsworth, JC Knight, and P St J Russell. Observation of soliton self-frequency shift in photonic crystal fibre. *Electronics Letters*, 38(4):167–169, 2002.

[109] Norihiko Nishizawa, Youta Ito, and Toshio Goto. 0.78-0.90-μm wavelength-tunable femtosecond soliton pulse generation using photonic crystal fiber. *IEEE Photonics Technology Letters*, 14(7):986–988, 2002.

[110] JW Walewski, MR Borden, and ST Sanders. Wavelength-agile laser system based on soliton self-shift and its application for broadband spectroscopy. *Applied Physics B*, 79(8):937–940, 2004.

[111] Jun Takayanagi, Toshiharu Sugiura, Makoto Yoshida, and Norihiko Nishizawa. 1.0–1.7-m wavelength-tunable ultrashort-pulse generation using femtosecond yb-doped fiber laser and photonic crystal fiber. *IEEE photonics technology letters*, 18(21):2284–2286, 2006.

[112] Gengji Zhou, Ming Xin, Franz X Kaertner, and Guoqing Chang. Timing jitter of raman solitons. *Optics letters*, 40(21):5105–5108, 2015.

[113] Ming-Che Chan, Shih-Hsuan Chia, Tzu-Ming Liu, Tsung-Han Tsai, Min-Chen Ho, Anatoly A Ivanov, Aleksei M Zheltikov, Jiun-Yi Liu, Hsiang-Lin Liu, and Chi-Kuang Sun. 1.2-2.2 μm tunable raman soliton source based on a cr: Forsterite-laser and a photonic-crystal fiber. In *Conference on Lasers and Electro-Optics*, page CThGG7. Optical Society of America, 2008.

[114] Jennifer H Lee, James van Howe, Chris Xu, and Xiang Liu. Soliton self-frequency shift: experimental demonstrations and applications. *IEEE Journal of Selected Topics in Quantum Electronics*, 14(3):713–723, 2008.

[115] AB Fedotov, AA Voronin, IV Fedotov, AA Ivanov, and AM Zheltikov. Powerful wavelength-tunable ultrashort solitons in a solid-core photonic-crystal fiber. *Optics letters*, 34(6):851–853, 2009.

[116] Tyler W Neely, Todd A Johnson, and Scott A Diddams. High-power broadband laser source tunable from 3.0 μm to 4.4 μmbased on a femtosecond yb: fiber oscillator. *Optics letters*, 36(20):4020–4022, 2011.

[117] James van Howe, Jennifer H Lee, Shian Zhou, Frank Wise, Chris Xu, Siddharth Ramachandran, Samir Ghalmi, and Man F Yan. Demonstration of soliton self-frequency shift below 1300nm in higher-order mode, solid silica-based fiber. *Optics letters*, 32(4):340–342, 2007.

[118] Martin EV Pedersen, Ji Cheng, Kriti Charan, Ke Wang, Chris Xu, Lars Grüner-Nielsen, and Dan Jakobsen. Higher-order-mode fiber optimized for energetic soliton propagation. *Optics letters*, 37(16):3459–3461, 2012.

[119] Kunimasa Saitoh, M Koshiba, T Hasegawa, and E Sasaoka. Chromatic dispersion control in photonic crystal fibers: application to ultra-flattened dispersion. *Optics Express*, 11(8):843–852, 2003.

[120] Aaron D Aguirre, Norihiko Nishizawa, James G Fujimoto, Wolfgang Seitz, Max Lederer, and Daniel Kopf. Continuum generation in a novel photonic crystal fiber for ultrahigh resolution optical coherence tomography at 800 nm and 1300 nm. *Optics Express*, 14(3):1145–1160, 2006.

[121] Haohua Tu, Yuan Liu, Jesper Lægsgaard, Utkarsh Sharma, Martin Siegel, Daniel Kopf, and Stephen A Boppart. Scalar generalized nonlinear schrödinger equation-quantified continuum generation in an all-normal dispersion photonic crystal fiber for broadband coherent optical sources. *Optics express*, 18(26):27872–27884, 2010.

[122] Alexander M Heidt, Alexander Hartung, Gurthwin W Bosman, Patrizia Krok, Erich G Rohwer, Heinrich Schwoerer, and Hartmut Bartelt. Coherent octave spanning near-infrared and visible supercontinuum generation in all-normal dispersion photonic crystal fibers. *Optics express*, 19(4):3775–3787, 2011.

[123] Lucy E Hooper, Peter James Mosley, Alistair C Muir, William J Wadsworth, and Jonathan C Knight. Coherent supercontinuum generation in photonic crystal fiber with all-normal group velocity dispersion. *Optics express*, 19(6):4902–4907, 2011.

[124] C Benko, A Ruehl, MJ Martin, KSE Eikema, ME Fermann, I Hartl, and J Ye. Full phase stabilization of a yb: fiber femtosecond frequency comb via high-bandwidth transducers. *Optics letters*, 37(12):2196–2198, 2012.

[125] Yuan Liu, Haohua Tu, and Stephen A Boppart. Wave-breaking-extended fiber supercontinuum generation for high compression ratio transform-limited pulse compression. *Optics letters*, 37(12):2172–2174, 2012.

[126] Scott R Domingue and Randy A Bartels. Three-photon excitation source at 1250 nm generated in a dual zero dispersion wavelength nonlinear fiber. *Optics express*, 22(25):30777–30785, 2014.

[127] Yuhong Yao and Wayne H Knox. Broadly tunable femtosecond mid-infrared source based on dual photonic crystal fibers. *Optics express*, 21(22):26612–26619, 2013.

[128] Yuhong Yao and Wayne H Knox. Speckle-free femtosecond red-green-blue (rgb) source from a fiber laser driven spectrally efficient two zero dispersion wavelength fiber source. *Optics express*, 23(1):536–544, 2015.

[129] Yuhong Yao, Govind P Agrawal, and Wayne H Knox. Yb: fiber laser-based, spectrally coherent and efficient generation of femtosecond 1.3-μm pulses from a fiber with two zero-dispersion wavelengths. *Optics letters*, 40(15):3631–3634, 2015.

Appendix A

The operation information of high power pump module in the CPA and PCMA system

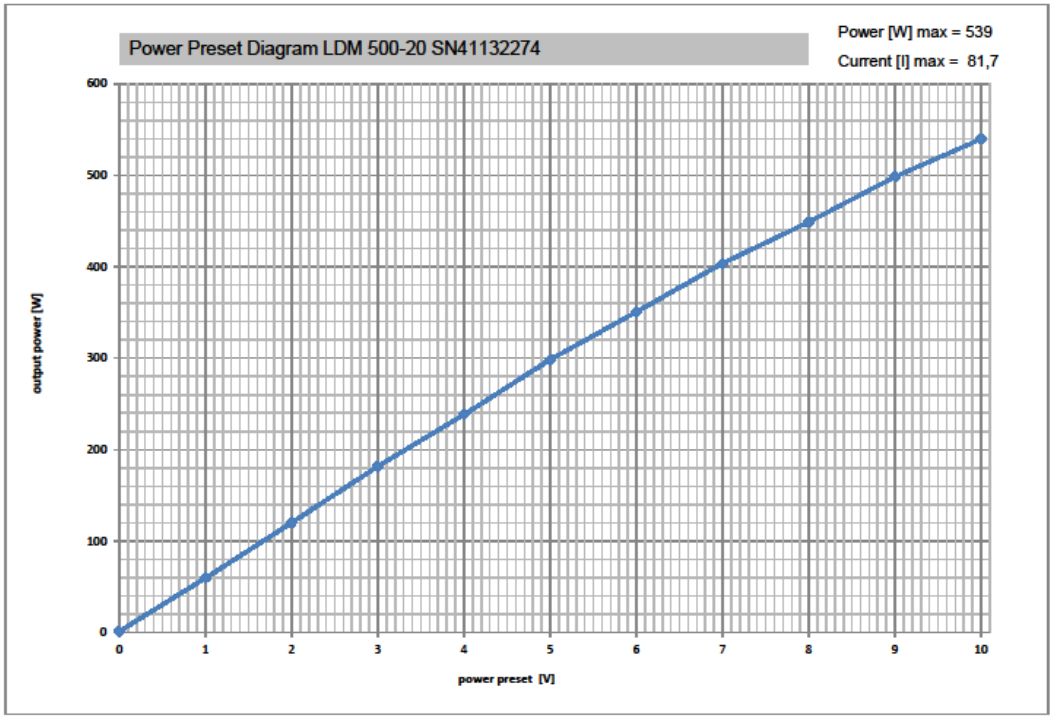

Fig. A.1 The output power of pump module versus the laser driving voltage.

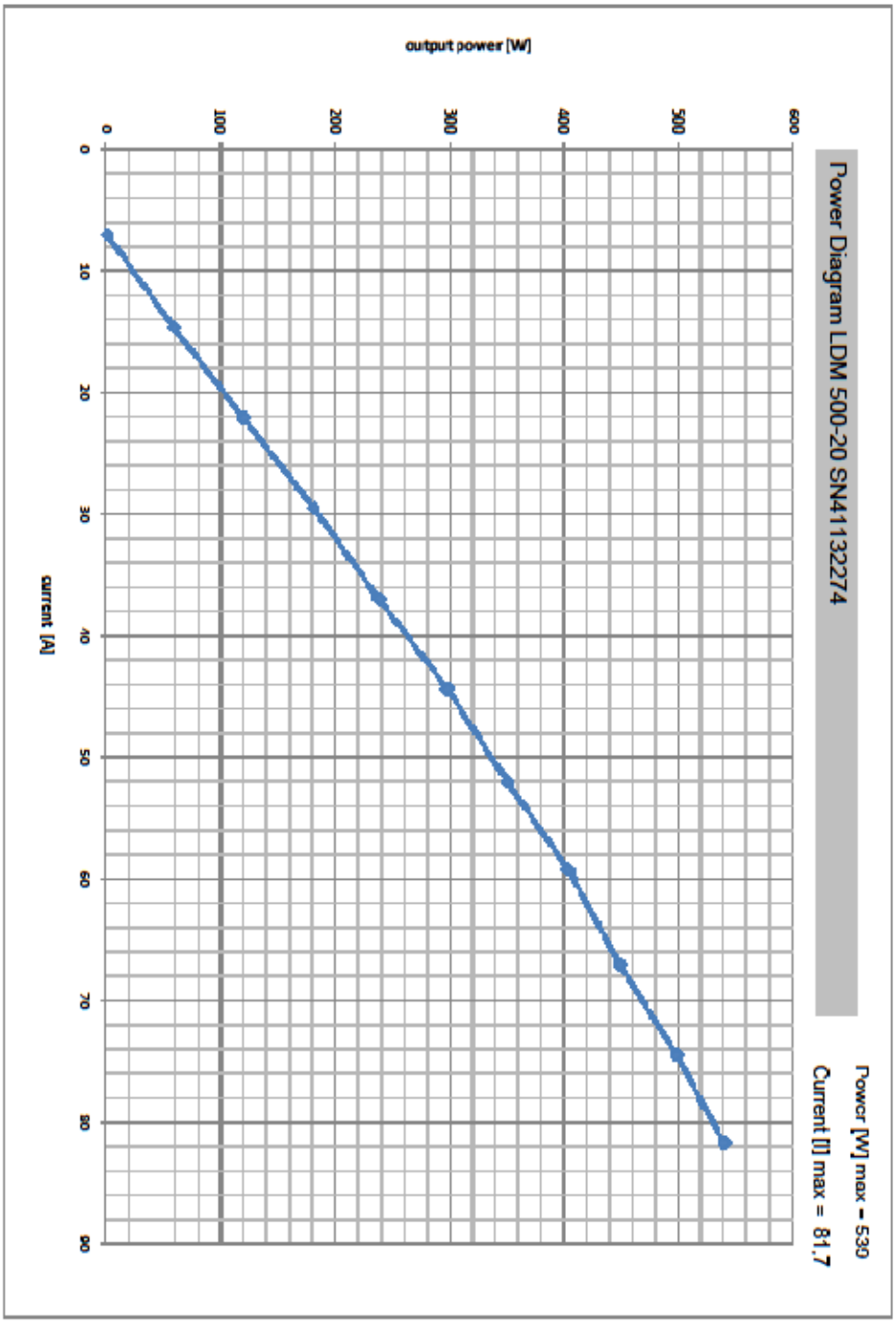

Fig. A.2 The output power of pump module versus the laser driving current.

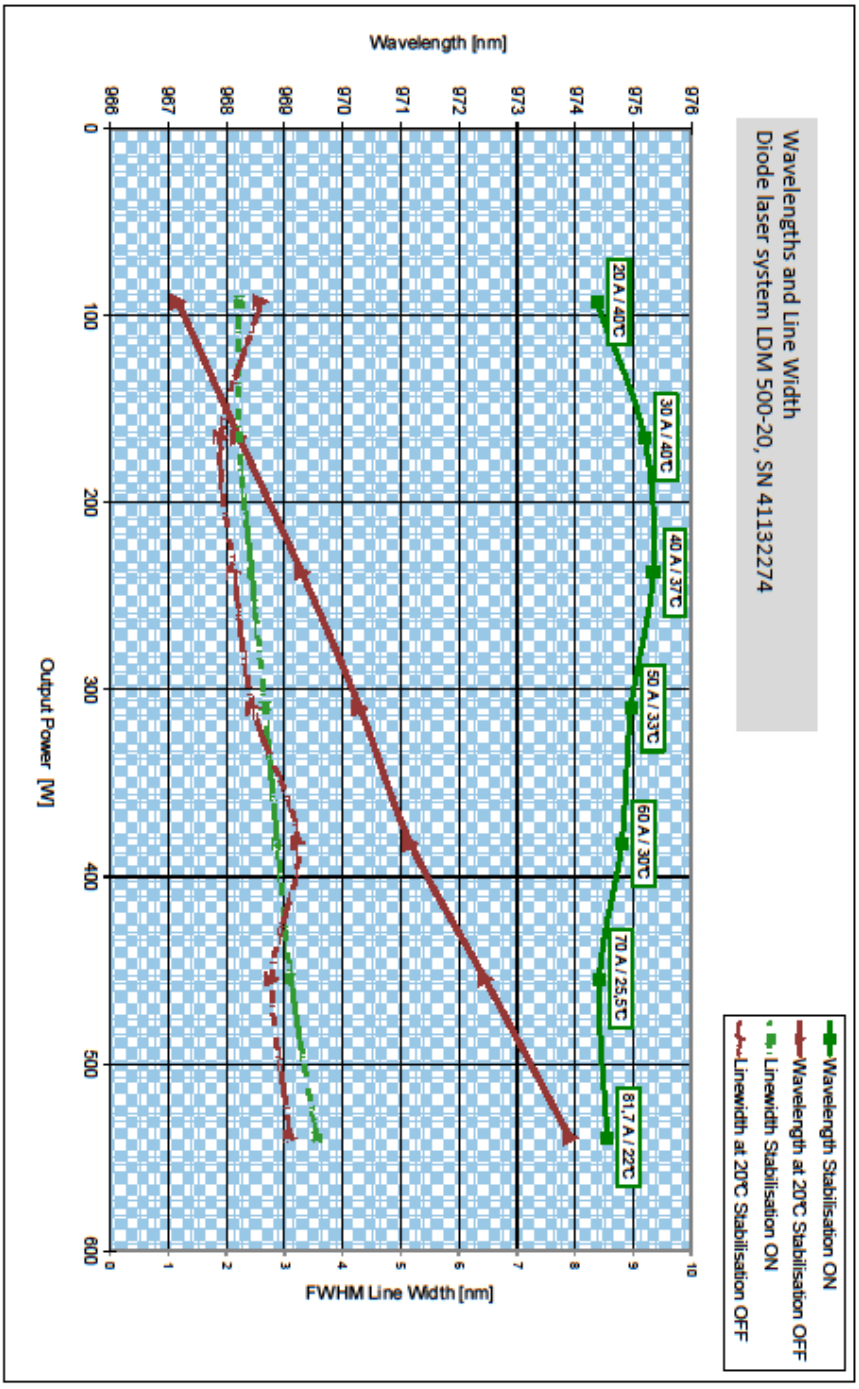

Fig. A.3 The central wavelength and linewidth stabilization performance of the pump module.